

Experimental Investigation of New Coating Methods for 3D-Printed Cathodes for Hydrogen Production

by

Muarij Khalil

A thesis submitted to the
School of Graduate and Postdoctoral Studies in partial
fulfillment of the requirements for the degree of

Master of Applied Science in Mechanical Engineering

Faculty of Engineering and Applied Science

University of Ontario Institute of Technology (Ontario Tech University)

Oshawa, Ontario, Canada

August 2023

© Muarij Khalil, 2023

THESIS EXAMINATION INFORMATION

Submitted by: **Muarij Khalil**

Master of Applied Science in Mechanical Engineering

Thesis title: Experimental Investigation of New Coating Methods for 3D-Printed Cathodes for Hydrogen Production

An oral defense of this thesis took place on August 11, 2023, in front of the following examining committee:

Examining Committee:

Chair of Examining Committee	Dr. Amirkianoosh Kiani
Research Supervisor	Dr. Ibrahim Dincer
Examining Committee Member	Dr. Martin Agelin-Chaab
Thesis Examiner	Dr. Xianke Lin

The above committee determined that the thesis is acceptable in form and content and that a satisfactory knowledge of the field covered by the thesis was demonstrated by the candidate during an oral examination. A signed copy of the Certificate of Approval is available from the School of Graduate and Postdoctoral Studies.

ABSTRACT

This thesis presents a novel approach for preparing electrodes for hydrogen evolution reaction. A new approach where the electrolysis cathodes are 3D-printed and coated for alkaline water electrolysis. Copper, iron, and molybdenum are considered with nickel as coatings using electrodeposition. The results are obtained from electrochemical measurements and hydrogen production testing. The electrochemical activity of the electrodes is improved with the addition of catalysts. Higher current densities are obtained at the same potential for electrodes with more metal deposition of the same coating metal. Relatively low overpotentials of 270 mV and 275 mV are obtained at 10 mA/cm² current density for nickel-iron and nickel-copper coated 3D-printed electrodes respectively. A new flow-through electrode design introduced showed to have 70% higher efficiency than the coated 3D-printed electrode of the conventional design. 3D printing provides a safe design place for exploring unconventional electrode designs for improving electrolysis performance and efficiency.

Keywords: Hydrogen production; electrolysis; cathodes; current density; energy; efficiency

AUTHOR'S DECLARATION

I hereby declare that this thesis consists of original work of which I have authored. This is a true copy of the thesis, including any required final revisions, as accepted by my examiners.

I authorize the University of Ontario Institute of Technology (Ontario Tech University) to lend this thesis to other institutions or individuals for the purpose of scholarly research. I further authorize the University of Ontario Institute of Technology (Ontario Tech University) to reproduce this thesis by photocopying or by other means, in total or in part, at the request of other institutions or individuals for the purpose of scholarly research. I understand that my thesis will be made electronically available to the public.

Muarij Khalil

STATEMENT OF CONTRIBUTIONS

I hereby certify that I am the sole author of this thesis and that no part of this thesis has been published or submitted for publication. I have used standard referencing practices to acknowledge ideas, research techniques, or other materials that belong to others. Furthermore, I hereby certify that I am the sole source of the creative works and/or inventive knowledge described in this thesis.

ACKNOWLEDGMENTS

I would like to express my deepest gratitude to my supervisor Dr. Ibrahim Dincer for his support, and confidence in me which has encouraged me in completing this thesis. His expertise and invaluable insights have allowed me to learn and grow. His guidance was key in motivating me to achieve my best.

I would like to thank my parents, and my brothers for their support and understanding. I would also like to thank my friends who have always been there for me and have continuously encouraged me. Their tremendous support has only motivated me and inspired me to reach my goals.

I would like to extend my appreciation to everyone at the Clean Energy Research Laboratory, at Ontario Tech University who has helped me by providing the necessary support with my experiments and academic studies.

TABLE OF CONTENTS

Thesis Examination Information	ii
Abstract	iii
Author’s Declaration	iv
Statement of Contributions.....	v
Acknowledgments	vi
Table of Contents	vii
List of Tables.....	x
List of Figures	xi
List of Abbreviations and Symbols.....	xv
Chapter 1: Introduction	1
1.1 Current State of Energy and Shift Towards Renewable and Clean Energy	1
1.2 Significance of Hydrogen as an Energy Fuel.....	3
1.3 Hydrogen Production Methods	4
1.4 Electrolysis Types	5
1.5 Electrolysis Materials and Manufacturing	5
1.6 Additive Manufacturing and 3D Printing Technologies.....	6
1.7 Motivation	6
1.8 Objectives.....	7
1.9 Novelties.....	8
Chapter 2: Literature Review and Background.....	9
2.1 Alkaline Water Electrolysis	10
2.2 Traditional Electrodes for Hydrogen Evolution Reaction.....	10
2.3 Additive Manufacturing Technologies and Materials for 3D-Printed Electrodes ..	12
2.4 Electrodeposition Fundamentals and Process	14
2.4.1 Electrodeposition Techniques.....	14
2.4.2 Electrochemistry of Metals.....	14
2.4.3 Electrodeposition Thermodynamics	17
2.4.4 Electrodeposition Kinetics.....	18
2.5 Electrocatalysts and Coatings.....	19
2.5.1 3D-printed based Electrodes and Coating Methods in Alkaline Media	19

2.5.2 3D-Printed based Electrodes in Non-Alkaline Electrolysis Applications	22
2.5.3 Coatings on Industrially Prepared Metallic Electrodes	23
2.6 Electrolysis Stack Configurations and Design	24
2.7 Gaps in the literature	26
Chapter 3: Experimental Apparatus and Procedure	27
3.1 Electrode Preparation and Coating Techniques	27
3.1.1 Electrode Design.....	27
3.1.2 3D Printing and Coating Procedure Plan.....	29
3.1.3 Electrodeposition on Conductive Paint 3D-printed Electrodes	30
3.1.4 Electrodeposition on Conductive PLA 3D-printed Electrodes.....	31
3.2 System Components and Materials	32
3.3 Experimental Setup and Procedure	36
3.3.1 Electrodeposition and Electrode Coating Apparatus	37
3.3.2 Electrode Testing Apparatus for Hydrogen Potential.....	38
3.3.3 Electrolyte Bath Compositions	39
3.3.4 Electrochemical Testing	43
3.4 Experimental Uncertainty and Error Analysis	45
Chapter 4: Modelling and Analysis	48
4.1 Electrochemistry Analysis.....	48
4.1.1 Thermodynamic Analysis.....	48
4.1.2 Kinetic Analysis.....	49
4.2 Metal Deposition	51
4.2.1 Electrodeposition and Electrode Coating Parameters.....	51
4.2.2 Voltage Supplied and Electrode Resistance	55
4.3 Thermodynamic Analysis and Hydrogen Yields	57
Chapter 5: Results and Discussion.....	59
5.1 Coated Electrodes and Deformations	59
5.2 3D-printed with Nickel Conductive Paint Coated and Electroplated Electrodes....	62
5.2.1 Nickel Electrodes.....	62
5.2.2 Nickel Alloy Electrodes.....	65
5.2.3 Impudence Measurements	68
5.2.4 Overpotential Results.....	70

5.3 Conductive PLA Electroplated 3D-printed Electrodes	71
5.3.1 Nickel Electrodes.....	72
5.3.2 Nickel Alloy Electrodes.....	74
5.3.3 Impudence Measurements	82
5.3.4 Overpotential Results.....	84
5.4 Flow Through Coated Electrodes.....	86
5.4.1 Current Density Measurements	86
5.4.2 Impudence Measurements	87
5.4.3 Overpotential Results.....	89
5.5 Comparative with Related Literature Studies	91
5.6 Electrolysis Cathodic Testing Results for Hydrogen Potential.....	93
5.6.1 Hydrogen Production Rates.....	94
5.6.2 Hydrogen Rates for Extended Testing Run Time.....	97
5.6.3 Energy and Exergy Efficiency Results	100
Chapter 6: Conclusions and Recommendations	106
6.1 Conclusions	106
6.2 Recommendations	108
References.....	110

LIST OF TABLES

Table 3.1 Equipment and component specifications.....	33
Table 3.2 Chemicals and specifications.....	35
Table 3.3 Electrochemistry testing setup components.....	44
Table 3.4 Experimental components and equipment errors.....	46
Table 3.5 Experimental uncertainties for measured parameters.....	47
Table 4.1 Electrodeposition parameters for nickel alloy coatings for NCP electrodes...	52
Table 4.2 Electrodeposition parameters for nickel coated NCP electrodes.....	53
Table 4.3 Electrodeposition parameters for nickel coated CPLA electrodes.....	54
Table 4.4 Electrodeposition parameters for nickel-copper coated CPLA electrodes.....	54
Table 4.5 Electrodeposition parameters for nickel-molybdenum coated CPLA electrodes.....	54
Table 4.6 Electrodeposition parameters for other metal coatings for CPLA electrodes..	55
Table 4.7 Electrodeposition parameters for metal coatings on D2 electrodes.....	55
Table 4.8 Measured resistances for nickel-coated NCP 3D-printed electrodes.....	56
Table 4.9 Measured resistances for metals on nickel-coated NCP 3D-printed electrodes.....	56
Table 4.10 Measured resistances for coatings on CPLA 3D-printed electrodes.....	57

LIST OF FIGURES

Figure 1.1 Investments in Energy Sector to Reach Net-Zero Emissions 2021 - 2030 (data from [3]).....	2
Figure 1.2 Factors for reducing emissions by 2050 (data from [5])	3
Figure 1.3 Hydrogen Production Paths (adapted from [9])	4
Figure 2.1 3D-printed flow through electrode studied by Sullivan et al. [49].....	22
Figure 2.2 Alkaline electrolysis stack configurations (a) convectional assembly (b) zero-gap assembly (adapted from [58])	25
Figure 3.1 Electrode designs (a) initial design (b) slightly modified design	28
Figure 3.2 Flow through electrode design (D2).....	28
Figure 3.3 Anycubic Kobra 3D printer used for 3D printing.....	29
Figure 3.4 Schematic diagram for electrodeposition	30
Figure 3.5 3D-printed with non-conductive PLA and NCP coated (a) 3D-printed PLA electrode (b) after nickel conductive painted electrode	31
Figure 3.6 Conductive PLA 3D-printed Electrodes (a) original design electrode (b) D2 electrode	32
Figure 3.7 Experimental procedure flow chart	37
Figure 3.8 Experimental setup for electrodeposition and electrochemistry testing	38
Figure 3.9 Electrolysis cathodic testing and hydrogen measurement apparatus.....	39
Figure 3.10 Conductivity of the copper electrolyte bath with increase in bath temperature	42
Figure 3.11 Gamry calibration configuration and Universal Dummy Cell [76].....	45
Figure 5.1 Coated CPLA 3D-printed electrodes (a) Ni (b) Ni-Cu (c) Ni-Fe (d) Ni-Mo..	59
Figure 5.2 Coated flow through CPLA 3D-printed Electrodes (a) Ni (b) Ni-Cu (c) Ni-Fe	60
Figure 5.3 Deformations while coating (a) breakage due to high voltage (b) impurities as a result of the PLA surface (c) pockets underneath coatings after testing.....	61
Figure 5.4 LSV measurements of nickel NCP 3D-printed electrodes in distilled water .	63

Figure 5.5 LSV measurements of nickel NCP electrodes in 1 mol KOH solution.....	63
Figure 5.6 LSV measurements of NCP 3D-printed electrodes coated with nickel bath of composition X.....	64
Figure 5.7 LSV measurements of NCP 3D-printed electrodes coated with nickel bath of composition Y.....	65
Figure 5.8 CV measurements of nickel alloys coated NCP 3D-printed electrodes in distilled water.....	66
Figure 5.9 CV measurements of nickel alloys coated NCP 3D-printed electrodes in 1 mol KOH solution.....	67
Figure 5.10 LSV measurements of nickel alloys coated NCP 3D-printed electrodes in 1 mol KOH solution.....	67
Figure 5.11 Bode plot for magnitude for NCP 3D-printed coated electrodes.....	68
Figure 5.12 Bode plot for phase angle for NCP 3D-printed coated electrodes.....	69
Figure 5.13 Nyquist plot for NCP 3D-printed coated electrodes.....	69
Figure 5.14 LSV measurements used for overpotential calculation for NCP 3D-printed coated electrodes.....	70
Figure 5.15 Overpotentials for NCP 3D-printed coated electrodes.....	71
Figure 5.16 CV measurements of nickel-coated CPLA 3D-printed electrodes for different nickel depositions in distilled water.....	72
Figure 5.17 CV measurements of nickel-coated CPLA 3D-printed electrodes for different nickel depositions in 1 mol KOH solution.....	73
Figure 5.18 LSV measurements of nickel-coated CPLA 3D-printed electrodes for different nickel depositions in 1 mol KOH solution.....	74
Figure 5.19 CV measurements of nickel alloy coated CPLA 3D-printed electrodes in distilled water.....	75
Figure 5.20 CV measurements of nickel alloy coated CPLA 3D-printed electrodes in 1 mol KOH solution.....	76
Figure 5.21 LSV measurements of nickel alloy coated CPLA 3D-printed electrodes in 1 mol KOH solution.....	76
Figure 5.22 CV measurements of nickel-copper coated CPLA 3D-printed electrodes for different copper depositions in 1 mol KOH solution.....	77

Figure 5.23 LSV measurements of nickel-copper coated CPLA 3D-printed electrodes for different copper depositions in 1 mol KOH solution.....	78
Figure 5.24 LSV measurements of nickel-copper coated vs copper-coated CPLA 3D-printed electrodes in 1 mol KOH solution	79
Figure 5.25 CV measurements of nickel-molybdenum coated CPLA 3D-printed electrodes for different molybdenum depositions in 1 mol KOH solution.....	80
Figure 5.26 LSV measurements of nickel-molybdenum coated CPLA 3D-printed electrodes for different molybdenum depositions in 1 mol KOH solution.....	81
Figure 5.27 LSV measurements of nickel-molybdenum coated vs nickel-molybdenum co-deposited CPLA 3D-printed electrode in 1 mol KOH solution.....	81
Figure 5.28 Bode plot for impedance magnitude for CPLA 3D-printed coated electrodes	83
Figure 5.29 Bode plot for phase angle for CPLA 3D-printed coated electrodes	83
Figure 5.30 Nyquist plot for CPLA 3D-printed coated electrodes	84
Figure 5.31 LSV measurements of coated CPLA 3D-printed electrodes for overpotential	85
Figure 5.32 Overpotentials for CPLA 3D-printed coated electrodes.....	85
Figure 5.33 CV measurements of flow through coated electrodes and the uncoated electrode in 1 mol KOH solution	87
Figure 5.34 Bode plot for impedance magnitude for flow through (D2) coated electrodes	88
Figure 5.35 Bode plot for phase angle for flow through (D2) coated electrodes.....	88
Figure 5.36 Nyquist plot for flow through (D2) coated electrodes.....	89
Figure 5.37 LSV measurements of flow through coated electrodes in 1 mol KOH solution.....	90
Figure 5.38 Overpotentials for flow through coated electrodes.....	91
Figure 5.39 A comparison of current density obtained for the nickel-copper coated electrodes from this study with Huner et al. [45] study	92
Figure 5.40 A comparison of overpotential obtained for the nickel-iron coated electrodes from this study with Han et al. [48]	93

Figure 5.41 Average hydrogen mass flow rate for coated NCP 3D-printed electrodes for a run time of 15 minutes	95
Figure 5.42 Average hydrogen mass flow rate for coated CPLA 3D-printed electrodes for a run time of 15 minutes	96
Figure 5.43 Average hydrogen mass flow rate for coated CPLA 3D-printed electrodes for flow through electrodes versus initial design for a run time of 15 minutes.....	97
Figure 5.44 Average hydrogen mass flow rate for Ni-Cu and Ni-Fe coated NCP 3D-printed electrodes for a run time of 15 minutes versus 30 minutes	98
Figure 5.45 Average hydrogen mass flow rate for Ni-Cu and Ni-Fe coated CPLA 3D-printed electrodes for a run time of 15 minutes versus 30 minutes	99
Figure 5.46 Average hydrogen mass flow rate for Ni-Cu coated CPLA 3D-printed flow through (D2) and solid (initial design) electrodes relation with operation time.....	100
Figure 5.47 Energy and exergy efficiencies for coated NCP 3D-printed electrodes	101
Figure 5.48 Current densities at 2.5V for coated NCP 3D-printed electrodes measured by potentiostat versus actual during hydrogen production	102
Figure 5.49 Energy and exergy efficiencies for coated CPLA 3D-printed electrodes...	103
Figure 5.50 Current densities at 2.5V for coated CPLA 3D-printed electrodes measured by potentiostat versus actual during hydrogen production	103
Figure 5.51 Energy and exergy efficiencies for coated flow through electrodes.....	104
Figure 5.52 Energy efficiencies for Ni-Cu and Ni-Fe coated CPLA 3D-printed flow through (D2) versus solid (initial design) electrodes	105

LIST OF ABBREVIATIONS AND SYMBOLS

Nomenclature

Avg	Average
E	Electrode potential (V)
F	Faraday's constant (C/mol)
I	Current (A)
J	Current density (A/cm ²)
J_o	Exchange current density (A/cm ²)
\dot{m}	Mass flow rate (kg/s)
M	Molar mass (g/mol)
N	Number of electrons
R	Resistance (Ω)
SD	Standard deviation
t	Time (s)
U	Uncertainty (%)
V	Voltage (V)
W	Coating amount (g)

Greek Letters

η	Efficiency (%)
ϕ	Potential at equilibrium (V)
ϕ_E	Potential of the electrode (V)
η_o	Overpotential
α	Transfer coefficient

Acronyms

AC	Alternating current
Cu	Copper
CuSO ₄ ·5H ₂ O	Copper sulfate
CPLA	Conductive polylactic acid
CV	Cyclic voltammetry
DC	Direct current
EIS	Electrochemical impedance spectroscopy
FDM	Fused deposition modelling
Fe	Iron
HER	Hydrogen evolution reaction
H ₃ BO ₃	Boric acid
H ₂ SO ₄	Sulfuric acid
KOH	Potassium hydroxide
LSV	Linear sweep voltammetry
Mo	Molybdenum
NaOH	Sodium hydroxide
NCP	Nickel conductive paint
Ni	Nickel
NiCl ₂ ·6H ₂ O	Nickel chloride
NiSO ₄ ·6H ₂ O	Nickel sulfate
OER	Oxygen evolution reaction
PLA	Polylactic acid

CHAPTER 1: INTRODUCTION

In Paris, at the COP 21 the United Nations climate change conference, it was agreed that urgent and stronger climate change actions are required to achieve the goals of the Paris Agreement adopted on December 12, 2015 [1]. To reach Zero-carbon emissions by 2050, everyone, including government officials, businesses, and individuals, have a role to play. There has been a rapid increase in the usage of fossil fuels. In 2022, global carbon emissions from combustion, and industrial processes grew by 0.9% (321 Mt to 36.8 Gt) alone [2]. There is an immediate need for new environmentally friendly fuels for replacing fossil fuels.

1.1 Current State of Energy and Shift Towards Renewable and Clean Energy

The usage of fossil fuels has risen since the 18th century when industrial revolution started. For decades, the share of fossil fuels in the energy sector has been 80%, and by 2030 it is only projected to decrease by 5% to a share of 75%. A rise of approximately 2.5 °C in global average temperatures is expected [3]. Although the projected outcome is better than expected a few years ago, there is still a need for drastic changes in the energy sector to avoid extreme impacts on climate conditions.

Government officials and businesses play a crucial role in the Zero-carbon emissions matrix. Officials need to implement strict policies that will help fight climate change. More investments are needed in renewable energy and clean sources-related projects to shift away from fossil fuels. Figure 1.1 shows the investments in 2021 for fossil fuels versus clean energy, and the investments that are required by 2030 for the net zero scenario. The investments for clean energy are expected to reach above 2 trillion USD by 2030, however, they would need to be above 4 trillion USD for net zero emissions [3]. Strategies to attract new investors toward clean energy projects are needed to obtain significant results.

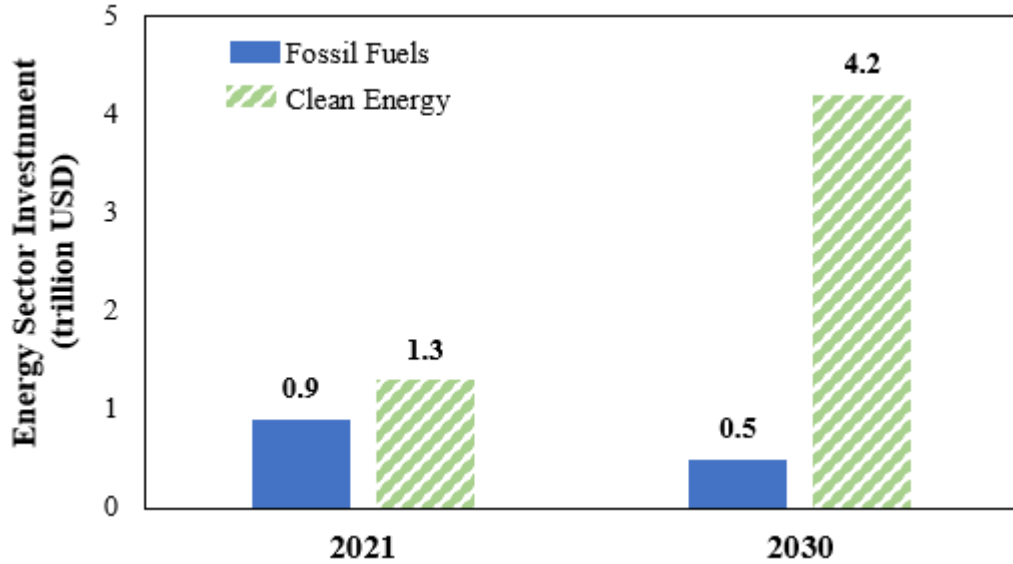


Figure 1.1 Investments in Energy Sector to Reach Net-Zero Emissions 2021 - 2030 (data from [3])

A combination of different clean energy approaches is required to meet climate change initiatives. To stay on the path to net zero carbon emissions, the development of clean energy technologies such as renewables, and electric vehicles is required. International Energy Agency provides a road map in the energy industry to reach net zero emissions by 2050 in the energy sector [4]. The majority of the reductions in CO₂ emissions by 2030 will be due to the technologies already available. More than half the reductions in carbon emissions projected by 2050 will need to be a result of new innovations, the majority of which are still in the prototype phase. There needs to be a huge decline in the usage of fossil fuels (coal, oil, gas, etc.), which means stopping sales of cars that require internal combustion engines. For the net zero scenario, there needs to be net zero emissions from electricity by 2040 on a global level. To do so, there needs to be an increase in battery storage capacities, more clean energy sources, and hydrogen production technologies. By 2045, the majority of the vehicles will be electrical, or fuel cell based [4]. Figure 1.2 shows the contribution of various technological avenues that will be needed to reduce carbon emissions by 2050. The majority of the contributions will come from advances in energy efficiency and more renewable energy projects. Electrification and hydrogen will also play a crucial role in reducing carbon emissions. The other 20% technological avenues contribution is from CO₂ removals and capture. A total of 36.9 GT in CO₂ emissions is expected from the avenues shown in Figure 1.2 [5].

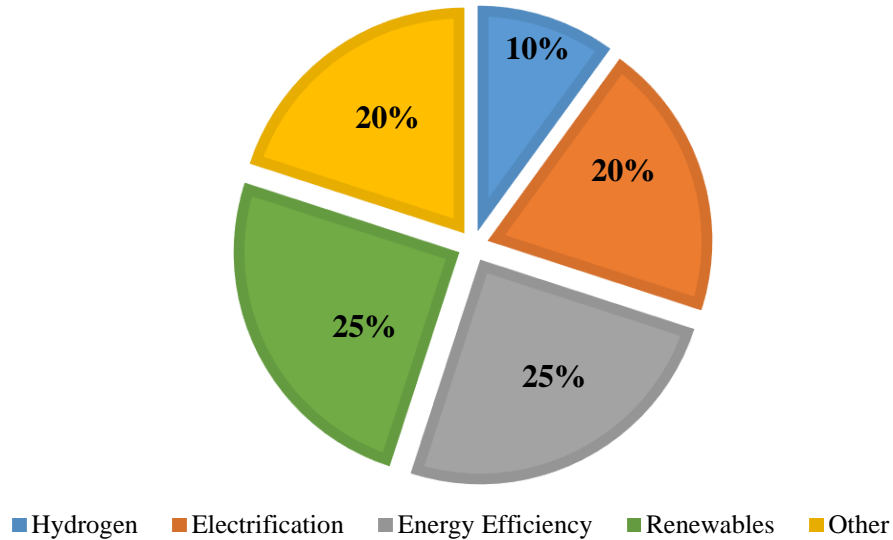


Figure 1.2 Factors for reducing emissions by 2050 (data from [5])

1.2 Significance of Hydrogen as an Energy Fuel

Recently, hydrogen has been emerging as a popular clean fuel. Hydrogen can be produced from many sources and produces zero emissions when used as a fuel. Initially, hydrogen was used as a rocket fuel, the National Aeronautics and Space Administration (NASA) started using liquid hydrogen in the 1950s [6]. Today, hydrogen has become in demand as an energy source for many applications. Many of its uses include industrial processes, power generation, and transport. Currently, hydrogen is most used in industrial processes for methanol, ammonia, steel production, and oil refining [7]. In addition, hydrogen can also be burned directly and used as a fuel source to produce electricity in power plants. Fuel cells are another application where hydrogen and oxygen atoms are combined to produce electricity which can be used to power vehicles. Alternatively, hydrogen can also be used with internal combustion engines, however, this approach results in nitrogen oxide emissions and has lower efficiency than using fuel cells [6]. Hydrogen can be critical for tackling climate goals. It has many advantages, it has the potential to store, produce and move energy [7].

1.3 Hydrogen Production Methods

Hydrogen can be produced using various sources and utilized in many industries. Hydrogen production can be categorized by different colors depending on the source used, which involves green, blue, and grey hydrogen, and various others. Figure 1.3 shows the different hydrogen production approaches and the uses of hydrogen. Grey hydrogen production is one of the most common routes used today. It is produced from coal, natural gas, or biomethane using a process called steam reforming. In this process, natural gas and hot water are combined to produce steam from which hydrogen is one of the outputs. However, carbon dioxide is also produced as one of the bioproducts, which is not captured. Blue hydrogen is produced from sources including natural gas, biomethane, and also biomass using steam reforming. It is like grey hydrogen production, except that carbon capture and storage as required to capture the carbon dioxide [8]. For green hydrogen production, electricity produced from renewable sources can be used to split water using an electrolysis. From this approach oxygen and hydrogen are produced electrochemically. The hydrogen is stored and then utilized as a clean energy fuel.

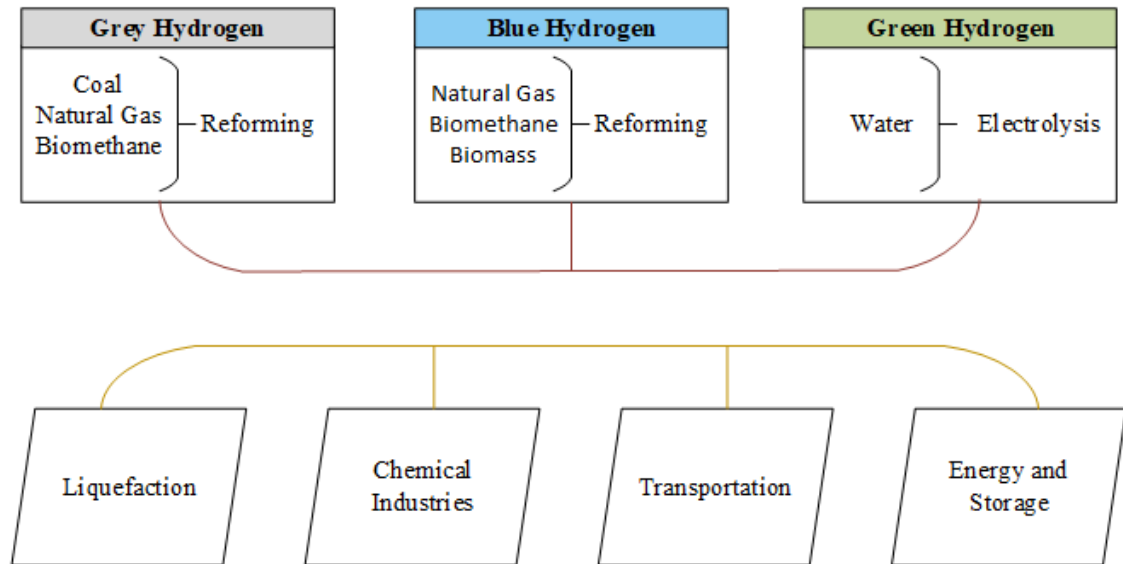


Figure 1.3 Hydrogen Production Paths (adapted from [9])

1.4 Electrolysis Types

There are many commercially available electrolyzers that can be used to produce hydrogen. The major types of electrolyzers include alkaline electrolysis, polymer electrolyte membrane (PEM) electrolysis, and solid oxide electrolysis. The main differentiation between the electrolyzers is the type of electrolyte they use. For alkaline based electrolyzers, a liquid alkaline solution of potassium hydroxide (KOH) or sodium hydroxide (NaOH) is used as the electrolyte to produce OH^- ions from the cathode to anode. PEM electrolyzers consist of a solid plastic-based membrane electrolyte which is used to promote the electrochemical reaction to produce oxygen at the anode and hydrogen at the cathode. Solid oxide electrolyzers involve a solid ceramic material that is used to conduct oxygen ions as an electrolyte. However, solid oxide electrolyzers must operate at high temperatures between 700 °C to 800 °C [10]. Alkaline electrolyzers are generally cheaper compared to the other types whereas PEM electrolyzers are more expensive and have larger capacities. In general, the reaction in water electrolysis can be categorized by oxygen evolution reaction (OER) and hydrogen evolution reaction (HER). Water is oxidized at the anode to produce oxygen for OER and reduced at the cathode to produce hydrogen. The anode of the electrolysis is generally associated with OER and the cathode with HER.

1.5 Electrolysis Materials and Manufacturing

Some of the manufacturers in the global top 20 hydrogen electrolyser manufacturers (2023) include Bloom Energy, Cummins Inc, Green Hydrogen Systems, Nel ASA, and Siemens [11]. One of the challenges surrounding the energy industry is hydrogen production and availability at large scale to meet low carbon initiatives. Alkaline electrolyzers consist of two electrodes, which is separated by a diaphragm. PEM electrolyzers have a polymeric membrane between the electrodes responsible for conducting H^+ . Regardless of the different types, and the different components involved, the manufacturing for all electrolyzers is relatively similar. Electrolyzers can be composed of multiple cells known as stacks connected in series to increase their capacity. Each cell consists of two electrodes, one of which is the anode and the other which is the cathode. A membrane or a diaphragm is added depending on the type. There are also other components involved such as bipolar

plates which provide support and circulate the flow. In addition, there are also porous layers involved which separate and allow the oxygen and hydrogen gases to flow [12]. The electrolysis itself requires some cooling devices, electricity, and water which are installed at the end. A key component in the electrolysis configuration is the electrode. Nickel is commonly used for electrodes in alkaline electrolysis. Even for some traditional electrodes, researchers have always explored the possibility of applying metallic coatings mainly nickel-based alloys, which have the potential for improving catalytic activity [13].

1.6 Additive Manufacturing and 3D Printing Technologies

3D printing is an additive manufacturing technique that has become a popular approach in recent years for fabricating a variety of objects and geometries. The technique involves using a computer to create three-dimensional (3D) parts by depositing materials layer by layer. The technology was first developed in 1986 by Charles Hull, in a process called stereolithography (SLA) [14]. Since then, the technology has come along with other technological developments including powder bed fusion, and inkjet printing, that all contribute to additive manufacturing. There are many benefits to additive manufacturing technologies. Using 3D printing technologies allows for more flexibility and freedom to create any part which is less costly to produce with this technology. In addition, the typical manufacturing process involves using molds, and complex operations to produce a specific object which are eliminated with 3D printing. Additive manufacturing can drastically save time and simplify the process. When a part is required to maintain a certain operation, parts can be produced on demand. A titanium bracket produced by Airbus using additive manufacturing is 30% lighter and does not compromise performance and durability compared to the conventionally manufactured titanium bracket [15].

1.7 Motivation

Electrolysers are an important part of green hydrogen production. Hydrogen can be produced using excess power generated from renewable energy sources. For some years, electrolysis capacity has been growing at a promising rate. Installation of prospect projects can grow the installed electrolyser capacity from 134 to 240 GW, which is twice from expected two years ago. However, still, a significant expedition in work is required to reach net zero goals. To align with current goals capacity needs to be above 700 GW [16].

Water electrolysis are a proposed technology for producing hydrogen, however, approximately only 4% of hydrogen is currently produced using this method. One of the challenges in implementing this technology is the cost of manufacturing, with electrodes being one of the most expensive components in the assembly. Newly emerging technology such as additive manufacturing can be integrated to reduce production costs and make the manufacturing process easier. 3D printing allows for rapid prototyping, once in development, individual businesses can produce electrolyzers instantly. Easing the assembly of the electrolysis will make these devices more accessible for hydrogen production and will allow more users to be able to produce hydrogen on a lower budget.

1.8 Objectives

The main objective of the thesis will be to develop and investigate 3D printing for alkaline water electrolysis for water splitting. The cathode plays a crucial part in the hydrogen evolution reaction (HER) for hydrogen production. Different strategies for 3D-printed electrodes for HER will be investigated in this thesis. The optimum goal will be to determine if the 3D printing electrode is a feasible approach for hydrogen production in terms of its electrochemical activity in alkaline media. The thesis will focus on the following key objectives of the course of the study period:

- To develop efficient and cost-effective cathodes for water alkaline electrolysis for hydrogen evolution reaction (HER).
- To investigate different coatings and methods for 3D-printed electrodes.
- To assess the performance of the coated electrodes using electrochemical measurements and analysis.
- To evaluate the performance of the coated electrodes with variations in coating deposition amounts.
- To compare the performance of different electrode designs based on geometry.
- To implement a method for testing the cathodes for hydrogen production to evaluate performance through hydrogen production rates and efficiencies.

1.9 Novelties

There were various novelties introduced in the thesis project as part of three main integrals. Firstly, new approaches for fabricating electrodes for water alkaline electrolysis are established. The main innovation is the 3D printed electrodes developed by utilizing fused deposition modelling (FDM) techniques and electrochemical coating processes. The second element part of which novelties are present, are the coatings investigated in the research. New coatings and techniques yet to be considered by other researchers for 3D printed electrodes for hydrogen evolution reaction are investigated. The final component where novelties were introduced were as part of the hydrogen production portion of the thesis. The novelties in the thesis are listed as follows:

- A new alternative method for coating 3D printed electrodes is introduced. Instead of 3D printing with conductive based PLAs, the electrodes were first 3D printed with normal non-conductive PLA. Then the electrodes were painted with conductive paint before using electrodeposition to coat the electrodes.
- Electrodes with larger surface areas and different geometries not considered by previous researchers are investigated.
- For coatings, nickel-molybdenum and nickel-iron were considered for coatings using electrodeposition, yet to be studied for coatings on 3D printed electrodes. Nickel-iron based 3D printed electrodes have been considered by other researchers using other additive manufacturing techniques such as photo-curing.
- New and alternative chemical compositions of the electrolyte baths are also considered for electrodeposition.
- A new flow-through electrode design is presented for hydrogen production. In addition, a unique setup is implanted for easy and efficient hydrogen production testing of multiple electrodes.

CHAPTER 2: LITERATURE REVIEW AND BACKGROUND

One of the first steps as part of the thesis was an extensive literature review. The literature review aimed to identify past and current processes involved in 3D printed electrodes for hydrogen evolution reaction (HER) in alkaline media for water electrolysis. There has been an increased interest in 3D printing which has been shown to reduce manufacturing costs, save time, and make parts easily accessible. These can be benefited from by utilizing 3D printing technologies for hydrogen production. Insights into conventional electrodes used for hydrogen production in alkaline electrolysis are obtained to gain a better understanding of the standard. Some researchers have done some recent work where 3D-printed electrodes for hydrogen production were printed using a conductive material such as conductive PLA. To improve the performance, researchers have looked at many materials in which the electrodes can be coated post-printing. Electrodeposition is the most common process used currently; however different modifications are required based on the coating material. The optimum goal is to determine the most feasible materials that will have good conditions for hydrogen production.

The following key insights are obtained from the in-depth literature review performed which can be considered for the thesis:

- Using conductive PLA as the 3D printing materials have shown some potential in electrochemical water splitting applications.
- Ultrasonic cleaning before coating the conductive PLA can reduce impurities in the coated electrodes.
- Combination of titanium-nickel based electrode has shown to produce low overpotential at current density benchmark of 10 mA/cm².
- Adding activators to the electrolytes have shown to increase electrolysis efficiency in comparison to the standard 6 mol KOH electrolyte.
- Reducing distances between electrodes can increase efficiency.
- Porous electrodes have shown to improve mass transport and increase hydrogen production rate.

2.1 Alkaline Water Electrolysis

Alkaline water electrolysis (AWE) technology is currently used in many applications including water splitting for hydrogen production. One of the advantages of AWEs is that they can easily be scaled for large hydrogen production facilities, however, this can increase the capital investment cost and increase energy demands [17].

The concept behind using electrolysis for hydrogen is straightforward. Direct current is applied, and water is split into oxygen and hydrogen. As a result of the electrochemical reaction, hydrogen gas is produced at the cathode and oxygen gas is produced at the anode.

The following is the reaction at the cathode:



The following is the reaction at the anode:



The total reaction is given as follows:



In comparison to other electrolysis, AWE uses a solution with 25% to 30% of a catalyst mixed with water [18]. Either potassium hydroxide (NaOH) or sodium chloride (NaCl) is used for the catalyst. In typical industrial applications, alkaline electrolysis is operated at temperatures between 30°C to 100°C. These electrolytes speed up the reaction and allow the hydrogen and oxygen ions to be transported rather than being used up in the reaction.

Hydrogen production efficiency is generally around 80% with the reactions being more effective at 0.3 A/cm² or lower current densities [18].

2.2 Traditional Electrodes for Hydrogen Evolution Reaction

The most used material for cathodes in alkaline water electrolyzers is nickel with other catalytic coatings such as platinum. Whereas the anodes require materials with good properties for oxygen evolution. Metals including nickel, copper and stainless steel coated with other oxide such as magnesium, tungsten, and ruthenium are used for the anode [19].

Additionally, alkaline electrolyzers require a liquid alkaline based solution composed of 30wt% potassium hydroxide (KOH) or sodium hydroxide (NaOH) for operation.

Tang et al.[20] looked at the fabrication of nickel and molybdenum (Ni-Mo) based electrodes for an alkaline polymer electrolyte electrolysis. The technique used involved using NiMoO₄ powder mixed with ethanol using ultrasonic bending. The powder used was reduced in hydrogen (H₂) at 500°C, which was then transformed into a uniform and robust electrode consisting of nickel (Ni) and Mo (IV) oxides. The resulting Ni-Mo electrode showed exceptional catalytic activity. A very high current density of 700 mA/cm² with an overpotential of 150 mV was obtained in a 5M KOH solution at temperature of 70°C. The researchers suggested their new fabrication method is suitable for alkaline water electrolysis and alkaline polymer electrolyte water electrolysis.

Another study conducted by Allebrod et al. [21] prepared nickel foam and gas diffusion based electrodes using cobalt and molybdenum (Co-Mo). Circular-shaped foam pieces were used for nickel foam and Inconel foam. Cobalt and molybdenum were added to the electrodes to improve the performance. Cobalt and molybdenum were added, by first using 50%wt cobalt (II) hydroxide and 50%wt SrTiO₃ powder to add the cobalt layer. Molybdenum (VI) oxide with 30%wt and 70%wt SrTiO₃ powder was used to add the molybdenum layer. The alkaline electrolysis cells prepared were tested at a pressure of 40 bar and temperatures of 150°C, 200°C, and 250°C. The electrodes were tested at a temperature of 250°C. The current densities obtained at this temperature were 1.1 A/cm² and 2.3 A/cm² at the voltages of 1.5 V and 1.75 V, respectively. The efficiency of the cells at high temperatures was improved.

One study conducted by Nikolic et al. [22] looked at improving the efficiency of alkaline hydrogen electrolyzers using cobalt (Co) and tungsten (W) based activators. The processes involved adding situ activating compounds directly into the electrolyte. With this addition, the efficiency was increased by reducing the energy requirements during the process by 15%. The study showed that the efficiency at higher temperatures and higher current densities was increased.

Colli et al. [23] studied the catalytic activity of different electrodes based on electrocatalysts used along with traditional electrodes. In their study, the activities of

nickel, iron, cobalt, and chromium were explored. The study found that good stability and performance were obtained for Raney nickel (nickel-aluminum alloy) as the cathode and 316 stainless steel as the anode.

Rosalbino et al. [24] studied the electrocatalytic behavior of cobalt and nickel with rare earth elements (Co-Ni-R) for hydrogen evolution reaction. The rare elements investigated in combination with Co-Ni were cerium (Ce), yttrium (Y), praseodymium (Pr), and erbium (Er). The study experimentally found that high efficiencies were obtained for electrodes where $Co_{57}Ni_{3x_5}Ce_8$ and $Co_{57.5}Ni_{3x_6}Y_{6.5}$ were used.

Esmaili et al. [25] considered using molybdenum-oxo catalysts for cathodes in a low temperature electrolysis. The system was modeled to analyze and evaluate the energy efficiency and the exergy efficiency of the system considered. The study shows that the molybdenum-oxo catalyst only worked under neutral environmental conditions. The study found that at higher current densities, the system was inefficient and lead to damages in the electrolysis.

2.3 Additive Manufacturing Technologies and Materials for 3D-Printed Electrodes

Additive manufacturing (AM) is referred to methods that involve layer by layer printing using polymer-based materials. AM technologies have been found to be more feasible due to their lower production costs and easy operation. The types of materials used in AM technologies can consist of photopolymers, thermoplastics solid, thermoplastic powders, injecting powders and metal powders [26]. Part of AM technologies is a fused deposition modeling (FDM) technique which enables 3D printing with polymer-based materials and includes the use of polylactic-acid (PLA). This involves using extrusion to 3D-print geometries. The materials for this technique are prepared using multiple liquefaction processes and directly depositing the material using a nozzle. This technique is beneficial for rapid prototyping and is the most widely used in the industry currently. Some researchers have considered 3D-printing the electrodes using conductive PLA, which are usually graphene-based. In alkaline media, only a few studies have been considered using conductive PLA to 3D print electrodes for hydrogen production due to complications that

can arise with using the material. Some studies have also considered using other additive manufacturing for exploring the possibilities with 3D-printed electrodes.

A study conducted by Browne et al. [27] suggested that 3D-printed electrodes have inherent impurities which make them catalysis for water splitting. The study states that the commercially available graphene or PLA filaments traditionally used for 3D printing electrodes themselves contain impurities. The study showed that thermal treatment after the 3D-printed properties had better hydrogen evolution reaction and oxidation properties.

Ambrosi et al. [28] conducted a study to review 3D materials for use in electrolytic and electrochemical systems. The study points out that in electrochemical systems one of the key components is the electrode, for which a conductive material is required. The overall efficiency of the 3D-printed device would also be dependent on the electrode and therefore plays a crucial role. Currently, available 3D printing conductive materials are very limited and mainly carbon-based. This makes them challenging to work with when it comes to their catalytic performance. Based on the studies evaluation, only a combination of traditional manufacturing technologies and additive manufacturing can be combined to obtain optimal solutions. Future work is needed to develop technologies and processes solely based on 3D printing technologies for large scale.

Other additive manufacturing technologies have also been considered for electrochemical energy applications. Other common techniques used by researchers have involved direct laser metal deposition (DLMD) and photo-curing. DLMD is a laser additive manufacturing (LAM) technology which uses laser beams to perform laser-based bed fusion or direct metal deposition. This technique is still in development, but some researchers have studied this approach for various metal depositions for applications that require high accuracy and precision. Photo-curing 3D printing is another technique that is used for high precision applications. There are various photo-curing techniques which exist and include, DLP, SLA and LCD to name a few. In general, photo-curing involves using photosensitive liquid resin which is cured using a light source [29]. Some researchers have also considered photo-curing techniques for 3D printing electrodes for electrolysis-based applications.

2.4 Electrodeposition Fundamentals and Process

Researchers have looked at potential electrocatalysts and coatings for 3D printing in electrolysis for hydrogen production. The literature review identified that electroplating is the most common technique used for coating 3D-printed electrodes with conductive PLA. It is an electrodeposition process in which an electrical current is applied to deposit metal ions to opposite charges electrodes [30]. Traditionally, electrodeposition is performed in an aqueous bath. There are many techniques used to perform electrodeposition. In addition, the thermodynamic and kinematic aspects are required to understand the electrodeposition process.

2.4.1 Electrodeposition Techniques

Researchers have looked at various techniques for electroplating materials using electrodeposition. The general technique consists of a circuit using an anode, cathode, and electrolytic bath. Electric current is applied which moves from the anode to the cathode, both submerged in a conductive electrolytic bath. The cathode is the working electrode on which electrodeposition is performed. The anode acts as the counter electrode used to complete the circuit, the anode can be either inert or soluble [31]. If the anode is soluble, it will dissolve as current is applied and parts of the anode will be coated on the coated. In this case, the same material as the coating material is used for the anode.

Some researchers have performed electrodeposition using a three-electrode system. Rathousky et al. [32] used a three-electrode setup in a study to prepare a TiO_2 film. Platinum was used as the counter electrode and Ag/AgCl as the reference electrode. The bath was composed of a TiCl_3 solution. The materials used to prepare the electrolytic bath depend on the cathode plating material. Past work and research have been done to determine the different materials and compositions of the substance for different electrolytic baths.

2.4.2 Electrochemistry of Metals

Researchers have looked at electrodeposition of various metals and alloys. Some background is required to understand how different metals react electrochemically. For

electrodeposition, an electrolyte with chemical reagents is required. The electrochemical behavior of certain metals can be described as follows.

Nickel

One commonly used metal in electrodes is Nickel. For centuries, Nickel alloys have been used for many materials such as coins, and household items because they have high oxidation resistance while having very good strength. For the electroplating of nickel, electrolytes containing Ni^{2+} ions are required. Nickel ions can be obtained from the following electrolytes, nickel sulfate ($\text{NiSO}_4 \cdot 6\text{H}_2\text{O}$), nickel sulfamate ($\text{Ni}(\text{NH}_2\text{SO}_3)_2 \cdot 4\text{H}_2\text{O}$), and nickel chloride ($\text{NiCl}_2 \cdot 6\text{H}_2\text{O}$). Additionally, another main component of the electrolyte is boric acid (H_3BO_3) [33]. Other species in the electrolyte are required to increase the bath's conductivity, reduce the surface tension, and are used as buffers to maintain the pH between 3.5 and 4.5 [33].

The reaction for nickel dissolved in an acidic solution would be given as:



The reaction for nickel in an alkaline solution is given as:



Aluminum

Aluminum is a very abundant metal with very good corrosion and wear-resistant properties. However, aluminum is very reactive in chemical form, and new aluminum surfaces can form a protective oxide layer at room temperature. Aluminum comes from a group of metals that have negative electrode potentials. This makes aluminum electrochemically impossible for electrodeposition in the conventional aqueous bath [34]. Electroplating aluminum is still possible using a more specialized process using molten salts or special organic solvents.

Due to the high negative potential in alkaline media, the electrodeposition of aluminum is not possible in aqueous solutions because of the hydrogen evolution reactions that occurs at the cathode.

The reduction potential for aluminum in acidic or neutral solutions can be defined as:



In alkaline media the reaction is given as:



The electrode potential for the hydrogen evolution at the cathode in acidic or neutral solutions is given as:



In alkaline media, the cathodic hydrogen evolution is given as:



Some researchers have looked at aluminum electrodeposition using acidic electrolyte baths and ethers-based solutions. Still, many researchers have found aluminum electroplating very difficult. Zhang et al. [35] looked at aluminum electrodeposition using aluminum chloride in a diglyme solution.

Copper

Copper along with silver, and gold belong to the 1B group from the periodic table. Copper has excellent electrical conductivity and has a good resistance to corrosion. It is often used with other metals as an alloy. Electrodeposition of copper can be performed for plating purposes; it is often carried out in acidic baths. Vincenzo and Cavallotti [36] carried out electrodeposition in a copper sulfide (CuSO_4) and sulfuric acid (H_2SO_4) bath at a pH of 3. The standard 0.25 mol CuSO_4 and 1.5 mol H_2SO_4 bath was used, and 0.8 mol CuSO_4 for the pH 8 electrolyte bath.

Iron

After aluminum, iron is the second most common metal used. In its pure form, iron is a soft silvery-white metal, and has very less use in its pure form. Iron is often used along with other transition metals to improve its strength. Iron has many uses, widely used in medical and for power source applications. For example, iron batteries in aqueous potassium hydroxide (KOH) electrolyte have shown some promising results [37]. Traditional iron electroplating can be deposited using a sulfate-chloride electrolyte bath.

Developed way back iron was deposited using a composition 250 g/L of iron sulfate, 42 g/L of iron chloride, and 20 g/L of ammonium chloride [38]. The recommended pH for iron electrodeposition is 3.5 to 5.5 between room temperature to room temperature to 32°C with a current density of 0.32 A/cm² to 0.053 A/cm². Further, iron can also be co-deposited with nickel using a nickel sulfate and iron sulfate bath. In a study by Philip et al. [39] 0.08 mol/L nickel sulfate, 0.02 mol/ L iron sulfate, and 0.1 mol/L boric acid was used to co-deposit nickel and iron. The pH was adjusted with sulfuric acid to between 3.0 to 3.5.

Molybdenum

Molybdenum is a silvery grey metal found in many minerals. It has good electrical conductivity, resistance to corrosion, and stability which makes it excellent for alkaline electrolysis. Molybdenum has commonly been used as a material for electrodes in electrolysis and can be combined with other metals as an alloy to improve its strength. Molybdenum can be electroplated using electrodeposition. Cao et al. [40] conducted a study where they used an ammonium molybdate solution to electroplate molybdenum. The study found that the addition of ammonium played a critical role in molybdenum electrodeposition and resulted in higher current efficiencies. In the study 0.25 mol/L sodium molybdate, and 0 to 1 mol/L ammonium sulfate was investigated. The study looked at two pH levels, 5 and 9. Better results were obtained for molybdenum coatings applied at a pH of 9.

2.4.3 Electrodeposition Thermodynamics

In the electrodeposition process, electrochemical reductions occur from the electrolyte with at least two components.



where n is the number of electrons and \bar{i} and \bar{i} are the current densities of the reduction and oxidation reaction.

The equilibrium potential of the half-cell reaction can be calculated as [41]:

$$E_{\text{eq}} = E^{\circ} + \frac{2.3RT}{nF} \log \frac{b_o}{b_R} \quad (2.11)$$

where T is the absolute temperature in Kelvin (K), R is the universal gas constant (8.314 J/mol·K), and F is the Faraday constant (96485 C/mol¹). The components, b_o , and b_R are the effective concentrations of the oxidation species, and the reduction species in mol/L. E° is the electrode potential at standard state conditions of 1 atm, 25°C and at 1 mol ion concentration.

When the electrode is submerged in the electrolyte, there becomes a difference between the potential of the electrode and the electrolyte [42]. This is known as the absolute potential of the electrode and is given as follows:

$$E_{\text{abs}} = \phi^s - \phi^l \quad (2.12)$$

2.4.4 Electrodeposition Kinetics

The kinetics of electrodeposition can be used to compute the reaction rates and different parameters associated. Two common parameters used to evaluate reactions are overpotential, and current density. Through the electrodeposition circuit, the current travels from the anode to the cathode. If the electrons being removed are faster than the rate of reaction, due to the shortage of electrons at the anode a change occurs in the equilibrium state. The same can occur at the cathode when there are more electrons than the amount of cathode takes. At this state, the electrodes become polarized. The overpotential of the electrode is given as [43]:

$$\eta_o = \phi_E - \phi \quad (2.13)$$

where ϕ_E is the potential of the electrode (E) and ϕ is potential at equilibrium (E_{eq}).

The most common expression which relates overpotential and current density is the Butler-Volmer expression [43]. The expression is generally solved using computation techniques. The Bulter-Vomer expression is given as follows:

$$\frac{i}{i_0} = e^{\alpha_a \left(\frac{F\eta_{o,S}}{RT} \right)} - e^{-\alpha_c \left(\frac{F\eta_{o,S}}{RT} \right)} \quad (2.14)$$

The amount of metal deposited during the electrodeposition can be calculated using Faraday's law given by equation (2.15):

$$W = \frac{ItM}{nF} \quad (2.15)$$

where W is the amount of coating deposited on the electrode in grams (g), I is the current in amps (A), t is the deposition time in seconds (s), M is the molar mass of the metal plated in grams per mol (g/mol), n is the number of electrons involved and F is the Faraday's constant.

2.5 Electrocatalysts and Coatings

This section looks at some past work that has been done in coating 3D-printed electrode materials for HER in alkaline media. There has been significantly more research for electrodes in other non-alkaline electrolyzers (PEM) 3D printed-based electrodes. To get a better understanding of the coating materials, a literature review was also performed for coatings performed for 3D-printed electrodes in other types of electrolyzers and for conventional plating performed on metallic materials.

2.5.1 3D-printed based Electrodes and Coating Methods in Alkaline Media

Very few researchers have looked at electrocatalysts and metal coatings for 3D-printed based electrodes in hydrogen evolution reactions. Huner et al. [44] conducted a study where they tested a nickel and platinum (Ni-Pt) coating on 3D-printed electrodes printed with graphene-based PLA. The 3D-printed and coated electrodes were investigated for hydrogen evolution reactions. In their study, the electrodes were first designed in SolidWorks with a length of 50 mm, width of 5 mm, and thickness of 1 mm. The electrodes were printed using the Ultimaker +2 used the Black Magic 3D conductive graphene PLA filament. The 3D-printed electrodes need to be conductive to perform the electrodeposition process. The 3D-printed electrodes were initially cleaned using an ethanol ultrasonic bath for 5 min, then washed with deionized water, and dried with nitrogen gas. For electrodeposition, the 3D-printed electrode is used as the working electrode (cathode) and a platinum sheet of 0.1 mm thickness is used as the counter electrode. In the process, the nickel coating was first deposited, then the nickel-coated electrodes were placed in the

platinum-based electrolyte bath to deposit platinum. The electrolyte bath for nickel electroplating consisted of nickel sulfate ($\text{NiSO}_4 \cdot 6\text{H}_2\text{O}$), nickel chloride ($\text{NiCl}_2 \cdot 6\text{H}_2\text{O}$), and boric acid (H_3BO_3). The composition of the platinum bath consisted of potassium hexachloroplatinate (K_2PtCl_6) and potassium chloride (KCl). The nickel-coated electrodes were used to deposit three different compositions of the platinum on the chemical composition named as NiPt1, NiPt2, and NiPt3. 0.176 g/L K_2PtCl_6 for NiPt1, 0.352 g/L K_2PtCl_6 for NiPt2, and 0.528 g/L K_2PtCl_6 for NiPt3 with 7.46 g/L KCl was used for the different electroplating baths. The researchers found that the NiPt3-coated electrode had three times higher current density than the NiPt1-coated electrode, which increased from 61.46 mA/cm^2 to 121.67 mA/cm^2 .

In another study by Huner et al. [45] a similar experimental procedure was used to electrodeposit compositions of Nickel and Copper (Ni-Cu) on 3D-printed electrodes. The 3D-printed electrodes with the same dimensions as the previous study were prepared using conductive PLA filament. The electrodes printed using the Ultimaker +2 printer were printed using a nozzle temperature of 220°C and a bed temperature of 60°C. The electrode layer thickness used was 0.1 mm, using a 0.4 mm nozzle diameter at a 50 mm/s nozzle speed. Like the previous study, the nickel coating was deposited first, then separate baths were used to co-deposit copper using three different compositions of the electrolyte bath. The copper electrolyte bath used was composed of 125 g/L copper sulfate ($\text{CuSO}_4 \cdot 5\text{H}_2\text{O}$) and 10 mL sulfuric acid (H_2SO_4), with all baths prepared in 100 mL of high-purity deionized water. In the study, the 3D-printed electrodes were coated with three different copper compositions. Sample NixCux consisted of a 10 mL Cu solution, NixCu2x with 20 ml, and NixCu3x with 30 ml. The results showed that compared to the uncoated electrodes the current density was increased by 78.1% at a voltage of -1.6 V and increased by 79.56% for a voltage of -1.4 V. Further, the resistance of the coated electrodes was also decreased by 99.5%. The NixCu3x showed to have the lowest resistance and higher current densities than the other samples. The NixCu3x had a current density of 40.12 mA/cm^2 at -1.4 V, and a resistance of 0.951 $\text{k}\Omega$ at a frequency range of 1 kHz to 10 kHz.

Huner et al. [46] performed another study for conductive PLA filament graphene-based 3D-printed electrodes. In the study, they applied an electrochemical process to electroplate

nickel and cobalt (NiCo). They used a very similar process as to their previous 3D-printed electrode studies. The same electrode dimensions and the 3D printing process were used. The nickel and cobalt deposited on the 3D-printed electrodes were deposited together in the same electrolyte bath using electrodeposition. The electrolyte bath was composed of nickel sulfate ($\text{NiSO}_4 \cdot 6\text{H}_2\text{O}$), boric acid (H_3BO_3), and cobalt sulfate heptahydrate ($\text{CoSO}_4 \cdot 7\text{H}_2\text{O}$). A 50 ml volume was used for the bath, with a constant concentration of 0.5 mol/L for boric acid for all baths prepared in the study. Three different electrode samples were prepared and tested based on different Ni and Co compositions. The electrodes were prepared at molar ratios of Ni:Co, 1:4, 1:1, and 4:1. The 1:1 (M) ratio was composed of 0.5 mol/L for both Ni and Co. The Ni:Co, 1:4 sample showed to have more stability and higher kinetic activity for hydrogen evolution reaction. At a voltage of 1.1 V the current density was found to be 30.22 mA/cm².

A similar approach was used in a study by Bui et al. [47] who also 3D-printed electrodes for alkaline membraneless electrolysis. The electrodes were first 3D-printed then nickel (Ni) was deposited using electrodeposition. The performance of the electrodes was evaluated for water electrolysis in a solution of 1 mol sodium hydroxide (NaOH). They tested the electrodes for oxygen evolution reaction and hydrogen evolution reaction. A simple membraneless electrolyser was developed by combining the electrodes in a monolithic lid for collecting the oxygen and hydrogen gases. The efficiency of the electrodes was found to be low, however it showed to be beneficial to explore new designs.

In a study conducted by Han et al. [48] a photo-curing method for 3D printing nickel-based electrodes for HER in alkaline media was studied. The method they used can directly manufacture nickel-based electrodes. In the study, a titanium, iron, and cobalt with nickel (Ti-Ni, Fe-Ni, Co-Ni) electrodes were 3D-printed. The technique used involved producing a ceramic paste from nickel oxide (NiO) powders, titanium carbide (TiC), and stabilized zirconia (YSZ) was created. For the iron depositions, ferric oxide (Fe_2O_3) was used and cobalt powder was used for cobalt depositions. Using the prepared paste the electrodes were directly printed using direct photo-curing 3D printing. The study found that Ti-Ni based electrode had a low overpotential of 34 mV at a current density of 10 mA/cm².

In an interesting study, Sullivan et al. [49] evaluated the performance of nickel and molybdenum (Ni-Mo) electrocatalysts for a flow-through electrode configurations. The 3D-printed electrode Sullivan et al. developed can be seen in Figure 2.1. The technique they used for 3D printing the Ni-Mo based electrode involved ink formation using so-gelation and carbonization. Using the developed ink, the Ni-Mo electrodes were 3D printed. Low overpotential were obtained for high quantity Mo electrodes. An average of 45 mV overpotential was obtained at current density of 10 mA/cm². In addition, the study found that the flow through configuration really helped to remove bubbles in comparison to traditional configurations.

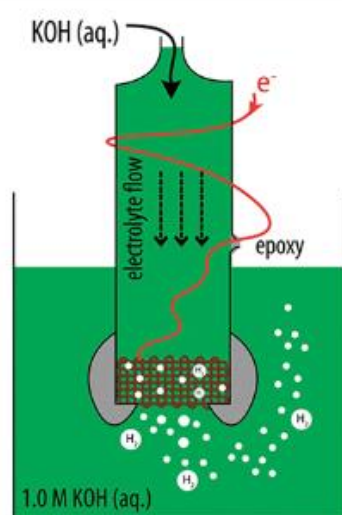


Figure 2.1 3D-printed flow through electrode studied by Sullivan et al. [49]

Zhou et al. [50] showed that 3D-printed electrodes using anodized steel is a promising technology for large scale electrolysis applications. The process used for fabrication consisted of direct energy deposition (DED) technique used to prepare the martensitic steel. For the alkaline electrolyser the steel cathode and anode were tested in a 1 mol potassium hydroxide solution (KOH). The study found that for cell voltages of 3.03 V and 3.18 V only a current density of 500 mA/cm² and 570 mA/cm² was required.

2.5.2 3D-Printed based Electrodes in Non-Alkaline Electrolysis Applications

Some researchers have studied coatings on 3D printed electrodes for other non-alkaline based electrolysers such as proton exchange membrane (PEM) electrolysis. The different

techniques considered by researchers are for improving the efficiency and the chemical properties of the 3D-printed electrodes.

Chisholm et al. [51] prepared 3D-printed electrodes for a PEM electrolysis for water splitting. The electrodes were printed using polypropylene (PP) using the 3dTouch 3D printer. The 3D-printed plates were ultrasonically cleaned in a detergent solution before coating. First, the 3D-printed plates were coated with silver paint, air dried for 1 hour and then cured at 120°C for 20 minutes. Then the electrodes were further plated in silver using a 3-electrode system using platinum as the counter electrode and silver wire as the reference electrode to plate silver. They then prepared a PEM electrolysis for water splitting to demonstrate that it possible to develop an electrochemical device using 3D printing technology.

A study conducted by Wright et al. [52] used 3D-printing techniques and electroless processes to produce electrodes for electrolysis. Titanium was deposited using electroless and the electrode was considered for a CO electrolysis. The results showed that the performance of the 3D-printed electrode was similar to the conventional machined electrode. The cells performed at a current density of up to 250 mA/cm² and were stable for a 24-hour operation.

Yang et al. [53] developed a fully printed PEM electrolyser using 3D printing. They used a laser powder bed printer from which they were able to directly 3D-print conductive cells. In the study, different cathodes were evaluated. The 3D-printed electrolyser was highly efficient, they found that at a current density of 2 A/cm² and an operating temperature of 80°C, an efficiency of 86.68% was obtained.

2.5.3 Coatings on Industrially Prepared Metallic Electrodes

Metallic coatings have traditionally been used in many applications such as jewelry plating or for coating other metals for improving strength and corrosion. Many researchers have looked at different processes for electroplating various industrially prepared materials which can better help understand the coating processes for 3D-printed materials.

Prochniak and Grden [54] applied a nickel plating using an electrolytic bath prepared using Ni powder in HNO_3 . With their approach, no additional treatment was required, and the coating was directly applied after dilution with water. The coatings were deposited from both an acidic solution and an alkaline bath. The results showed that coating applied from the acidic solution bath more stable in terms of both physical and chemical aspects.

One study conducted by Ying [55] looked the deposition of copper and nickel (Ni-Cu) using a citrate solution. In the study, the electrodeposition was performed for both a stationary and rotating electrode. The electrolytic bath was prepared using copper sulfate and nickel sulfate in a citrate bath using sodium citrate. The copper and nickel alloy deposition occurred at an electrode potential of -1 V to -1.2 V.

In a study conducted by Wang et al. [56] electrodeposition was used to apply nickel-iron coatings on stainless steel electrodes for oxygen evolution reactions in alkaline media. The Ni-Fe deposited electrodes showed to have an overpotential of 514 mV at a 10 mA/cm^2 current density.

Gutierrez et al. [57] used electrodeposition to prepare nickel coated 304 stainless steel electrodes. They analyzed the effect on hydrogen production due to variations in potential, time and the amount of nickel which was deposited. The study found that the highest hydrogen production concentration was obtained for the nickel coating with the electrode with the most nickel deposited.

2.6 Electrolysis Stack Configurations and Design

Typically, alkaline electrolyzers can have two stalk configurations. Figure 2.2 shows the conventional assembly (with a gap assembly), and the more commonly used configuration today is the zero-gap assembly.

The conventional assembly has a gap between the electrodes and the separator, where the separator is used to separate the oxygen and hydrogen gasses. The zero-gap assembly has the electrodes pressed into the separators. The zero-gap assembly minimizes ohmic losses that occur due to the electrolyte. Various researchers have studied different modifications to the stalk configurations discussed and their effect on electrolyser performance.

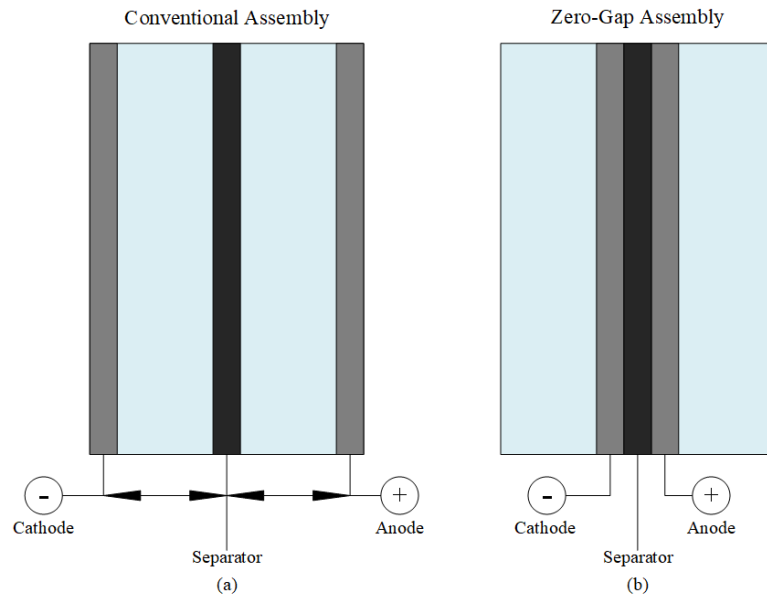


Figure 2.2 Alkaline electrolysis stack configurations (a) conventional assembly (b) zero-gap assembly (adapted from [58])

A study conducted by Silva et al. [59] developed and studied the performance of two stack configurations for alkaline electrolysis. The two configurations considered in the study were mono-polar and bi-polar which were compared through 3D modeling and comparison. The main difference between the two configurations was the distance between the electrodes. The results of the study showed that the performance of the electrolysis could be improved by reducing the distance in between the electrodes. The bi-polar stack had a better performance in terms of flow rater, power, and efficiency.

Rajaei and Haverkort [60] conducted a study to evaluate the performance of a compact electrochemical stack design arranged in a checkboard configuration. The study was performed using 3D-printed metal prototyping for alkaline water electrolysis. The results showed that the design took up at least 1.5 to 2 times less volume compared to conventional ‘sandwich’ type configurations.

In a study conducted by Yang et al. [61] non-conductive bipolar plates were printed for a PEM water electrolysis. The study proposes the use of low-cost PLA for the plates which is mainly used to distribute water and gas products. The results showed that the hydrogen

production rated for the PLA bipolar plates was six times higher than the traditionally graphite based bipolar plates.

One study conducted by Sandeep et al. [62] looked at an experimental investigation of porous electrodes on an engineering scale for hydrogen production. The electrodes were used with a zero-gap bipolar electrolysis configuration to minimize the cell voltage required. To minimize production cost, the current density needs to be maximized at the minimum voltage required. The study considered the losses that occurred due to ohmic and activation overpotential at various temperatures. The efficiency was found to be higher for higher operating temperatures.

2.7 Gaps in the literature

There has only been a handful of previous studies using a 3D printer and electrodeposition techniques for 3D printing electrodes for hydrogen evolution reactions. These studies have only considered a few metallic coatings with much smaller electrode surface areas. The metal coating applied, and coating technique used plays a crucial role on the durability and the performance of the electrodes. No studies have been reported on using nickel-molybdenum and nickel-iron for coatings on 3D printed electrodes using electrodeposition. Other researchers have looked at using other additive manufacturing techniques such as photo-curing for 3D printing nickel-iron based electrodes. However, these approaches are much more complex and would be more costly to implement than the electrodeposition technique considered. So far, earlier studies have only considered rectangle electrode geometries with smaller surface areas. Round electrodes, which are more commonly used in commercial applications provide a more even distribution of current. Current plays a crucial role in electrolysis, in general electrodes with larger surface area can sustain higher currents. Further, most studies on 3D printed electrodes have only considered electrochemical behaviour. Studies that have implemented the 3D printed electrodes into an electrolysis assembly have only reported to the efficiency to be low. However, actual numerical results related to hydrogen yields and efficiencies are not reported.

CHAPTER 3: EXPERIMENTAL APPARATUS AND PROCEDURE

The experimental setup and procedure used to prepare and test the electrodes are presented in this section. Novel methods and materials are introduced for the preparation of new and cheaper electrodes of alkaline water electrolysis for hydrogen production. A detailed outline of the materials and approaches used to prepare the electrodes is explained. In addition, the equipment and apparatus used to test the fabricated electrodes are also discussed.

3.1 Electrode Preparation and Coating Techniques

Additive manufacturing is investigated to prepare the electrodes for cost reduction and feasibility. Although there are many benefits to 3D-printing technologies, there are still some limitations that prevent this technology from being implemented in manufacturing of water electrolysis. 3D-printing is limited in terms of materials that are compatible with most printers in fused deposition modelling (FDM) techniques. These materials are generally polymer-based, mostly non-conductive. The materials that are conductive have very poor performance in electrical applications. This raises a concern; good conductive electrodes are crucial for hydrogen production and play a key role in efficiency. Metallic coatings are a common practice used to prepare traditional electrodes. This methodology is yet to be explored extensively for 3D-printed electrodes prepared using FDM techniques. 3D-printed electrodes can be coated to significantly improve their performance while reducing costs. This section introduces the techniques used to apply metallic coatings on 3D-printed electrodes using two different polylactic acid (PLA) materials. In addition, the design of the 3D-printed electrodes is also discussed.

3.1.1 Electrode Design

The electrodes are designed in SolidWorks and then converted into STL files to be 3D printed. The electrodes designed are selected to be circular. Round electrodes can provide a more even distribution of current compared to other geometries. Current plays a crucial role in electrolysis, an even current distribution is important to obtain adequate electrolysis efficiencies. Figure 3.1 illustrates the electrodes designed for the study. Figure 3.1(a) shows the initial design that is selected and is a representation of a typical electrode used in

traditional electrolysis configurations. Figure 3.2 (b) shows the slightly modified design to accommodate the electrodeposition process. Traditional electrodes can vary by size depending on the capacity. Generally, the capacity of the electrolysis is increased by increasing the number of stacks rather than the size of the electrode itself. The size of the electrodes for experimental purposes was selected as a 50 mm diameter electrode with a thickness of 1 mm, with an area of 19.63 cm^2 (1963 mm^2). The modified electrode has the same dimensions, except a 10 mm long with 1 mm thickness strip was added at the end of the electrode to extend the surface for electrodeposition.

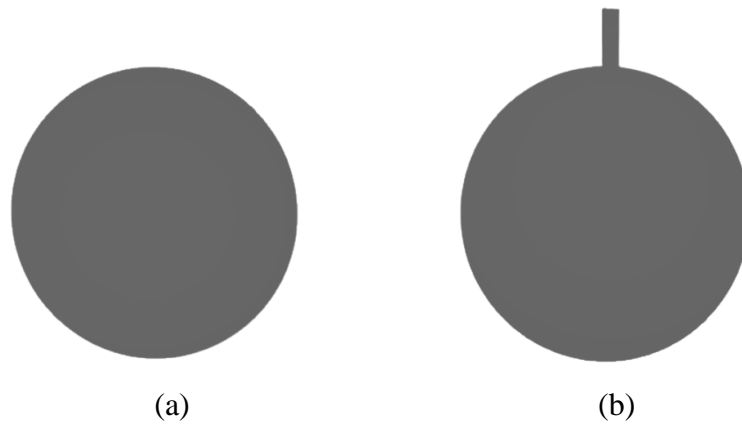


Figure 3.1 Electrode designs (a) initial design (b) slightly modified design

One of the advantages of additive manufacturing is that there is much more flexibility in the design. Complex shapes can easily be 3D-printed without the need for expensive and intricate manufacturing processes. Further to the thesis project, a flow-through electrode design (named D2 for reference) as illustrated in Figure 3.2 is considered.

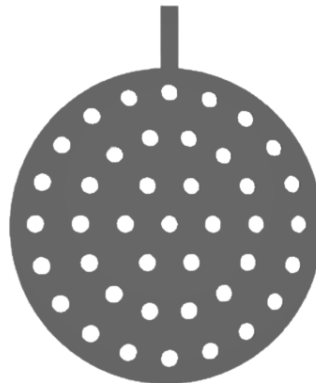


Figure 3.2 Flow through electrode design (D2)

Using a porous electrode can help increase the rate at which the gases evacuate the electrolysis, especially for zero-gap configurations where the electrodes are closely packed. Traditional electrodes are generally solid, plate-like (Figure 3.1 (a)) in geometry due to the increased costs and complex procedures that would require modifying the electrode design. With 3D printing technologies, more advanced and involved designs can easily be investigated for water electrolysis for hydrogen production.

3.1.2 3D Printing and Coating Procedure Plan

A common approach is selected to prepare all electrodes investigated. The electrodes are first 3D-printed and then coated with various coatings. The Anycubic Kobra illustrated in Figure 3.3 is used to 3D print all electrodes for the experiments.



Figure 3.3 Anycubic Kobra 3D printer used for 3D printing

Many coating approaches are traditionally used for metal plating. Electrodeposition is selected as the best approach for coating. This technique has proven to result in good and consistent coatings. In addition, it is low cost, resulting in strong bonds and adhesion between layers. Electrodeposition can be performed for a variety of metallic coatings and is easy to operate if the conditions of the electrolyte bath are controlled. Figure 3.4 shows the schematic of the setup implemented for the electrodeposition of metallic coatings on

the 3D-printed electrodes. The electrodeposition setup consists of an electrolyte bath composed of the metal ions of the metal being deposited. The bath generally consists of various chemicals, some which act as a source of metal ions and others improve the conductivity of the bath and help control the pH. A two-electrode system is introduced where a platinum or carbon anode is used as the counter electrode and the cathode is the part being coated. A hot plate can be used to heat up the electrolyte if needed, and a thermometer is used to monitor the temperature of the bath.

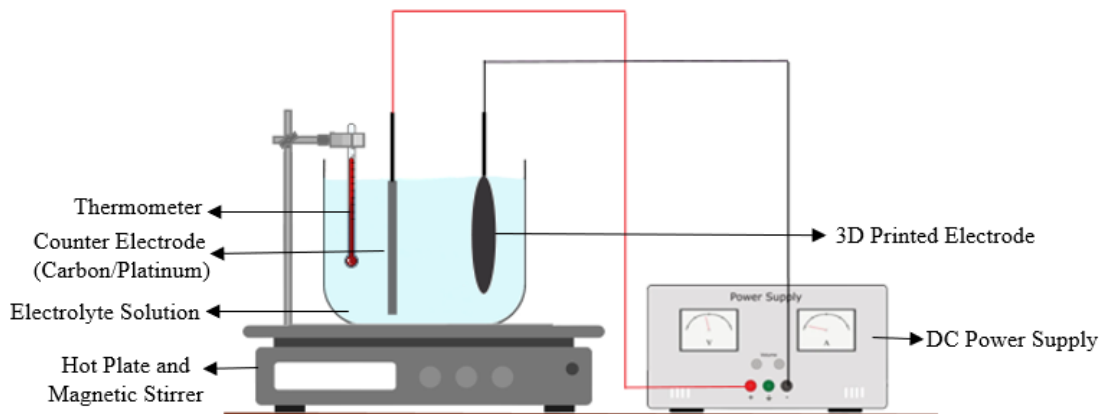


Figure 3.4 Schematic diagram for electrodeposition

One limitation of electrodeposition is that the material being coated (the cathode) must be conductive. Direct current is applied and flows through the electrolyte solution from the anode to the cathode. Due to the electric field formed, the ions from the electrolyte solution move toward the cathode and are reduced by producing a metallic layer of the metal being deposited.

3.1.3 Electrodeposition on Conductive Paint 3D-printed Electrodes

Traditional materials used to 3D print parts are generally non-conductive and therefore electrodeposition can not be performed using these materials. Various types of conductive metallic paints are available in the market and can be applied to non-conductive parts made of plastic before electrodeposition. This is the first approach investigated for the thesis project to prepare the 3D-printed electrodes. Conductive-based paints have lower conductivity and high resistance, hence metal deposition can significantly improve the

electrode's performance compared to just using the conductive paint. Additionally, electrodeposition is required to improve the life of the electrodes. Under direct contact with water over time the paint layer becomes weak, then starts to crack and break apart from the material. Nickel is selected as one of the main metals to be electrodeposited and investigated in the thesis. Therefore, nickel-based conductive paint are chosen to plate the 3D-printed electrodes before the electrodeposition of nickel. Two different types of nickel conductive paints (NCP) are investigated to determine the best one for electrodeposition. The MG Chemicals 841AR Nickel Conductive paint, which is an acrylic solution-based paint is used. The second type of paint used is the MG Chemicals 841WB Nickel Conductive paint, which is a water solution-based paint. Figure 3.5 shows the 3D-printed electrode which are printed with non-conductive PLA and then coated with the nickel conductive paint.

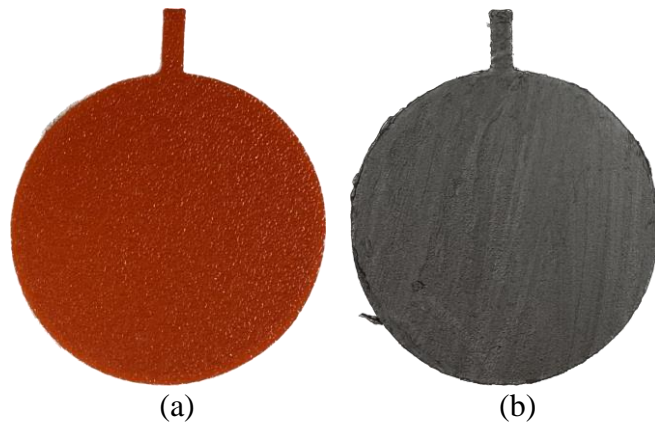


Figure 3.5 3D-printed with non-conductive PLA and NCP coated (a) 3D-printed PLA electrode (b) after nickel conductive painted electrode

3.1.4 Electrodeposition on Conductive PLA 3D-printed Electrodes

There are some available conductive materials such as conductive PLA which have been modified to generate electrical current. In addition, they are compatible with the standard (FDM) modeling 3D printers used with the traditional PLA's. Using conductive PLA, eliminates the need to first coat the electrodes with conductive paint and they can directly be used with electrodeposition. Figure 3.6 shows the electrodes printed with the conductive PLA for the original design and the flow-through design. The Proto-Pasta Conductive PLA is used to print the electrodes for experiments where nickel conductive paint is not used.

The electrodes are printed with the Anycubic Kobra 3D printer with a bed temperature of 50°C and a hot end temperature of 230°C.

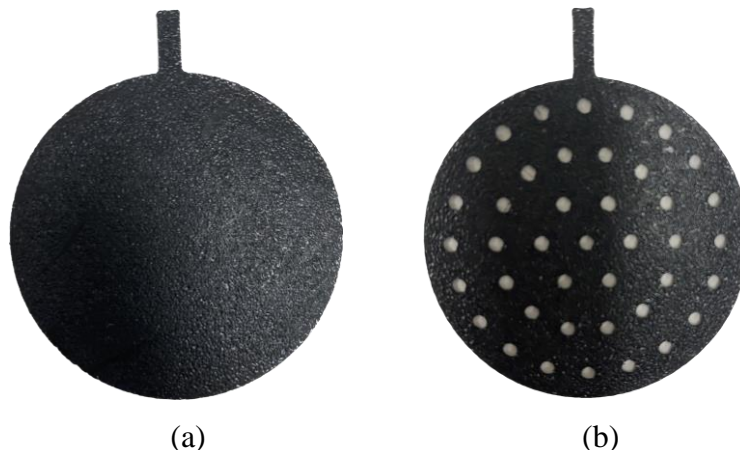


Figure 3.6 Conductive PLA 3D-printed Electrodes (a) original design electrode (b) D2 electrode









For coating the conductive PLA 3D-printed electrodes, cleaning the electrodes with an ultrasonic cleaner can help reduce impurities. Initially, the electrodes are cleaned in a distilled water bath in an ultrasonic cleaner. For comparison, they are also cleaned in a reagent alcohol-based solution mixed in water. The alcohol-based cleaning bath tends to work better than the water bath for reducing impurities in the coated electrodes.

3.2 System Components and Materials

The key system components used to implement the experimental setup are shown in Table 3.1 with their corresponding specifications. The components in the electrodeposition setup are the power supply which is used to supply direct current between the anode (counter electrode) and the cathode (3D-printed electrode). The magnetic stirrer is used to stir the electrolyte bath at a constant bath during the duration of the electrodeposition. Once the electrodes are coated, they are also tested for hydrogen potential. The hydrogen cell prepared for electrolysis testing uses a 316 stainless steel (60mm by 50mm) anode. The prepared electrodes are tested as a cathode for hydrogen evolution reaction. The MQ-8 hydrogen gas sensor with Audrino is used to measure the rate of hydrogen.

Table 3.1 Equipment and component specifications





Name	Reference	Image	Specifications
Wanptek DC Power Supply DPS3010 U	[63]		Output Voltage: 0-30 V Output Current: 0-10 A Temperature: 0-40 °C Resolution: 00.01 V, 0.002 A
Fisher Scientific Isotemp Hotplate with Magnetic Stirrer	[64]		Stirring Range: 60- 1200 rpm Temperature Range: 5 to 400 °C Plate Capacity: 35 lbs
Mettler Toledo, AB204-S/FACT Scale	[65]		Range: Up to 220 g Temperature Sensitivity (10 to 30 °C): 2.5 ppm/°C Time (setting): 4s
Fisher Scientific FS20D Ultrasonic Cleaner	[66]		Cleaner power: 80 W Heater Power: 63 W (up to 60°C) Operating frequency: 40 kHz
Mastercraft Digital Temperature Reader	[67]		Response Time: 500 ms Temperature Readability Range: -30 to 480 °C Temperature (Operating): 0 to 50°C
Vernier Conductivity Probe	[68]		High Range: 0 to 20,000uS/cm Response Time: 98% in 5s Temperature Range: 0 to 80 °C
Mastercraft 052-0060-2 Multimeter	[69]		Resistance Readability: 200, 2k, 20k, 200k, 2000kΩ Temperature: 0 to 50 °C Readings accurate after 1 year of calibration at 18 to 28 °C

Corning 450 pH/ion meter	[70]		pH Operating Range: pH – 1.999 to 19.999 Resolution: 0.001/0.01/0.1 pH Temperature: –30 to 130 °C Recommended Calibration: Every 24 hours
Wagner Furno Heat Gun	[71]		Two Speeds: Low, High Heating Setting (Drying Paint): Low
Platinized Titanium Mesh electrode	-		Dimensions (mesh): 50 mm (length) by 25 mm (width)
ProtoPasta Conductive PLA	[72]		Strength: Fair (less layer adhesion) Stiffness: Low, semi-flexible Heat Resistance: below 50 °C Density: 1.15 g/cm ³ (1500 kg/m ³)
MG Chemicals 841AR Nickel Conductive paint	[73]		Volume Resistivity: 0.0040Ωcm Temperature: -40 to 120 °C
MG Chemicals 841WB Nickel Conductive paint	[74]		Volume Resistivity: 0.027Ωcm Temperature: -40 to 120 °C
MQ-8 Hydrogen Gas Sensor with Arduino	[75]		Hydrogen Detecting Range: 100-10000 ppm Circuit Voltage: 5V±0.1 Heating Voltage: 5V±0.1 Standard Conditions: 20°C±2°C temp, 65%±5% humidity
316 Stainless Steel Anode	-		Dimensions: 60mm (length) x 50mm (width)

There are various chemicals used for different coating electrolyte baths during electrodeposition. Some chemicals such as potassium hydroxide (KOH), is used during testing. All chemicals used in the thesis are listed in Table 3.2.

Table 3.2 Chemicals and specifications

Chemical Name	Image	Supplier/ Product #	Description/Usage
Nickel Sulfate (NiSO ₄ ·6H ₂ O)		Sigma Aldrich/ 10101-97-0	Nickel sulfate is used for nickel ions in nickel coating electrolyte bath.
Nickel Chloride (NiCl ₂ ·6H ₂ O)		Sigma Aldrich/ 7791-20-0	Nickel chloride is used to increase conductivity in nickel coating electrolyte bath.
Boric Acid (H ₃ BO ₃)		Sigma Aldrich/ 10043-35-3	Boric acid for electrodeposition coating baths, mainly for nickel to control pH.
Copper Sulfate (CuSO ₄ ·5H ₂ O)		Sigma Aldrich/ 7758-99-8	Copper sulfate is used for source of copper ions in copper electrolyte bath.
Iron Sulfate (FeSO ₄)		Sigma Aldrich/ 13463-43-9	Iron sulfate is used for source of iron ions in iron electrolyte bath.
Iron Chloride (FeCl ₃ ·6H ₂ O)		Sigma Aldrich/ 10025-77-1	Iron chloride is used additionally in iron electrolyte bath to improve conductivity.
Ammonium Molybdate (NH ₄) ₆ Mo ₇ O ₂₄ · 4H ₂ O		Sigma Aldrich/ 12054-85-2	Ammonium molybdate is used a source of molybdenum ions in molybdenum electrolyte.

Sodium Hydroxide (NaOH)		Fisher Scientific	Sodium hydroxide is used in the electrolyte baths to increase the pH of the baths
Sulfuric Acid (H ₂ SO ₄)		Sigma Aldrich/ 7664-93-9	Sulfuric acid is used in the electrolyte baths to improve conductivity and to decrease the pH so the solution is more acidic
Potassium Hydroxide (KOH)		Fisher Scientific	Potassium hydroxide is used to test the electrodes in an alkaline-based solution
Regent Alcohol		Lab Chem	Ethanol and methanol based solution is used to clean the 3D-printed electrodes in the ultrasonic cleaner before coating

3.3 Experimental Setup and Procedure

This section introduces the experimental apparatus implanted to coat the electrodes and test the developed electrodes. There are various steps taken to prepare the electrodes first before they could be tested. There are two main types of tests conducted in the thesis. The first set of tests involved setting up an electrochemistry setup to measure the current and impedance response of the electrodes. The second set of tests involved measuring the electrodes for hydrogen potential using a prepared electrolysis testing cell. Figure 3.7 introduces the key steps that are taken to fabricate the electrodes and then test them using the different approaches.

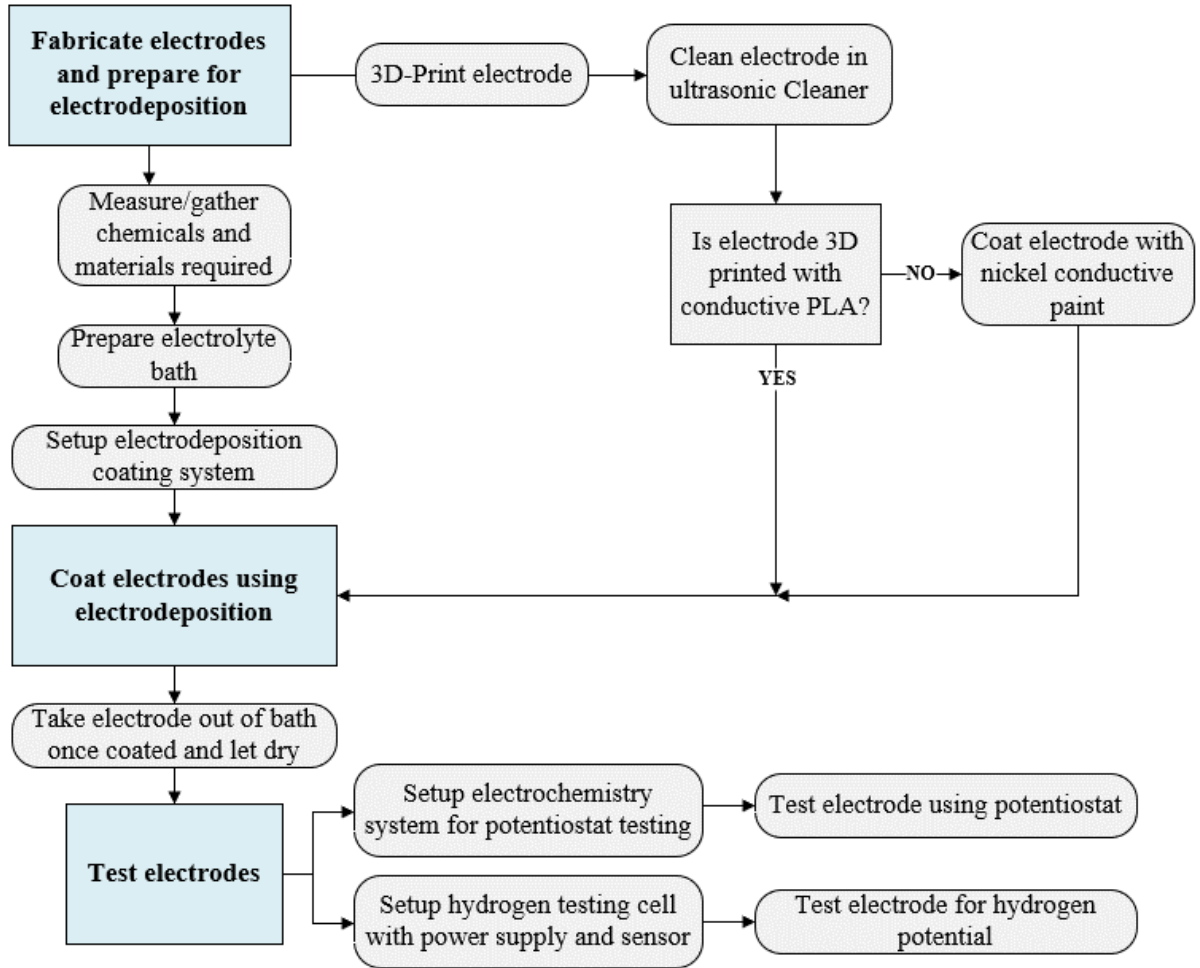


Figure 3.7 Experimental procedure flow chart

3.3.1 Electrodeposition and Electrode Coating Apparatus

An experimental setup to coat the electrodes is implemented based on the electrodeposition schematic diagram. A procedure for testing the electrochemical properties of the coated electrodes is also developed. Figure 3.8 shows a picture of the experimental setup that is established. The electroplating system consists of a platinum-coated titanium mesh electrode which is used as the counter electrode (anode). The part being coated (3D-printed electrode) is used as the cathode. Direct current is applied to the anode (+) and the cathode (-) which breaks down ions from the electrolyte bath and plates the part being coated (cathode). The composition of the electrolyte bath varies depending on the metal which is being coated.

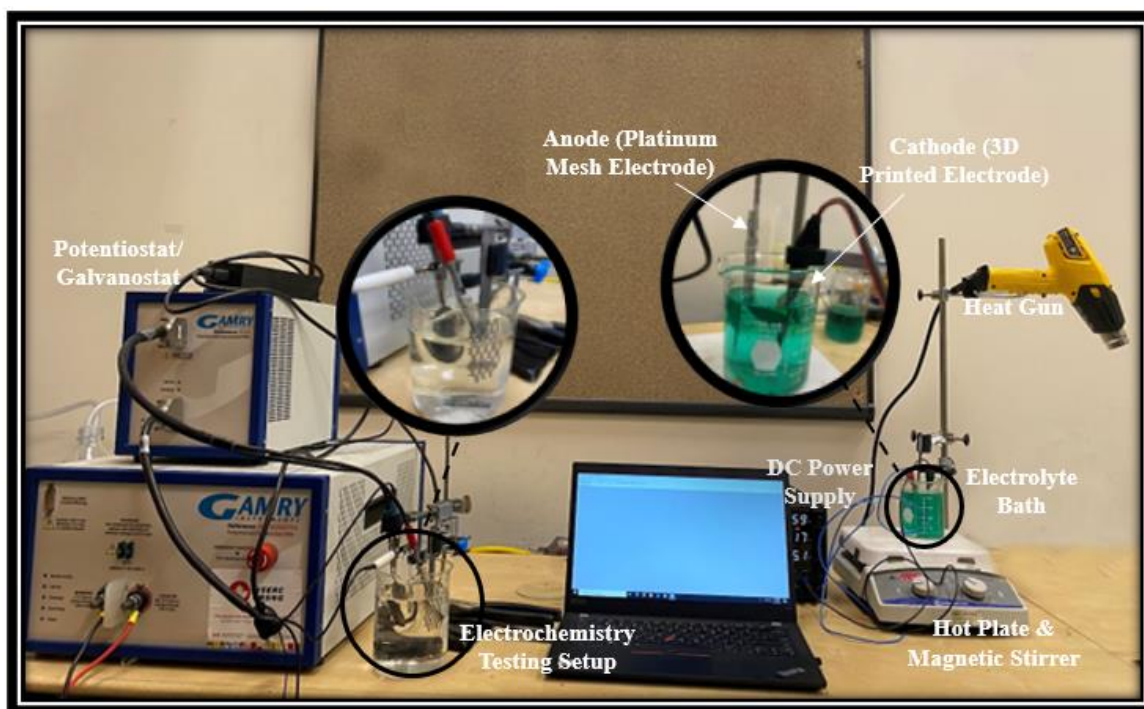


Figure 3.8 Experimental setup for electrodeposition and electrochemistry testing

The hot plate can be used to adjust the temperature of the electrolyte bath if needed. For the experiments performed this is not used and all coatings are applied at room temperature ($\sim 24\text{ }^{\circ}\text{C}$). The magnetic stirrer is used to magnetically stir the electrolyte while electrodeposition takes place. All coating baths are magnetically stirred at 200 rpm. In addition, the magnetic stirrer is also used to stir the chemicals in distilled water to prepare the electrolyte. For the electrodes which are first coated with nickel conductive paint, some of them are thermally dried using the heat gun after applying the paint. All electrodes are first cleaned with an ultrasonic cleaner using a reagent alcohol solution composed of ethanol and methanol with distilled water.

3.3.2 Electrode Testing Apparatus for Hydrogen Potential

For hydrogen testing, a setup is implemented to test the electrodes using a cell to imitate the conditions of a water electrolysis. Figure 3.9 shows the hydrogen testing apparatus used to test the prepared electrodes for hydrogen evolution reaction. A 316 stainless steel electrode is used for the anode. The coated 3D-printed electrodes are used as the cathode.

The hydrogen produced is collected and measured using the MQ-8 hydrogen gas sensor connected to Arduino.

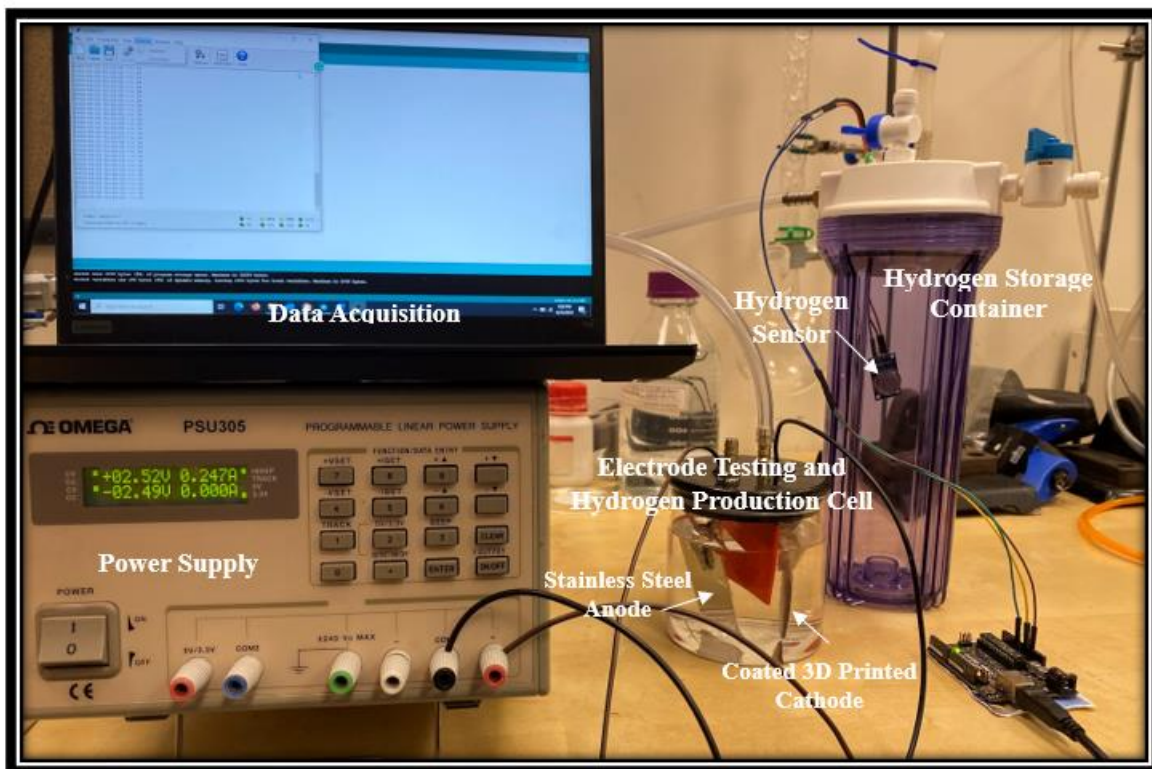


Figure 3.9 Electrolysis cathodic testing and hydrogen measurement apparatus

The hydrogen concentration measurements are recorded using Arduino connected to the sensor. A pipe connecting from the cathode testing cell is connected to the hydrogen collecting cylinder. The cathode and the anode are supplied with current for different durations of time at a voltage of 2.5 V. The hydrogen produced is measured at the end of the different testing time intervals. Although the measurements are recorded instantaneously, accurate measurements could only be recorded at end of each testing time due to the sensitivity of the sensor. The 3D-printed and coated electrodes are tested in a 1 mol KOH in 500 ml water solution as the electrolyte.

3.3.3 Electrolyte Bath Compositions

There are four main metal coatings that are investigated for electrodeposition on the 3D-printed electrodes. Nickel is one of the metals electroplated among the four metals.

Other metals include copper, iron, and molybdenum, which are coated on top of the nickel coating to determine their performance as an alloy. Further, iron and molybdenum are also co-deposited together to improve the adhesive and corrosive properties of the metals. For the conductive PLA 3D-printed electrodes, Copper is also coated without plating with nickel first of investigated the strength and performance of copper on its own. The compositions of the chemicals used to prepare the electrodes varies depending on the metal being coated. In addition, different compositions are considered for different methods to investigate if there is a significant difference. All electrolyte baths are prepared in 200 ml of distilled water. This section discusses the compositions of different chemicals used based on recommendations from the literature, as well as the modified versions which are investigated. The prepared baths with the initial concentration are reused for other coatings of the same metal. It is a common practice to use electrolyte baths in metal coatings if parameters such as pH level, temperature, and conductivity of the bath are controlled. The baths after each coating are closely monitored for pH, conductivity, and temperature. The baths are cooled before using them for a new coating, and additional chemicals are added from time to time to increase the conductivity. The pH of all baths is adjusted with sulfuric acid (for too-basic solutions) and sodium hydroxide (for too-acidic solutions) until the desired pH is reached. Electrolyte baths are changed from time to time when needed.

3.3.3.1 Nickel Electrolyte Bath

For nickel electroplating generally nickel sulfate ($\text{NiSO}_4 \cdot 6\text{H}_2\text{O}$), nickel chloride ($\text{NiCl}_2 \cdot 6\text{H}_2\text{O}$), and boric acid (H_3BO_3) are used in combination for nickel electrodeposition. Nickel sulfate serves as a source of ions for electrodeposition, whereas nickel chloride is supposed to help dissolve nickel chloride (in the case of a nickel electrode). In addition, nickel chloride can improve the conductivity of the bath and result in harder nickel deposits. Boric acid is used as a buffer to increase conductivity and prevent the formation of hydroxides which can cause inefficient and poor plating. Huner et al. [45] used an electrolyte bath for nickel deposition on 3D-printed electrodes with the following compositions 132 g/mL nickel sulfate, 0.05 g/mL nickel chloride, and 0.0125 g/mL boric acid. They prepared the bath with 100 ml of deionized water. This composition used by them was modified to accommodate a 200 ml electrolyte bath. Further, reduced

compositions from the recommended are also considered to see if there are any significant differences.

The actual electrolyte bath used for nickel electrodeposition slightly differs for different approaches. For the nickel conductive painted (NCP) coated 3D-printed electrodes, the initial composition used for baths is half of the used by Huner et al. [45] which will be referred to as X in the thesis for simplicity. Composition X is composed of 13.2g of nickel sulfate, 2.5g of nickel chloride, and 1.25g of boric acid in 200 ml of distilled water. The composition of chemicals used based on Huner et al. studies is double of composition X and will be referred to as Y. Bath with composition Y is composed of 26.4g nickel sulfate, 5g nickel chloride, 2.5g boric acid in 200 ml.

For the electrodeposition of all conductive PLA 3D-printed electrode coatings, the same composition as Y is used (26.4g nickel sulfate, 5g nickel chloride, 2.5g boric acid). The composition of bath X is successful; however, bath Y is easier to coat the electrodes. One big difference is the conductivity of the bath which is less for X since it is composed of half of less chemical compositions as compared to Y. The conductivity of bath Y is measured as 4082 $\mu\text{S}/\text{cm}$ as compared to 3060 $\mu\text{S}/\text{cm}$ for X. The electrodes are electroplated between a pH of 3.5 and 4.5. For conductive PLA 3D-printed electrodes, it becomes more crucial to control and adjust the pH. After a few coatings, the pH of the nickel bath significantly fluctuates and becomes more acidic (approx. 0.9 – 1 pH). In this condition, it takes longer for the nickel ions to deposit on the electrode surface, and at times the reaction does not occur at all.

The possibility of using a nickel electrolyte bath without nickel chloride is also explored for the conductive PLA 3D-printed electrodes. The bath works very well with an addition of sulfuric acid which works as a substitute for nickel chloride and increases the rate of the reaction to deposit the nickel ions on the electrode surface. Very less amounts of sulfuric acid are required, 0.1 ml to 0.5 ml is added to the bath depending on the pH.

3.3.3.2 Copper Electrolyte Bath

For a copper electrodeposition bath copper sulfate ($\text{CuSO}_4 \cdot 5\text{H}_2\text{O}$) can be used as a source of copper ions. Generally, sulfuric acid is used along with copper sulfate to increase the

conductivity of the bath and adjust the pH. Huner et al. [45] uses a composition of 125 g/L copper sulfate and 10 ml sulfuric in 100 ml deionized water to electroplate copper on the 3D-printed electrodes first coated with nickel. A similar composition to their study is used to coat the electrodes with copper. The solution used is prepared in 200 ml distilled water. The composition is kept the same for all coatings. The bath consists of 25g copper sulfate with approximately 0.1 to 0.5 ml sulfuric acid with a pH of 2.5 to 3. The amount of sulfuric acid is significantly reduced from the amount used by Huner et al. [45]. This is done after measuring the pH of the solution using 5 ml sulfuric acid in a 200 ml solution which is measured as 0.5 pH and is way too acidic. All coatings are applied at a room temperature of 24 °C. Studies have found that the conductivity of the copper electrolyte bath decreases as temperature increases. In fact, several studies have looked at copper electrodeposition at freezing temperature for improving conductivity of the bath. The measured conductivity at room temperature is 4094 $\mu\text{S}/\text{cm}$, Figure 3.10 illustrates that the measured conductivity of bath is decreased as the temperature of bath increases.

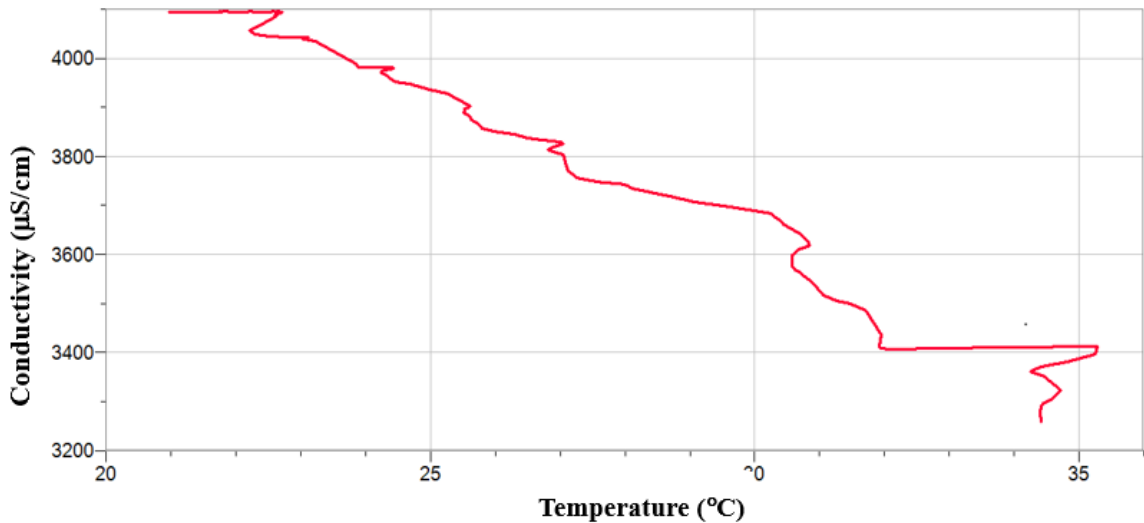


Figure 3.10 Conductivity of the copper electrolyte bath with increase in bath temperature

3.3.3.3 Iron and Nickel Iron Co-deposition Electrolyte Bath

An iron electrolyte bath with the composition of 33.3g of iron sulfate, 8.4g of iron chloride, and 2.67g of ammonium chloride in 200 ml of distilled water is prepared for electrodeposition of iron. The electrodes are first coated with nickel and then iron is plated.

The conductivity of the bath is measured as 4092 $\mu\text{S}/\text{cm}$ and the pH was as 3.5. Electroplating of iron alone resulted in rust formation after a day. To improve corrosive properties, nickel and iron are also co-deposited with and without the initial nickel coating. The composition of the electrolyte bath used is 13.2g of nickel sulfate, 1.11g of iron sulfate, and 1.23g of boric acid. The nickel-iron plating on the conductive surface PLA resulted in an inconsistent surface and some rust after taking it out of the bath. Co-deposition of nickel and iron is found successful when nickel is coated first on the conductive PLA 3D-printed electrode. This is directly due to the increase in nickel which improves the strength of the alloy and is more corrosion resistant.

3.3.3.4 Molybdenum Electrolyte Bath




Based on the literature, use of ammonium in molybdenum electrodeposition showed promising results. Cao et al. [40] used sodium molybdate with the addition of ammonium sulfate as the source of ammonium ions. A similar approach is taken for molybdenum electrodeposition except ammonium molybdate is used with the addition of sodium hydroxide to adjust the pH of the bath to 7. This electrolyte bath is used for nickel conductive painted (NCP) 3D-printed electrodes. For the electrolyte bath for conductive PLA 3D-printed electrodes, the pH is 5 and there was no addition of sodium hydroxide. All molybdenum coated are coated after the electrodes are plated with nickel first. Molybdenum is also co-deposited with nickel for comparison. The addition of sodium hydroxide is found to be necessary. The electrolyte without the use of sodium hydroxide resulted in a non-adhesive coating for the conductive 3D-printed electrodes. This was directly due to increased hydroxide layers formed which resulted in a portion of the molybdenum coating coming apart once current was applied during testing.

3.3.4 Electrochemical Testing

A major part of the thesis consists of electrochemical testing. Table 3.1 shows the components used in electrochemical testing. The Gamry reference 3000 potentiostat/galvanostat is used to conduct electrochemistry testing. Part of the setup, an Ag/AgCl electrode is used as a reference electrode placed in between the counter and the working electrode. A 25 mm by 50 mm platinum-coated titanium mesh is used as the

counter electrode. For the working electrode, the coated electrodes are used. The electrochemistry testing setup was tested in 400 ml of distilled water first, then in a 1 mol KOH solution in 400 ml prepared in distilled water. The electrochemistry system setup along with the Gamry Reference 3000 potentiostat is shown in Figure 3.8.

Table 3.3 Electrochemistry testing setup components

Component	Image	Description
Gamry Reference 3000 Potentiostat/ Galvanostat		Used for electrochemistry analysis. Is used to perform cyclic voltammetry, linear sweep voltammetry, and electrochemical impedance spectroscopy analysis.
Ag/AgCl Reference Electrode		Reference electrode used in electrochemical testing setup.
Platinized Titanium Mesh electrode		Counter electrode for electrochemical testing. Dimensions: 50 mm (length) by 25mm (width).

There are various steps involved in collecting electrochemical measurements. The Gamry potentiostat has to be set up with the software to run the experiments. To record the measurements Gamry Instrument Framework software is used. The potentiostat and galvanostat is first calibrated in the software for DC and AC measurements before testing. Figure 3.11 illustrates the Universal Dummy Cell (UDC) which is used as part of the Gamry to calibrate the potentiostat. The corresponding colours are colour coded on UDC and are also shown.

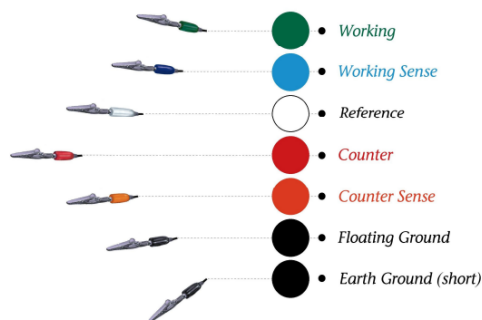


Figure 3.11 Gamry calibration configuration and Universal Dummy Cell [76]

The cables with their corresponding colour are connected to the corresponding component in the electrochemistry setup. The working sense is first connected with the working cable before connecting it to the working electrode (3D-printed coated electrode). There are three main analysis that the Gamry Reference 3000 is used to perform in Gamry Framework. Cyclic voltammetry, linear sweep voltammetry, and electrochemical impedance spectroscopy analysis are performed, and the corresponding measurements are recorded.

3.4 Experimental Uncertainty and Error Analysis

Error analysis is performed to be able to effectively evaluate the experiments and the results obtained. It is important to assess the uncertainties associated with the experimental components used to take measurements. Errors in the experiment can directly impact the results if not assessed. Table 3.4 shows the different errors associated with the different experimental components used. The errors are obtained for each corresponding component from the manual provided by the manufacturer. The experimental uncertainties can be associated with systematic errors and random errors. Systematic errors are those that are caused by the equipment itself. These are generally provided by the manufacturer. For this study, the systematic errors are provided in Table 3.4 for the components used in the experiments.

Table 3.4 Experimental components and equipment errors

Component	Parameter	Error/Accuracy
Wanptek DC Power Supply DPS3010 U	Input Voltage	± 10%
	Accuracy	0.5% + 3 digits
Mettler Toledo AB204-S	Mass	± 0.2 mg
Fisher Scientific Stirring Hotplate	Stirring Speed	± 2.0%
	Heating	± 10.0°C
Mastercraft Temperature Reader	Temperature (between 0 – 100 °C)	± 2.0%
Vernier Conductivity Probe	Conductivity (high range)	± 2% Custom Calibration ± 4% Custom Calibration
Corning 450 pH/ion meter	pH	±0.001
Adrino hydrogen sensor	Under standard detecting conditions	≥5% (only approximated trend is reflected by the sensor)
Mastercraft 052-0060-2 Multimeter	Resistance (Range)	200Ω: ±1.2%+5 2kΩ, 20kΩ, 200kΩ: ±1.0%+5 2000kΩ: ±1.5%+5
Gamry Reference 3000 Potentiostat/ Galvanostat	Applied potential	≤ 0.1% ± mV offset
	Current	< 0.2%

Random errors are categorized as those that resulted in the actual experiments. There are many factors that can contribute to random errors. These could include human error or other factors that can cause fluctuations in the data gathered. Random errors can only be determined using measured data. To eliminate and evaluate random errors, the experiments and the measurements taken are repeated three times. The uncertainty related to the different measured parameters can be calculated by equation 4.23:

$$U = \sqrt{(R^2 + S^2)} \quad (3.1)$$

where U is the experimental error (%), R is the random error (%), and S is the systematic error (%).

The random errors can be calculated by equation 3.2:

$$R = \frac{SD}{AVG} \times 10 \quad (3.2)$$

where R is the error (%) due to random errors, SD is the standard deviation, and Avg is the average of the measurements recorded.

The uncertainty of the measured parameters is evaluated using this approach. Table 3.5 shows the experimental uncertainties calculated based on systematic and random errors. To calculate the random error, three different measurements are taken for each parameter.

Table 3.5 Experimental uncertainties for measured parameters

Component	Measured Parameter	Reference Measurement			Systematic Error (%)	Random Error (%)	Uncertainty (%)
		1	2	3			
Mastercraft Temperature Reader	Temperature (°C)	24	25	24	2	2.37	3.10
Vernier Conductivity Probe	Conductivity (μS/cm)	4098	4092	4088	4	0.12	4.00
HQ-8 hydrogen sensor	Concentration (ppm)	529	579	587	5	5.56	7.48
Mastercraft 052-0060-2 Multimeter	Resistance (Ω)	1.4	1.3	1.4	1.2	4.22	4.39
Gamry Reference 3000 Potentiostat/ Galvanostat	Current Density (mA/cm ²)	53.62	56.41	54.52	0.3	2.58	2.60

The key measurement parameters used to evaluate the performance of the coated 3D-printed electrodes are the current density, and the concentration of the hydrogen. The uncertainty for the hydrogen concentration is very high (7.48%). The % uncertainty in the measurement is due to the sensor itself. This error can drastically increase if the measurements are taken outside of the standard conditions specified for measurements. In addition, the concentration of oxygen can also have an impact. To minimize the uncertainty error, the hydrogen measurements are taken three times, and the average of the three is used to evaluate the results.

CHAPTER 4: MODELLING AND ANALYSIS

This chapter of the thesis presents the various analyses performed. Part to the different coatings considered, electrochemical analysis is performed. The various electrochemical models used are also discussed and evaluated. Further, an analysis for the actual coatings deposited on the electrodes is performed. This considers the amount of coatings applied at the specific current and electrodeposition duration. This analysis considers the measured resistance of the different electrodes and evaluates the applied voltage which is required at the desired current. In addition, analysis related to prepared cathodes for hydrogen production is introduced. Thermodynamic analysis is performed, as well as the analysis used to evaluate the energy and exergy efficiencies is presented. Lastly, this section covers the error analysis related to different measurement components. The uncertainties of the measured parameters are analyzed.

4.1 Electrochemistry Analysis

Thermodynamic and kinetic analysis is performed as part of electrochemistry analysis. Thermodynamics analysis is introduced in this section to evaluate the reactions of the coating metals which occur part of electrodeposition. Kinetic analysis is presented to better understand the activities of the coated electrodes.

4.1.1 Thermodynamic Analysis

There are four main metallic coatings that are investigated at a time using electrodeposition. These consisted of nickel, copper, nickel-iron, and molybdenum. Further to the study, iron is also deposited on nickel-coated electrode, and copper directly on conductive PLA, and possibility of co-deposition of nickel-molybdenum is also explored.

Nickel sulfate is used as the source of ions in the electrolyte bath for nickel electrodeposition. The half-reaction of the nickel deposition at the cathode is given as:



The dissolution of the nickel sulfate can be given as:



For copper electrodeposition, copper sulfate is used as the source for the copper ions, and the half-reaction is given as:



The dissolution of the copper sulfate can be given as:



Iron is deposited using iron sulfate as the source of ions and nickel-iron is co-deposited using nickel sulfate and iron sulfate. The half-reaction for the deposition of iron can be given as:



The dissolution of the iron sulfate can be given as:



For nickel and iron co-deposition, the half reactions occur simultaneously and the Ni^{2+} and the Fe^{2+} are deposited at the same time as NiFe.

Ammonium molybdate is use as the source of molybdenum ions for molybdenum electrodeposition. The half reaction is given as follows:



The dissolution of ammonium molybdate can be given as:



4.1.2 Kinetic Analysis

Kinetic analysis is required to better understand the electrochemical activity of the prepared electrodes. Current density and overpotential are important parameters which can provide more insights into the behaviour of the electrodes. Overpotential is the difference in potential (voltage) that is required for an electrochemical reaction to occur versus the potential at equilibrium. The overpotential can be defined by equation 4.9 where η is the overpotential (in volts) of the electrode. ϕ_E is the potential of the electrode and ϕ is potential at equilibrium.

$$\eta_o = \phi_E - \phi \quad (4.9)$$

The overpotential can be categorized by two main components, the activation overpotential, and the ohmic overpotential. The activation overpotential is related to the energy that is required by the electrode to continue the reaction. Several factors such as catalysts, electrode material, and the area of the electrode can impact the activation overpotential. Ohmic overpotential is associated with the resistance that is encountered as the current flows the electrodes and the electrolyte.

The current density can be related with overpotential using the Butler-Volmer given as follows:

$$J = J_o \left[\exp\left(\alpha \frac{\eta_{o,s}}{2.303RT}\right) - \exp\left((1 - \alpha) \frac{\eta_{o,s}}{2.303RT}\right) \right] \quad (4.10)$$

The Butler-Volmer can be simplified based on some assumptions to drive the Tafel equation, which also relates the current density with the overpotential. The Tafel equation assumes backward or forward charge transfer reactions, whereas the Butler-Volmer considers both forward and backward reactions. The Tafel equation is given as:

$$J = J_o \left[\exp\left(\alpha \frac{\eta_{o,s}}{2.303RT}\right) \right] \quad (4.11)$$

where J is the current density, and J_o is the exchange current density in A/cm^2 . α is the transfer coefficient, used to indicate the fraction of the reaction which is involved in the charge transfer. α is generally between 0 to 1 and can be taken as 0.5 for single electron transfer reactions. η is the overpotential, R is the ideal gas constant ($8.314 J/molK$) T is the temperature in Kelvins (K).

4.1.2.1 Kinetic Measurement Models

Kinetic analysis results can also be obtained through modeling and data collection. The Gamry Framework software used can collect cyclic voltammetry (CV), linear sweep voltammetry (LSV), and electrochemical impedance spectroscopy (EIS) measurements. Both CV and LSV are models that can be used to relate the current density of the electrode with its potential. The main difference between the two models is the potential and current

response at which the voltages are applied. CV applies a potential in the forward direction first, then the potential is reversed to measure the current response in both directions between a selected limit. CV can provide insights into the reversibility of the system and the redox activity of the electrode. LSV only applies a linear potential in the forward direction to measure the current response. LSV models can be useful in determining the overpotentials of an electrode at a specific current density. The LSV curve can be used to determine the potential at which the current density is zero. This potential is subtracted from the potential at the current density of interest for a particular electrode. Electrochemical impedance spectroscopy (EIS) is another electrochemical model which can be used to study the impedance behaviour of the electrode. EIS applies an alternating current across the electrode system for a range of frequencies. EIS measurements can be represented in Bode and Nyquist plots. Bode plots can be used to analyze the magnitude of the impedance and the phase angle over a range of frequencies. The Nyquist plot can be used to see the relation between the negative imaginary part of the impedance versus the real part of the impedance. Both models can be helpful in providing the resistive and capacitive activity of the electrode.

4.2 Metal Deposition

The amount of metal coating deposited during the electrodeposition is considered in this section. The metal deposited onto the electrode during electrodeposition can be calculated using the Faraday's law as given as follows:

$$W = \frac{ItM}{nF} \quad (4.12)$$

where W is the amount of coating deposited on the electrode in grams (g), I is the current in amps (A), t is the deposition time in seconds (s), M is the molar mass of the metal plated (g/mol), n is the number of electrons involved and F is the Faraday's constant (96485 C/mol)

4.2.1 Electrodeposition and Electrode Coating Parameters

The coating parameters used during electrodeposition for the different coatings considered are presented. The amount of metal deposited for each coating is calculated and given in

this section. Based on traditional electrodeposition techniques, the current at which each coating is performed is selected. For nickel, electrodeposition is typically performed at a current density of 0.025 A/cm². Copper can be electrodeposited at a wide range of current densities depending on the coating amount and temperature. Typically, up to a current of 0.03 A/cm² has proven to be successful. The current density for iron varies, and generally, iron is co-deposited with other metals due to its high tendency to corrode. Molybdenum is typically electrodeposited at a higher current density. In neutral electrolyte baths, molybdenum has successfully been electrodeposited with a current density of 0.4 A/cm².

4.2.1.1 3D-Printed and Nickel Conductive Paint Coated Electrodes

The electrodeposition parameters used for coating the nickel conductive paint (NCP) coated over the 3D-printed electrodes are outlined. The calculated deposition amounts for each coating is also presented. Table 4.1 shows the electrodeposition for parameters used to coat the three nickel alloys considered. For all coatings listed, nickel is coated first on the electrode and then the alloy is coated. For iron and nickel, both are co-deposited together on top of the initial nickel coating. All deposition amounts for the nickel coating are the same.

Table 4.1 Electrodeposition parameters for nickel alloy coatings for NCP electrodes

Sample	Current (A)	Time (h)	Deposition (g)	Current (A)	Time (h)	Deposition (g)
Ni-Cu	Nickel			Copper		
	0.8	3	2.62	0.7	3	2.49
Ni-Fe	Nickel			Nickel Iron Co-deposition		
	0.8	3	2.62	0.8	3	2.62Ni, 2.5Fe
Ni-Mo	Nickel			Molybdenum		
	0.8	3	2.62	1.2	3	2.14

Table 4.2 shows the electrodeposition parameters and the deposition amounts of the different nickel NCP 3D-printed samples coated. The different paint specifications used to prepare the 3D-printed electrodes for electrodeposition are also listed in this table.

Table 4.2 Electrodeposition parameters for nickel coated NCP electrodes

Sample	Specification	Electrolyte Composition	Time (h)	Current (A)	Deposition (g)
A	1 coat of acrylic-based nickel paint and thermal heat dried	X	3	0.8	2.62
B	2 coats of acrylic-based nickel paint and thermal heat dried	X	4	0.8	3.49
C	2 coats of acrylic-based nickel paint and air dried	X	3	0.8	2.62
D	2 coats of acrylic-based nickel paint and thermal heat dried	Y	3	0.8	2.62
E	1 st coat of water-based paint, 2 nd coat of acrylic-based nickel paint, and thermal heat dried	Y	3	0.8	2.62
F	1 st coat of acrylic-based paint, 2 nd coat of water-based nickel paint, and air dried	X	3	0.8	2.62
G	2 coats of acrylic-based nickel paint and air-dried	Y	3	0.8	2.62
H	2 coats of water-based nickel paint and thermal heat dried	Y	3	0.8	2.62
I	1 st coat of water-based paint, 2 nd coat of acrylic-based nickel paint, and air dried	Y	3	0.8	2.62
J	2 coats of acrylic-based nickel paint and thermal heat dried	Y	4	0.8	3.49
K	2 coats of acrylic-based nickel paint and air dried	Y	3	0.8	2.62

4.2.1.2 Conductive PLA Electrodes

The parameters used to coat the CPLA 3D-printed electrodes are presented for each coating, in addition, the coating deposition amount is also listed. Table 4.3 shows the parameters and the coating for the four different depositions considered for the nickel-coated samples. All nickel-coated samples are proportional, Ni2x has double to amount of coating as Ni1x, Ni3x has three times of Ni1x and so forth.

Table 4.3 Electrodeposition parameters for nickel coated CPLA electrodes

Nickel Sample	Current (A)	Time (h)	Deposition (g)
Ni1x	0.8	1	0.87
Ni2x	0.8	2	1.75
Ni3x	0.8	3	2.62
Ni4x	0.8	4	3.49

Table 4.4 presents the parameters for the nickel-copper coated samples. First nickel is coated on the 3D-printed electrodes before coating with copper. The amount of the nickel coating is the same for all nickel-copper samples. The deposition amount of the copper coating is different for each. Ni-Cu1x and Ni-Cu2x are coated at the same current, only the electrodeposition time is doubled for Ni-Cu2x. Ni-Cu3x is coated at a lower current, but the electrodeposition time is increased.

Table 4.4 Electrodeposition parameters for nickel-copper coated CPLA electrodes

Nickel-Copper Sample	Nickel Coating			Copper Coating		
	Current (A)	Time (h)	Deposition (g)	Current (A)	Time (h)	Deposition (g)
Ni-Cu1x	0.8	2	1.75	0.7	1	0.83
Ni-Cu2x	0.8	2	1.75	0.7	2	1.66
Ni-Cu3x	0.8	2	1.75	0.6	4	2.84

Table 4.5 shows the electrodeposition parameters used to prepare the nickel-molybdenum samples. The electrodes are coated with nickel first, then molybdenum is coated. Two different deposition amounts of molybdenum are considered. Ni-Mo2x has two times more of the molybdenum coating as Ni-Mo1x. Both samples contain the same amount of nickel.

Table 4.5 Electrodeposition parameters for nickel-molybdenum coated CPLA electrodes

Nickel-Molybdenum Sample	Nickel Coating			Molybdenum Coating		
	Current (A)	Time (h)	Deposition (g)	Current (A)	Time (h)	Deposition (g)
Ni-Mo1x	0.8	2	1.75	1.2	2	1.43
Ni-Mo2x	0.8	2	1.75	1.2	4	2.85

Table 4.6 shows the parameters for some other coatings which are considered. Main differentiation for the NiFe and NiMo samples is that the two metals are co-deposited

without coating the electrodes with nickel first. Copper is also coated on one of the samples directly on the conductive PLA without another metal.

Table 4.6 Electrodeposition parameters for other metal coatings for CPLA electrodes

Sample	Current (A)	Time (h)	Deposition (g)
NiFe Co-deposition	0.8	3	4.37 Ni, 2.50 Fe
NiMo Co-deposition	1.2	4	5.24 Ni, 2.85 Mo
Cu	0.8	2	1.90

4.2.1.3 Conductive PLA Printed Flow Through Electrodes

The parameters used to coat the flow through CPLA 3D-printed electrodes are presented in Table 4.7. Only three samples for the flow through electrodes are considered. Nickel-copper and nickel-iron are coated in a similar manner to the other coated electrodes. For the nickel alloys, nickel is coated first on the conductive PLA then copper, and nickel-iron are coated on the samples. The amounts of nickel and the alloy deposited on the electrodes are shown.

Table 4.7 Electrodeposition parameters for metal coatings on D2 electrodes

Metal Coating	Nickel Coating			Other Metal		
	Current (A)	Time (h)	Deposition (g)	Current (A)	Time (h)	Deposition (g)
Ni	0.8	3	2.62	-	-	-
Ni-Cu	0.8	2	1.75	0.7	2	1.66
Ni-Fe	0.8	4	3.5	0.8	2	1.67

4.2.2 Voltage Supplied and Electrode Resistance

The resistance of the 3D-printed electrodes is measured before and after electrodeposition. In the case of nickel conductive paint coated first, the resistance of the electrodes is also measured after each coat. The Ohms law can be used to evaluate the relation between resistance, current and voltage. The Ohms law is given by equation 4.13:

$$V = I \times R \quad (4.13)$$

where V is the voltage in volts (V), I is the current in amps (A) and R is the resistance in Ohms (Ω). Based on the relation, at a given current, higher voltage will need to be supplied if the resistance is high. This can be used to evaluate the fluctuation in the voltage supplied by the power supply at different resistances. Table 4.8 shows the resistance of the nickel coated samples measured for different scenarios. The voltage which would be required to coat the electrode at the given current is also shown. At higher resistances, more voltage is required to coat the electrode at the same current.

Table 4.8 Measured resistances for nickel-coated NCP 3D-printed electrodes

Sample	Resistance after 1 st nickel paint coat (Ω)	Resistance after 2 nd nickel paint coat (Ω)	Resistance after electrodeposition - nickel (Ω)	Current (A)	Voltage at start (V)
A	6.1	3.6	1.4	0.8	2.88
B	6.4	3.3	0.6	0.8	2.64
C	4.5	4.0	0.9	0.8	3.2
D	6.3	3.5	1.0	0.8	2.8
E	7.8	4.1	1.4	0.8	3.28
F	3.5	2.7	0.7	0.8	2.16
G	5.3	4.6	1.3	0.8	3.68
H	4.3	3.0	0.8	0.8	2.4
I	4.4	3.1	0.8	0.8	2.48
J	4.5	3.2	0.5	0.8	2.56
K	4.5	3.4	1.1	0.8	2.72

Table 4.9 shows the voltage required at the start and the end of electrodeposition for second metal coating for NCP 3D-printed electrodes. The starting voltage is reduced as result of the nickel coating which is electrodeposited on the paint first. The voltage is adjusted accordingly during electrodeposition as the plating process progresses to maintain the current at a constant rate.

Table 4.9 Measured resistances for metals on nickel-coated NCP 3D-printed electrodes

Coating Metal	Resistance before (Ω)	Resistance after (Ω)	Current (A)	Voltage at start (V)	Voltage at end (V)
Cu	1.4	1.1	0.7	0.98	0.77
Fe	1.3	0.9	0.8	1.04	0.72
Mo	0.8	1.8	1.2	0.96	2.16

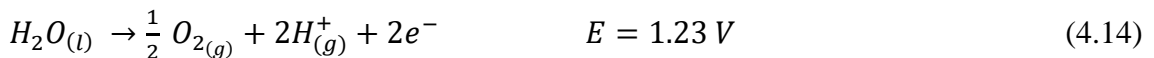
Table 4.10 shows the measured resistances and the voltage required for electrodeposition. For the nickel coatings, a much higher voltage is required for electrodeposition due to the high resistance of the conductive PLA. Coating the electrode with nickel first is beneficial to coat with the alloys since the required voltage significantly decreases. For co-depositing the alloys together, it is difficult to implement this approach. It is much more complex to coat two metals at once using a higher voltage. Applying a higher voltage at the start for co-deposition coatings didn't expedite the electrodeposition process at the start and resulted in the deformation of the PLA.

Table 4.10 Measured resistances for coatings on CPLA 3D-printed electrodes

Sample	Resistance before (Ω)	Resistance after (Ω)	Current (A)	Voltage at start (V)	Voltage at end (V)
Ni1x	1400	0.8	0.8	1120	0.64
Ni2x	13800	0.7	0.8	11040	0.56
Ni3x	14100	0.7	0.8	11280	0.56
Ni4x	1400	0.7	0.8	1120	0.56
Ni-Cu	0.7	0.6	0.7	0.49	0.42
Ni-Fe	0.7	0.5	0.8	0.56	0.4
Ni-Mo	0.7	1.5	1.2	0.84	1.8

4.3 Thermodynamic Analysis and Hydrogen Yields

Thermodynamic analysis is performed to evaluate the performance of the electrodes for hydrogen production as the cathode Direct current is applied at the anode and the cathode to split water. The oxygen and hydrogen are produced as the resulting gasses from the reaction. The reaction at the anode, the cathode, and the overall reaction is given by equations 4.14 to 4.16. The following oxygen evolution reaction occurs at the anode:



The following hydrogen evolution reaction occurs at the cathode:



The overall reaction of the electrolysis is given as follows:



The activation and ohmic overpotentials can also be defined for electrolysis. The activation potential of the anode can be defined as follows:

$$\eta_{ac,a} = \frac{RT}{F} \sinh^{-1}\left(\frac{J}{2J_{0,a}}\right) \quad (4.17)$$

The activation potential of the cathode can be defined as:

$$\eta_{ac,c} = \frac{RT}{F} \sinh^{-1}\left(\frac{J}{2J_{0,c}}\right) \quad (4.18)$$

The ohmic overpotential assuming the resistance only arises due to the flow of current through the current would be given by equation 4.17:

$$\eta_{oh} = \eta_{oh,electrolyte} = IR_{elec} \quad (4.19)$$

where I is the current and R_{elec} is Resistance of the electrolyte. The current (I) be found by multiplying the current density (J) with the area of the electrode. The potential of the electrolysis can be calculated as follows:

$$V = V_0 + \eta_{ac,a} + \eta_{ac,c} + \eta_{oh} \quad (4.20)$$

The energy and exergy efficiency can be expressed for the electrolysis using the energy inputs and outputs. The energy efficiency of the system is given as:

$$\eta_{en} = \frac{\dot{m}LHV}{\dot{E}_{in}} \quad (4.21)$$

The exergy efficiency of the system is given as:

$$\eta_{ex} = \frac{\dot{m}ex^{ch}}{\dot{E}x_{in}} \quad (4.22)$$

where LHV is the low heating value of hydrogen (120 MJ/kg), \dot{m} is the mass flow rate of the hydrogen produced, and ex^{ch} (116.6 MJ/kg) is the chemical exergy. \dot{E}_{in} is the energy input into the electrolysis. Only electrical power ($\dot{E}_{in} = VI$) is input into the system therefore energy input is equal to the exergy input.

CHAPTER 5: RESULTS AND DISCUSSION

The 3D-printed electrodes which are coated are further tested using electrochemical models with the Gamry Reference 3000. The electrochemical measurements taken included cyclic voltammetry (CV), linear sweep voltammetry (LSV), and electrochemical impedance spectroscopy (EIS). All electrodes prepared are tested, these include the NCP 3D-printed electrodes, the CPLA printed electrodes, as well as the flow through (D2) electrodes. CV and LSV measurements are taken and compared in 1 mol KOH in 400 ml distilled water solution. Additionally, some electrodes are tested in just distilled water to compare the performance without the addition of 1 mol KOH. This section presents the results which are collected from the electrochemical measurements. The coated electrodes and obstacles encountered during electrodeposition are also discussed.

5.1 Coated Electrodes and Deformations

This portion of the thesis presents the coated 3D-printed electrodes which are obtained using electrodeposition. The conductive PLA 3D-printed electrodes coated directly with various coatings are shown in Figure 5.1.

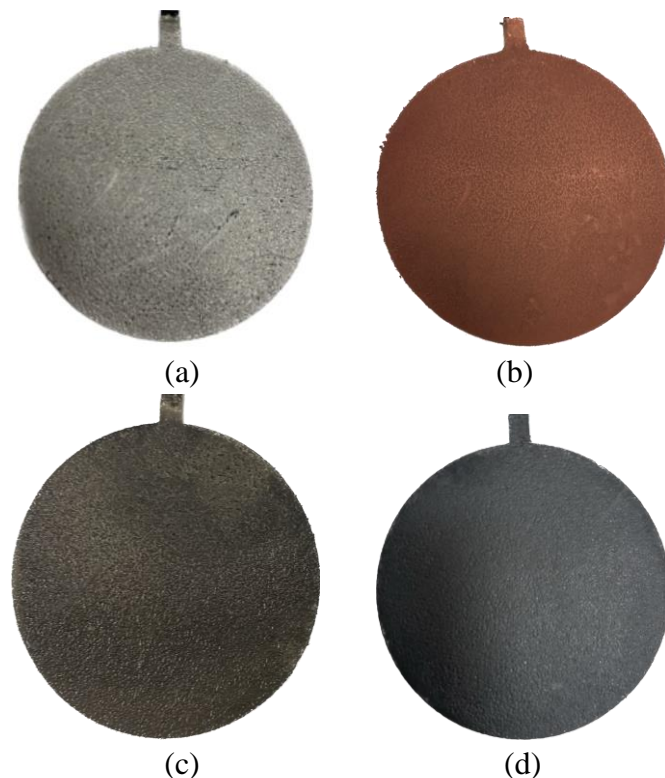


Figure 5.1 Coated CPLA 3D-printed electrodes (a) Ni (b) Ni-Cu (c) Ni-Fe (d) Ni-Mo

The coatings for the CPLA 3D-printed electrodes are very consistent compared to electroplated nickel conductive paint (NCP) coated 3D-printed electrodes. This is due to the uneven coatings of conductive paint, which is hard to control since the acrylic-based conductive paint is dense and hard to apply. The water-based nickel conductive paint used, resulted in deformations of the coatings after electrodeposition. Some electrodes are tested by applying one coat of water-based paint first and a second coat of acrylic paint (very stable for electrodeposition). However, due to the electrolyte, the underneath layers with the water-based conductive paint created pockets under the coated surface. The acrylic conductive painted 3D-printed electrodes worked well with electrodeposition, and no deformation in the coatings are noticed. However, some spots have more of the nickel coating, and resistance across the painted surface is inconsistent. There are some dark spots noticeable after electroplating. This is a result of a higher current distribution in some areas of the electrodes. This is noticed essentially around the area where the current is applied on the electrode for electrodeposition. Another disadvantage with using conductive paint to make the 3D-printed part conductive is that complex shapes are difficult to coat with the paint first. Figure 5.2 shows the nickel, nickel-copper, and nickel-iron coated flow through (D2) electrodes. The D2 electrodes are first printed with the conductive PLA and then coated using electrodeposition. Printing the flow-through electrodes with the non-conductive PLA would be challenging since it would be hard to paint them with the conductive paint for electrodeposition.

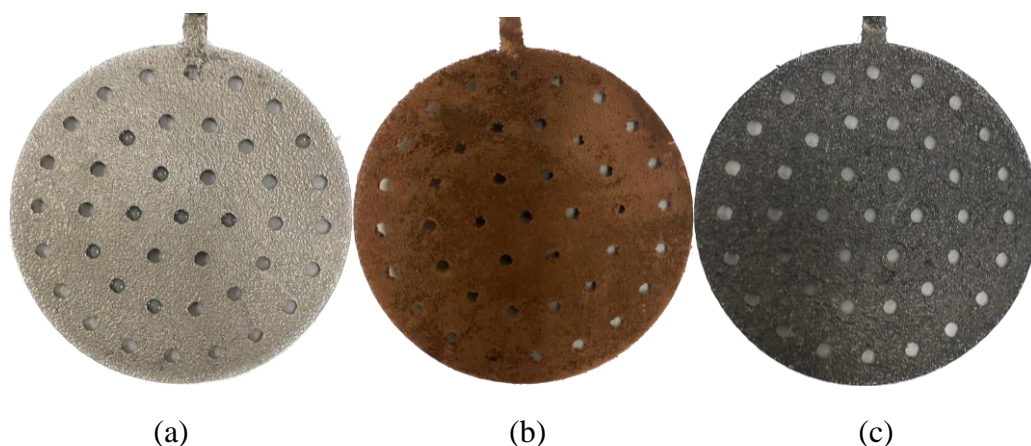


Figure 5.2 Coated flow through CPLA 3D-printed Electrodes (a) Ni (b) Ni-Cu (c) Ni-Fe

The flow-through electrodes have tiny holes which make them hard to coat with the conductive paint first before electrodeposition. In addition, it would also take a longer time to prepare the electrodes with the nickel conductive paint approach. The conductive PLA 3D-printed electrodes are ready for electrodeposition directly after ultrasonic cleaning. Whereas the electrodes printed with non-conductive PLA have to be cleaned then painted with conductive paint and dried for 24 hours after every coat (alternatively dried with the heat gun for 1 hour speeded up the process). Although the CPLA 3D-printed electrodes approach is much faster, the electrodes are much harder to coat compared to NCP 3D-printed electrodes. The resistance of the CPLA is much higher than the NCP, therefore the applied current at the same voltage is much lower for CPLA 3D-printed electrodes. To overcome this, the applied voltage is increased at the start to 10 V from 4 V (for NCP) until the plating process started, and when the applied current is observed to increase the voltage is reduced. The parameter for electrodeposition has to be controlled much more carefully for CPLA 3D-printed electrodes. Figure 5.3 shows some deformations which results due to various reasons while coating the CPLA 3D-printed electrodes.

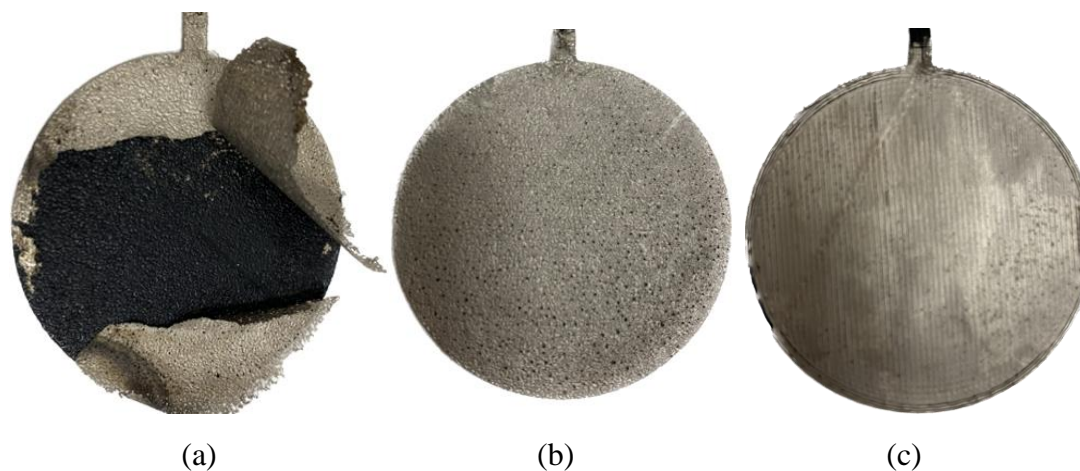


Figure 5.3 Deformations while coating (a) breakage due to high voltage (b) impurities as a result of the PLA surface (c) pockets underneath coatings after testing

Initially, applying a very high voltage for a long period of time during electrodeposition caused the coating to break apart from the PLA surface as seen in Figure 5.3 (a). The coatings which did not break are inconsistent (tiny holes are noticed) which is a direct result of impurities in the PLA. This also caused the water to go underneath the coating during electrochemical testing, which eventually resulted in pockets forming between the coated

metal layer and the PLA surface as seen in Figure 5.3 (c). This is easily fixed by cleaning the electrodes in an ethanol-methanol with distilled water solution bath in the ultrasonic cleaner. First, the electrodes are only cleaned in distilled water with the ultrasonic cleaner, which results in the impurities shown in Figure 5.3 (b)-(c). Electrodes aging is another impurity to consider. After a few tests, the performance of some electrodes declined depending on the coatings they are coated with.

5.2 3D-printed with Nickel Conductive Paint Coated and Electroplated Electrodes

First, the nickel conductive paint (NCP) coated 3D-printed electrodes are electroplated with nickel and then with nickel and various catalysts. The coated electrodes are tested in an electrochemistry setup. The results obtained for these electrodes are discussed in this section.

5.2.1 Nickel Electrodes

Various nickel electrodes are prepared using electrodeposition for the NCP coated 3D-printed electrodes. Main differentiation between the samples is the method they are prepared with. There are two types of nickel conductive paints which are used, acrylic based, and water based. During electrodeposition, the NCP coated electrodes with the water based broke part directly due the paint layer being separated from the 3D-printed electrode surface, therefore these electrodes are not tested. The samples which had no deformations are the ones coated with the acrylic based nickel paint which worked very well for electrodeposition. The specification of each sample differed based on the number of coats which are applied, as well as how the paint is dried. Table 4.2 lists the different specification of the electrodes on how each sample is prepared before electrodeposition. Another difference between the electrodes is the electrolyte bath which is used. Some electrodes are coated with half of the composition (X) of nickel electrolyte bath (Y). Electrolyte bath X is composed of 13.2 g of nickel sulfate, 2.5 g of nickel chloride, and 1.25 g of boric acid in 200 ml of distilled water. Electrolyte bath Y is composed of double the chemical compositions as bath X in the same amount of water (400 ml). All nickel electrodes are tested in distilled water, as well as a 1 mol KOH solution. Figure 5.4 shows the current densities of the nickel electrodes in water.

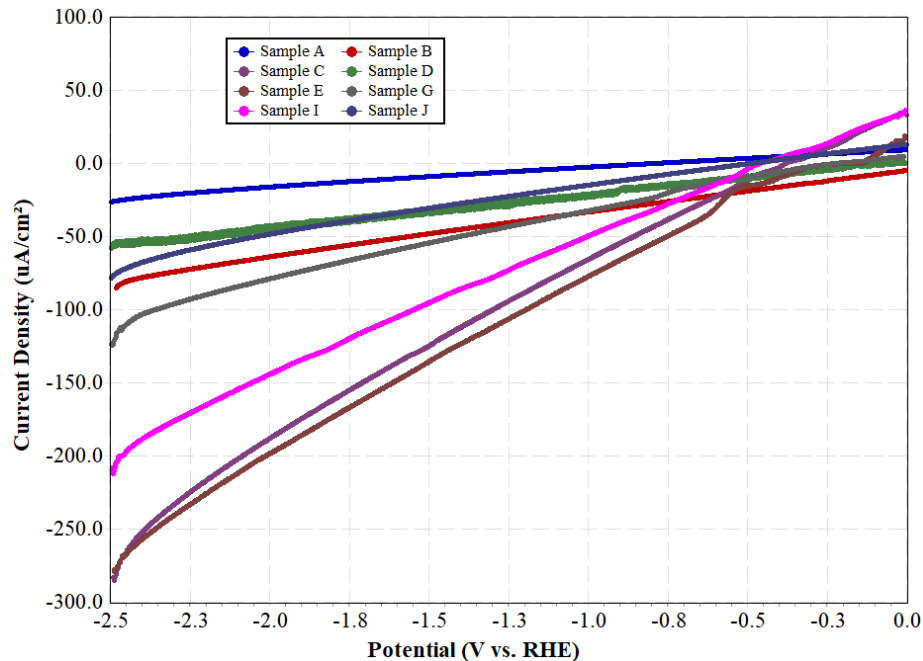


Figure 5.4 LSV measurements of nickel NCP 3D-printed electrodes in distilled water

Figure 5.5 shows the current densities measured in the 1 mol KOH solution. Immediately a major shift in the current densities is seen from the ones tested in distilled water. The conductivity of water is very low compared to the potassium hydroxide solution which is one of the main reasons for this.

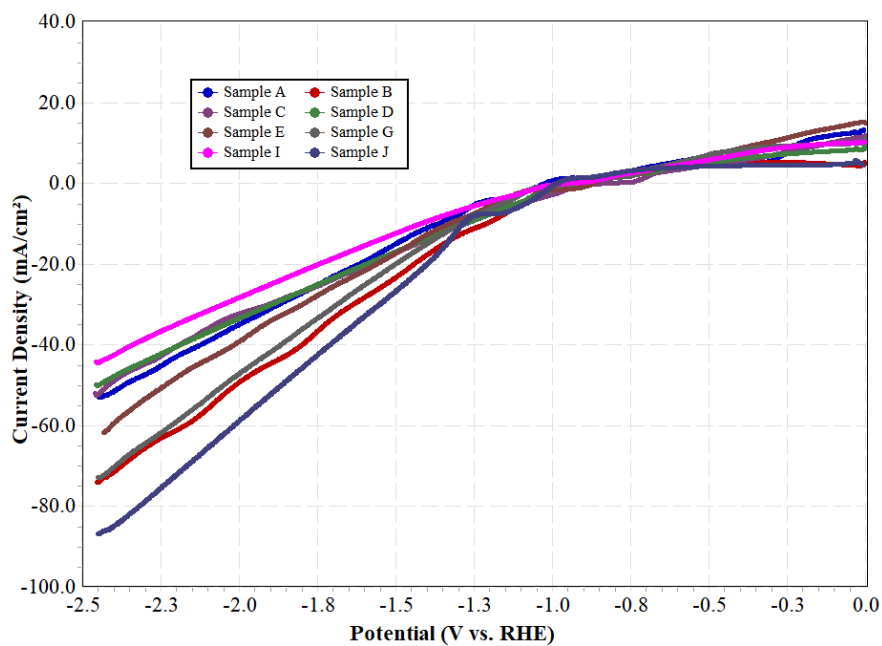


Figure 5.5 LSV measurements of nickel NCP electrodes in 1 mol KOH solution

Figure 5.6 shows the LSV measurements just for the nickel-coated electrodes which are coated with the electrolyte bath composed with less chemical compositions. In comparison to the samples, Sample B is coated for 4 hours whereas the others are only coated for 3 hours. There is a significant difference which can be seen in the current densities for higher deposited coatings.

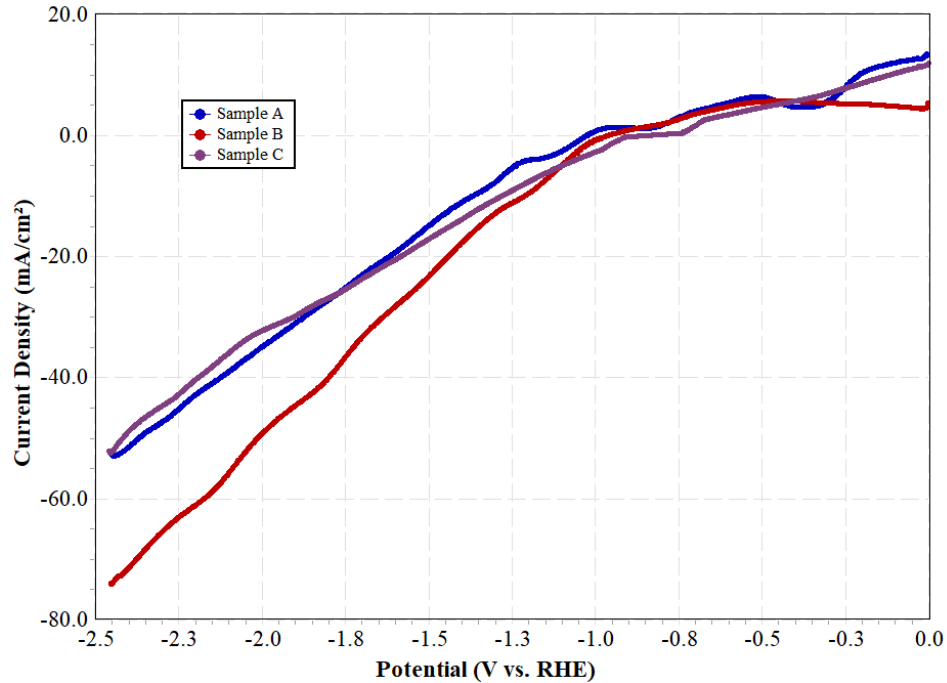


Figure 5.6 LSV measurements of NCP 3D-printed electrodes coated with nickel bath of composition X

Figure 5.7 represents the LSV measurements of the NCP electrodes which are coated with nickel using the electrolyte bath with composition Y. Sample J is the only sample coated for 4 hours and it had the highest current densities at the same potential compared to the other samples which are only coated for 3 hours (other electrodeposition parameters are the same). Sample A, B, and C which are coated with the bath with half the composition, the current densities tended to be lower for these electrodes. For the electrodes coated with bath with composition Y, it is important to note that the current densities fluctuated for the same electrodes with the same parameters used during electrodeposition. This is mainly due to uncontrolled factors during the nickel conductive painting processes. Although the amount of the nickel conductive paint applied is carefully applied to be the same on each electrode, there is still some error, and some paint coatings result in thicker than others.

The number of paint coats applied also plays a role in electrodeposition. Overall, the electrodes coated for a longer time, or at a higher current (with more thickness) have higher current densities. In this scenario, the electrodes coated for 4 hours have the best results.

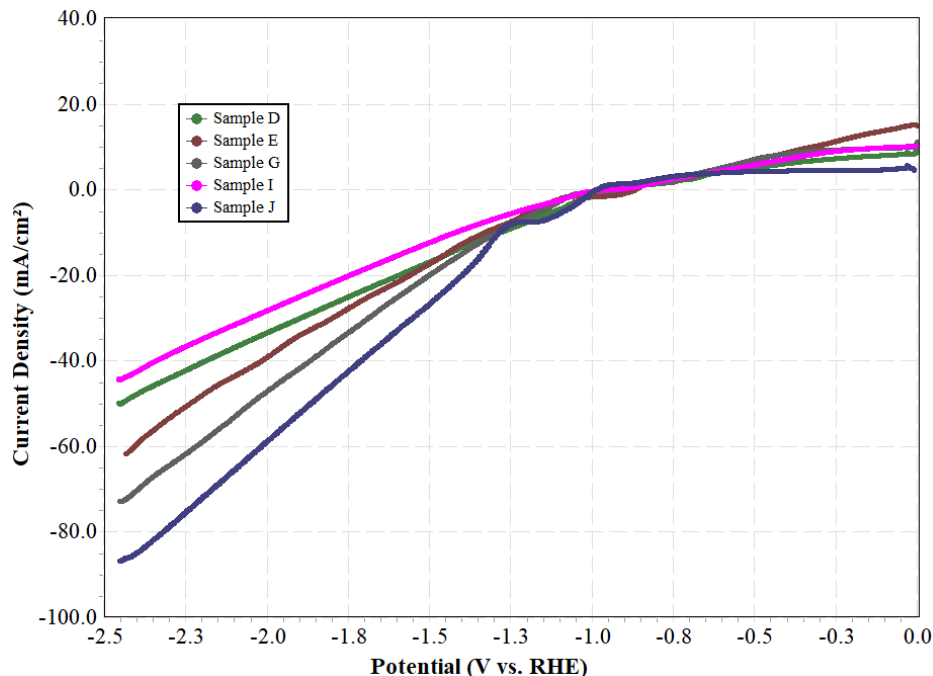


Figure 5.7 LSV measurements of NCP 3D-printed electrodes coated with nickel bath of composition Y

5.2.2 Nickel Alloy Electrodes

The NCP 3D-printed electrodes are also coated with nickel alloys to see the impact on the performance. First, the electrodes are coated with nickel, and the catalysts are coated to form nickel alloys. Three different alloy combinations are considered, nickel-copper, nickel-iron, and nickel-molybdenum. Similar to the nickel-coated electrodes, the alloy electrodes are also tested in distilled water as well as in 400 ml of 1 mol KOH solution. Figure 5.8 presents the CV measurements of the three nickel alloys in distilled water. As compared to nickel-coated electrodes, the current densities are slightly higher of the alloys, however they are still very low and would not perform very well just in water. This shows that the addition of potassium hydroxide is necessary to improve conductivity of the electrolyte.

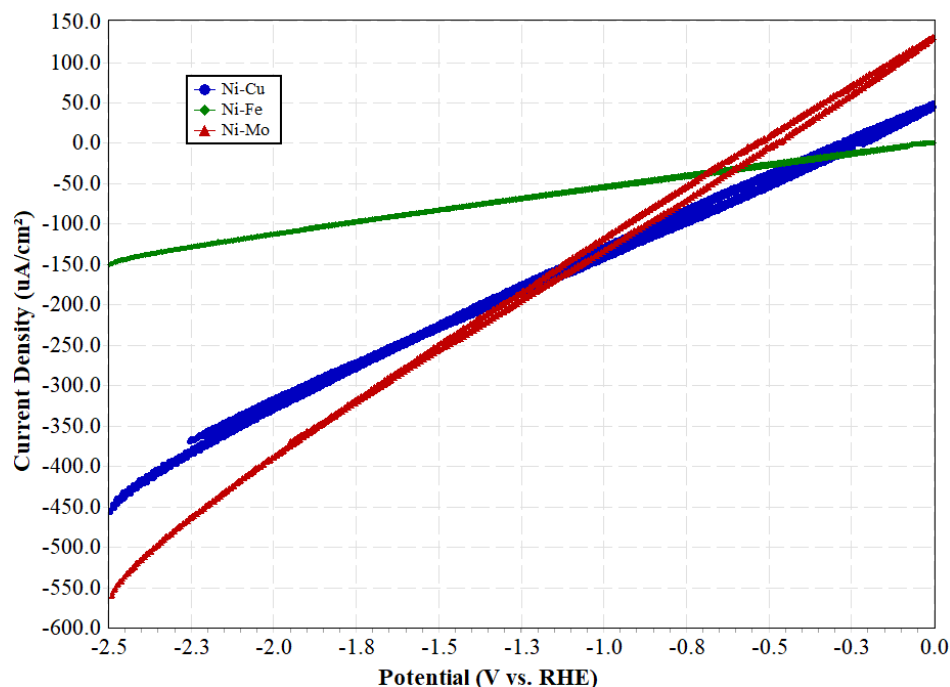


Figure 5.8 CV measurements of nickel alloys coated NCP 3D-printed electrodes in distilled water

Figure 5.9 shows the CV measurements for nickel alloy-coated electrodes in the 1 mol KOH solution. The current densities obtained in the solution are significantly higher. The curves obtained for the CV measurements represent an adequate current response. At lower potentials ($\sim 0V$) the performance of the alloys is relatively similar. At higher potentials, a higher current density can be observed for the Ni-Mo alloy.

Figure 5.10 shows the LSV measurements of the nickel alloy electrodes. LSV measurements make it easier to observe the electrochemical behaviour of the electrodes when only considering the forward response. The performance of the Ni-Cu and Ni-Fe electrodes in this case is relatively similar. At higher voltages, Ni-Cu electrodes tend to have a slightly higher current density than the Ni-Fe electrode. Molybdenum-coated electrode have the highest current density in comparison to all three alloys. Traditional molybdenum electrodes have shown some promising results as catalyst. Electrochemical response of the nickel-molybdenum electrode shows potential for molybdenum coatings as catalyst for hydrogen evolution reactions.

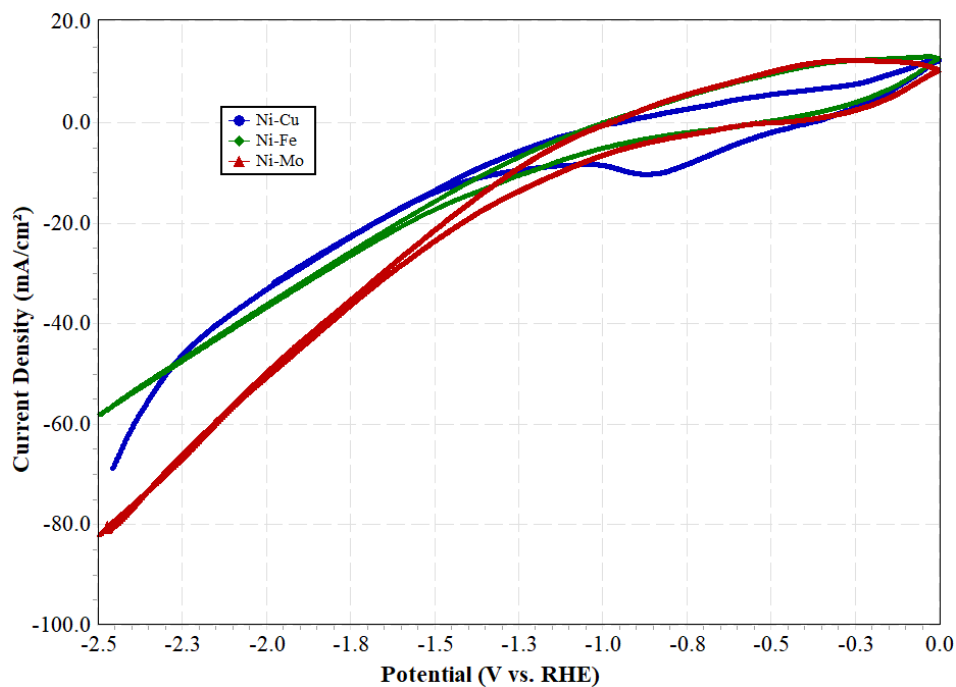


Figure 5.9 CV measurements of nickel alloys coated NCP 3D-printed electrodes in 1 mol KOH solution

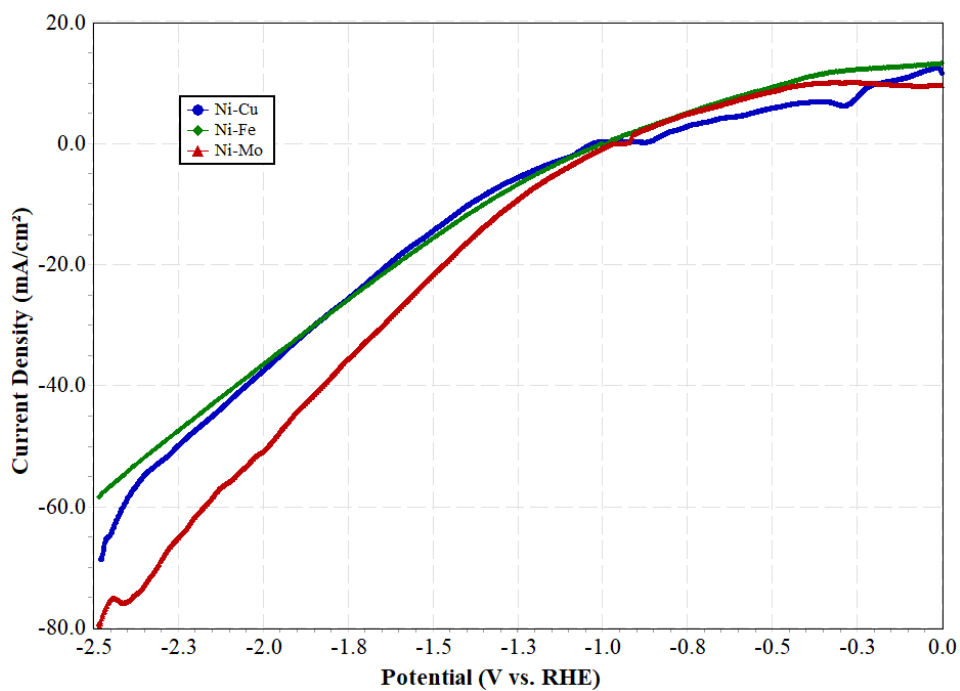


Figure 5.10 LSV measurements of nickel alloys coated NCP 3D-printed electrodes in 1 mol KOH solution

5.2.3 Impedance Measurements

Electrochemical impedance spectroscopy (EIS) measurements are used to evaluate the impedance activity of the electrodes. The measurements for impedance are performed in 1 mol KOH solution. Figure 5.11 shows the impedance magnitude over the frequency of 0.1Hz to 10kHz. The impedance behaviour of the electrodes is very similar, the magnitude tends to decrease as higher frequencies are reached. The plot represents a stable impedance behavior, there is a very less shift in the magnitude of the impedance.

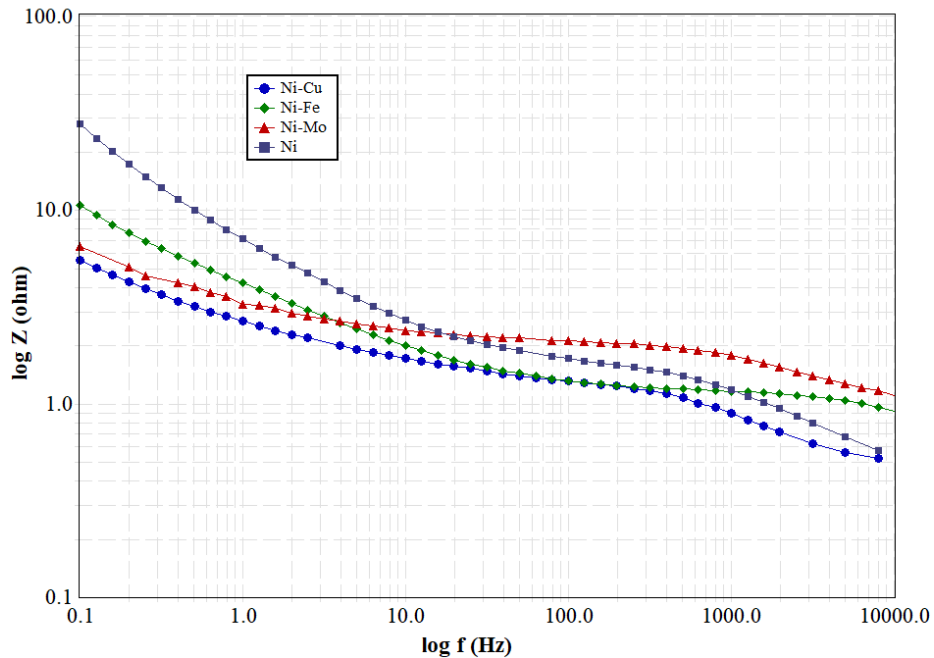


Figure 5.11 Bode plot for magnitude for NCP 3D-printed coated electrodes

Figure 5.12 represent the phase angle of the electrodes as the frequency is increased. The Ni-Cu, and Ni-Mo electrodes have a smoother phase shift, whereas the Ni electrode without any catalysts seems unstable in comparison.

Figure 5.13 represents the Nyquist plots of the NCP 3D-printed coated electrodes. The measured negative imaginary part of the impedance is represented over the real part of impedance. The Ni electrode has a very high impedance compared to the nickel alloys. In comparison, nickel alloys have much lower impedance. The Ni-Fe electrode among Ni-Cu and Ni-Mo electrodes have the highest imaginary impedance over the real part. The nickel-copper electrode has the lowest impedance.

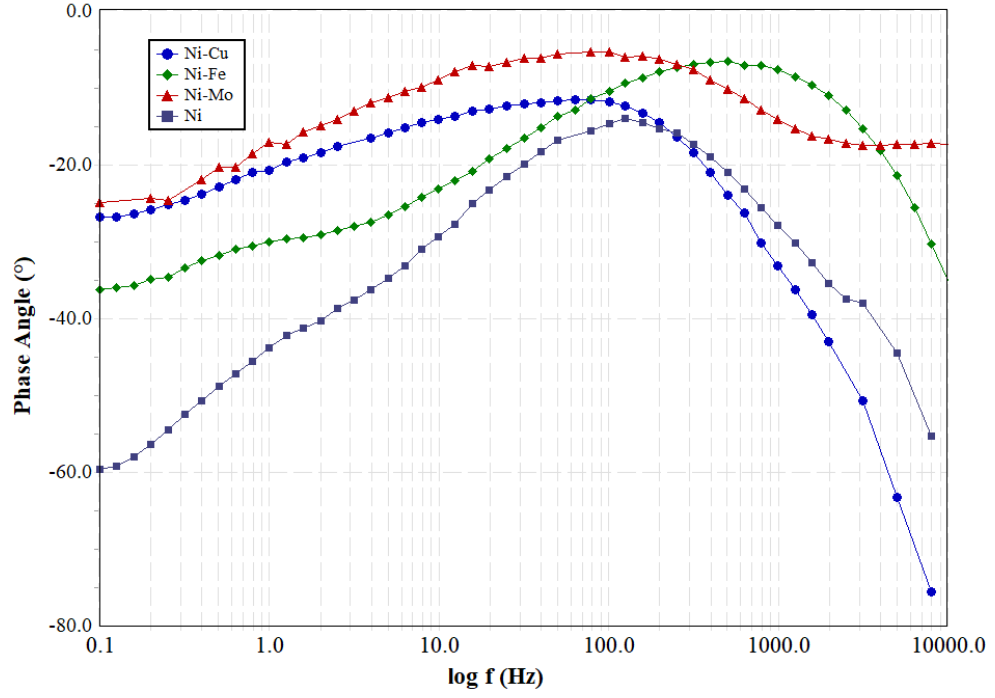


Figure 5.12 Bode plot for phase angle for NCP 3D-printed coated electrodes

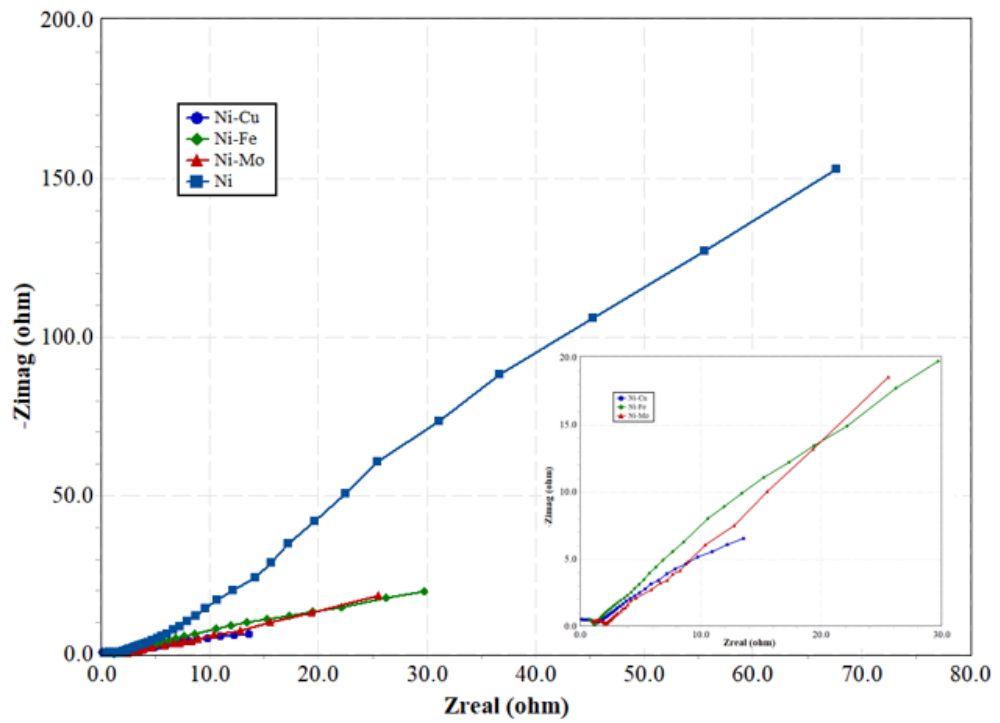


Figure 5.13 Nyquist plot for NCP 3D-printed coated electrodes

5.2.4 Overpotential Results

The overpotentials are calculated based on the LSV measurements obtained for the NCP 3D-printed and coated electrodes. Figure 5.14 represents the plot that is used to determine the potentials at the respective current densities. The plot also compares the LSV measurements of nickel to its alloys.

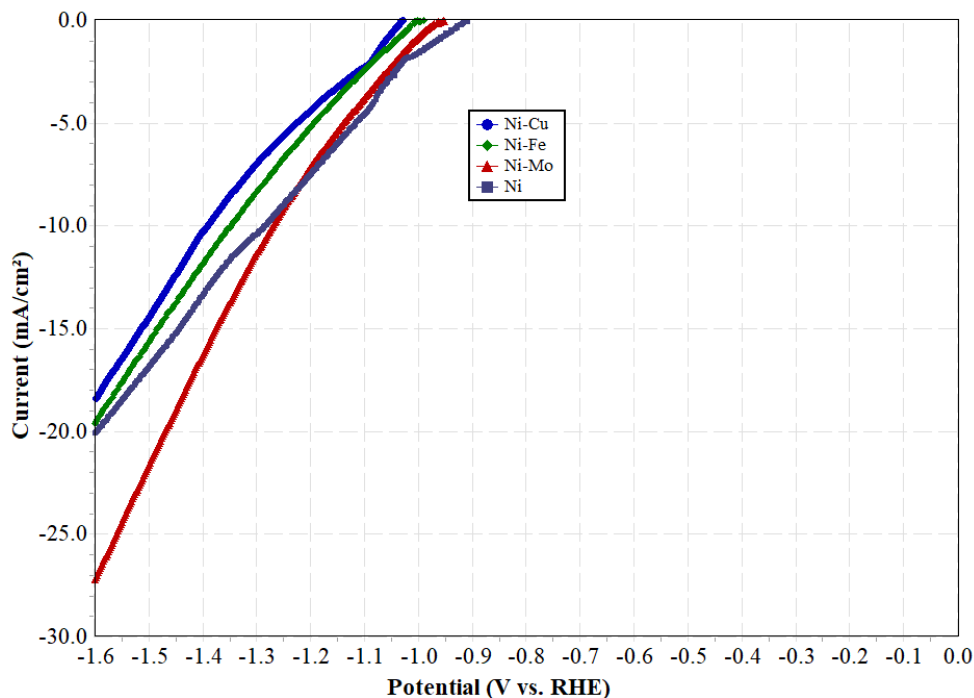


Figure 5.14 LSV measurements used for overpotential calculation for NCP 3D-printed coated electrodes

Figure 5.15 compares the overpotentials for the different electrodes at the current densities of 10 mA/cm² and 20 mA/cm². It can be observed that nickel has a higher overpotential compared to its alloys. The current density of the nickel electrode is very low compared to the alloy electrodes. The potentials at which the current density is zero, are recorded for the electrodes considered. The potentials at a current density of 10 mA/cm² and 20 mA/cm² are measured. The measurements are determined very carefully ensuring precision using the Gamry Echem Analyst software. The overpotentials are determined at the 10 mA/cm² and 20 mA/cm² ranges by subtracting the collected overpotential at a zero current density from the potentials at the respective current densities.

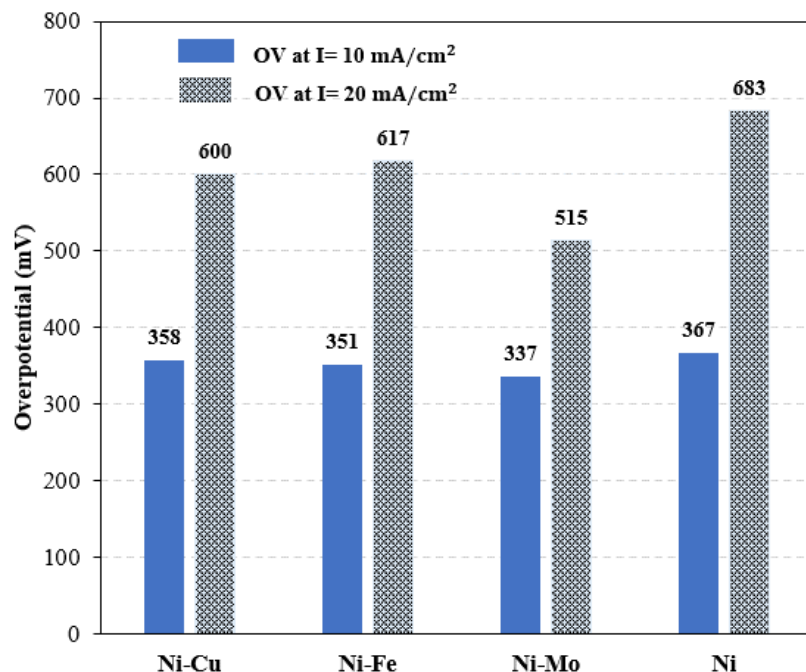


Figure 5.15 Overpotentials for NCP 3D-printed coated electrodes

The nickel electrode in the figure represents Sample B of the nickel-coated NCP 3D-printed electrode. This sample is selected for comparison because it had the same electrodeposition parameters and electrode preparation techniques as the one used to coat the nickel for the alloy electrodes. The Ni-Mo electrode has the lowest overpotential at both current densities. For a current density of 20 mA/cm² the overpotential drastically increases. However, for nickel this change is not significant as compared to Ni-Cu and Ni-Fe coated electrodes.

5.3 Conductive PLA Electroplated 3D-printed Electrodes

Electrochemical analysis and measurements are also performed for the conductive PLA (CPLA) 3D-printed electrodes. The analysis process is similar to the one for NCP 3D-printed and coated electrodes. For the CPLA electrodes, the electrodes are coated with the same metals, nickel, and its alloys nickel-copper, nickel-iron, and nickel molybdenum. However, various coating approaches are explored with the CPLA electrode coating baths. Some of the coatings without coating the electrode with nickel first are investigated by co-depositing the metals together. The results showed that first coating the electrodes is beneficial in improving the strength of the electrode. In addition, coating the electrodes before coating the alloy made the electrodeposition easier for the CPLA electrodes. Since the conductive PLA originally has a very high resistance, it is very hard to coat a lot of the

metals especially alloys together, which are more easily coated on other metals. The nickel electrodeposition is found to be the more efficient for coating the CPLA electrodes. The nickel coating electrolyte baths are found to be more effective in controlling the parameters of the bath in comparison to other electrolyte baths considered in the study.

5.3.1 Nickel Electrodes

For the CPLA-coated electrodes, only a few samples are prepared for comparison. The main differentiation between these electrodes is the deposition of the metal deposited on the electrodes. The same electrolyte bath with the same chemical compositions is used for the different nickel coatings. Figure 5.16 shows the CV measurements of four different depositions of the nickel coatings in distilled water. Electrode Ni1x is coated for 1h, Ni2x is coated for 2h, Ni3x for 3h, and Ni4x for 4h. All other electrodeposition parameters are kept the same therefore the nickel coatings are proportional to each other. The Ni2x has two times the coating of Ni1x. The sample Ni3x has 3 times coating amount of Ni1x, and Ni4x has approximately four times the coating amount of Ni1x.

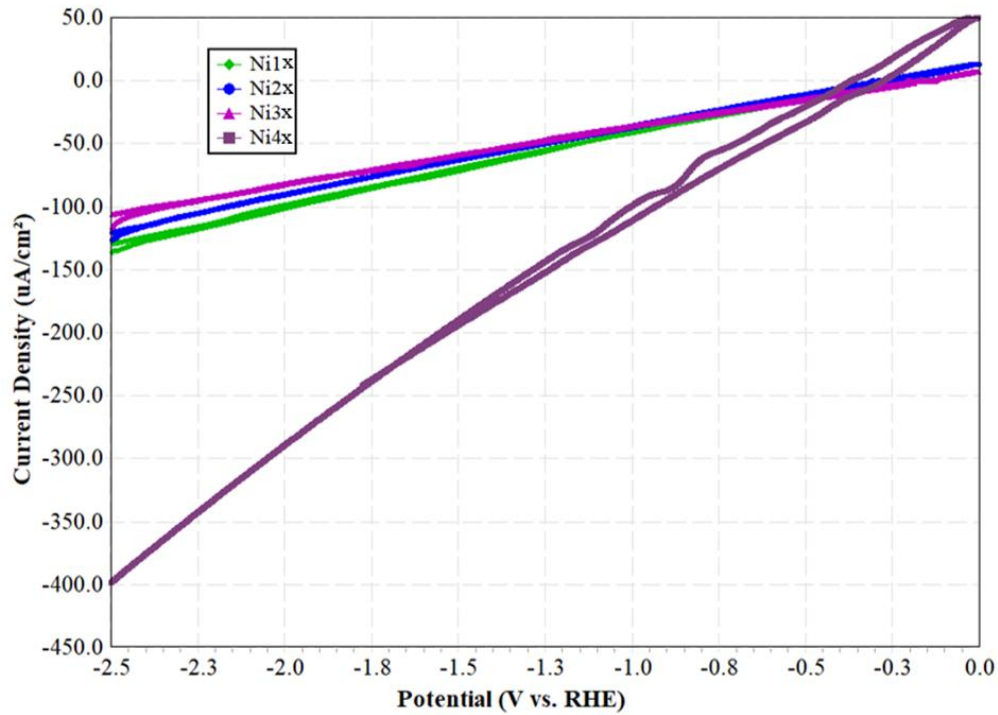


Figure 5.16 CV measurements of nickel-coated CPLA 3D-printed electrodes for different nickel depositions in distilled water

Figure 5.17 presents the CV measurements of the nickel coated CPLA 3D-printed electrodes for different nickel depositions in 1 mol KOH in 400 ml distilled water solution. The electrochemical activity of the nickel-coated electrodes is very low in distilled water. In comparison, nickel-coated electrodes for CPLA 3D-printed measured in the 1 mol KOH solution are significantly better. The performance of electrodes with deposition Ni1x, Ni2x, and Ni3x is relatively similar.

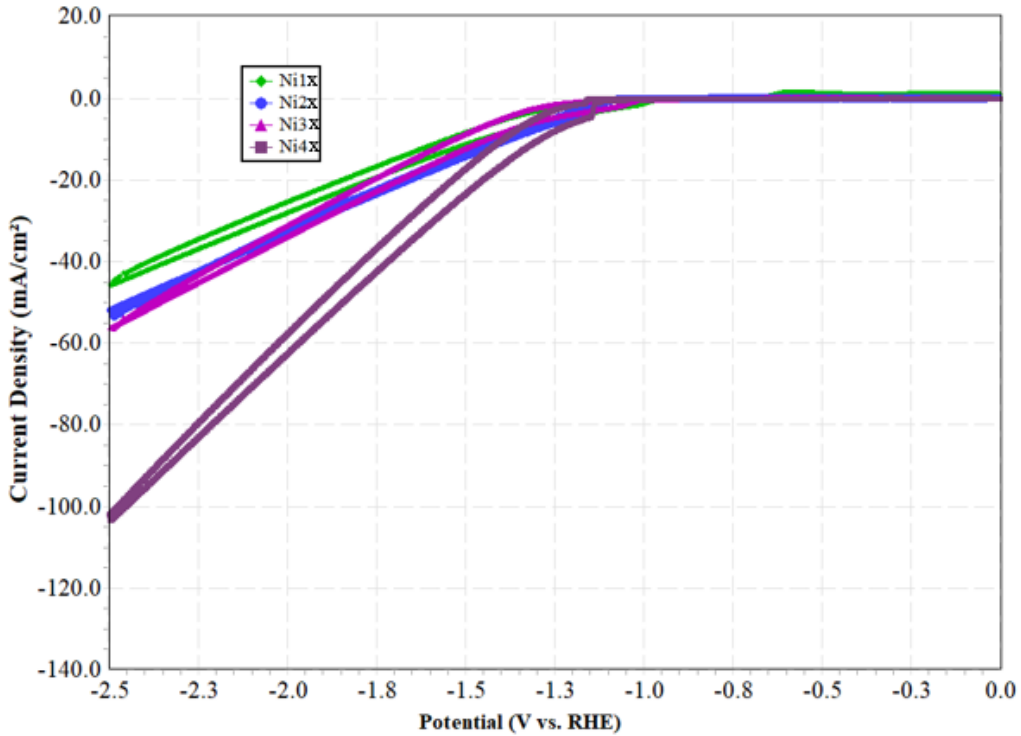


Figure 5.17 CV measurements of nickel-coated CPLA 3D-printed electrodes for different nickel depositions in 1 mol KOH solution

Figure 5.18 shows the LSV measurements of the different nickel depositions measured in 1 mol KOH solution. A better understanding of the forward current response of the electrode can be obtained from this illustration. It can be observed that the electrode with deposition Ni4x (4 times the coating amount than Ni1x) has very good current density compared to the other three nickel compositions. Although there is not much of a difference in the amount of the nickel coating on Ni3x compared to Ni4x, still the relation of Ni3x is more similar to Ni1x, and Ni2x than Ni4x. The current density tends to significantly increase at a certain coating amount because the metallic properties of the electrodes are improved.

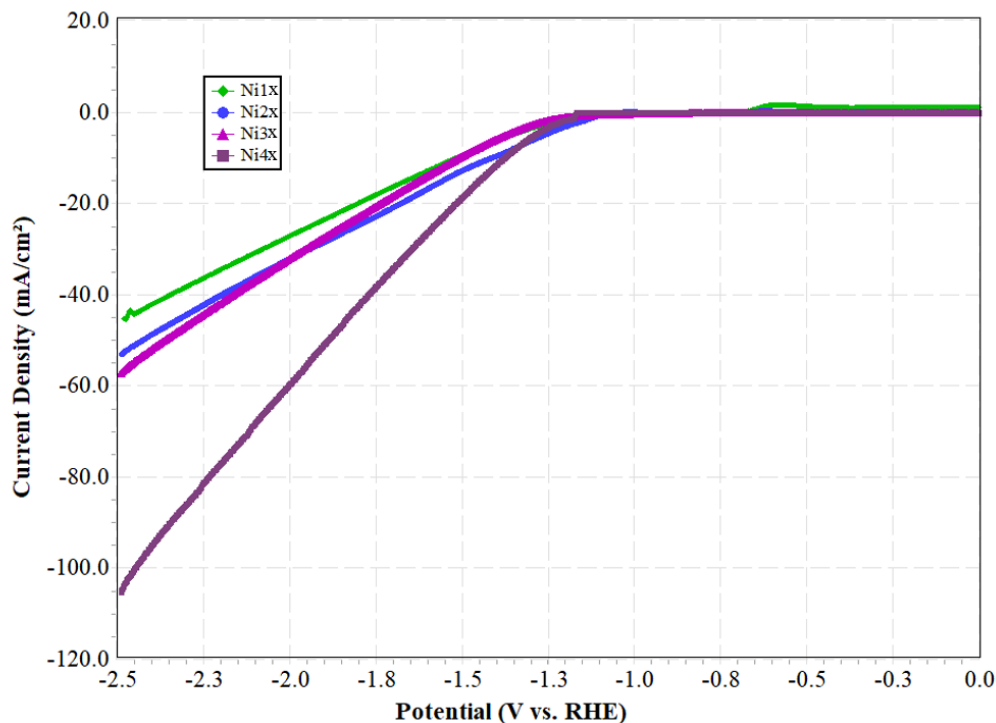


Figure 5.18 LSV measurements of nickel-coated CPLA 3D-printed electrodes for different nickel depositions in 1 mol KOH solution

5.3.2 Nickel Alloy Electrodes

The CPLA 3D-printed electrodes are further coated with nickel alloys to investigate their electrochemical behaviour. First, a nickel electrolyte bath is used to coat the electrodes, then the electrodes are coated with the alloy. Nickel-iron is co-deposited on top of the nickel coating to reduce the corrosion of iron. When nickel is coated with just iron, the electrode rust after a few hours. In addition, Nickel-iron is also co-deposited by coating the electrode with nickel first, but adhesion between the layers is weak and the coatings comes apart easily.

Figure 5.19 shows the CV measurements for nickel alloys in water. The results in distilled water are similar to the other previous electrochemical measurements performed in water. It is evident that the addition of potassium hydroxide significantly increases electrode performance due to the increased conductivity of the electrolyte. Other factors not studied in the present study, such as temperature of the electrolyte may also improve performance.

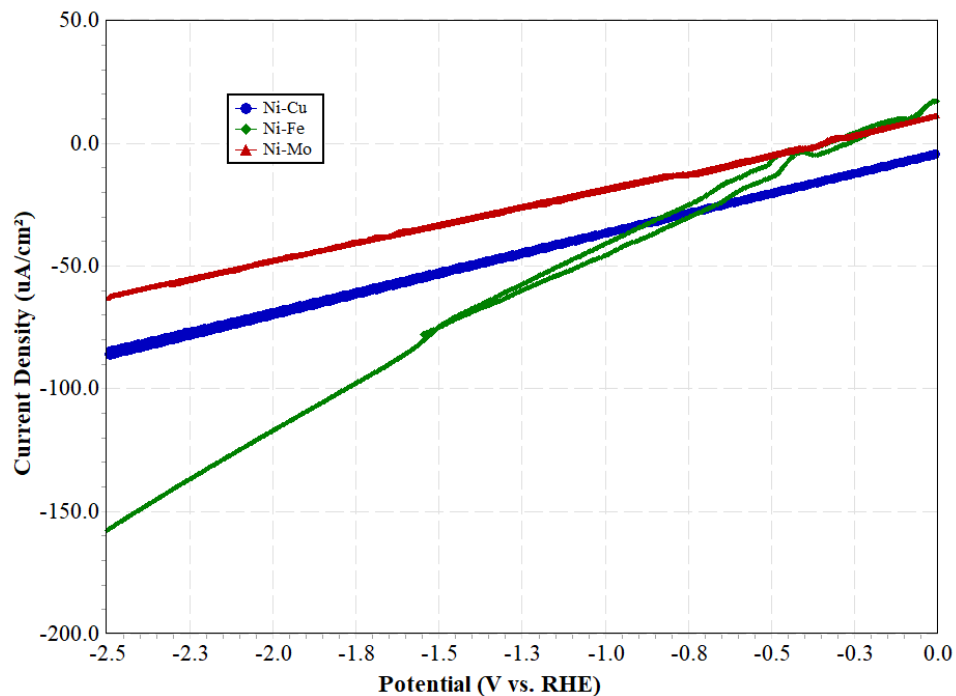


Figure 5.19 CV measurements of nickel alloy coated CPLA 3D-printed electrodes in distilled water

Figure 5.20 shows the CV measurements of the CPLA 3D-printed electrodes coated with alloys in 1 mol KOH solution. For the nickel alloy-coated electrodes, in distilled water there is no current backward current response. Both backward and forward responses are the same, and the current density is also very low. In 1 mol KOH solution, the current response of the electrodes is significantly higher.

Figure 5.21 shows the LSV measurements for the nickel alloy-coated electrodes in 1 mol KOH solution. It can be noted from the figure that the current densities of the three alloys are very similar for higher potentials, at 2.1 V and above. For voltages between 0.9 V and 1.7 V, the Ni-Cu electrode has a significantly higher current density compared to Ni-Fe and Ni-Mo. For nickel-molybdenum, the electrolyte bath used to coat the CPLA 3D-printed electrodes did not include sodium hydroxide, the pH is also lower compared to the bath used for the NCP 3D-printed coated electrodes. The molybdenum coating easily comes apart once current is applied to the electrode. The addition of sodium hydroxide with ammonium molybdate is necessary to reduce to the formation of hydroxides. Due to the coating coming apart from the nickel layer, there is a significant reduction observed in the current densities compared to the Ni-Mo coated NCP 3D-printed electrode.

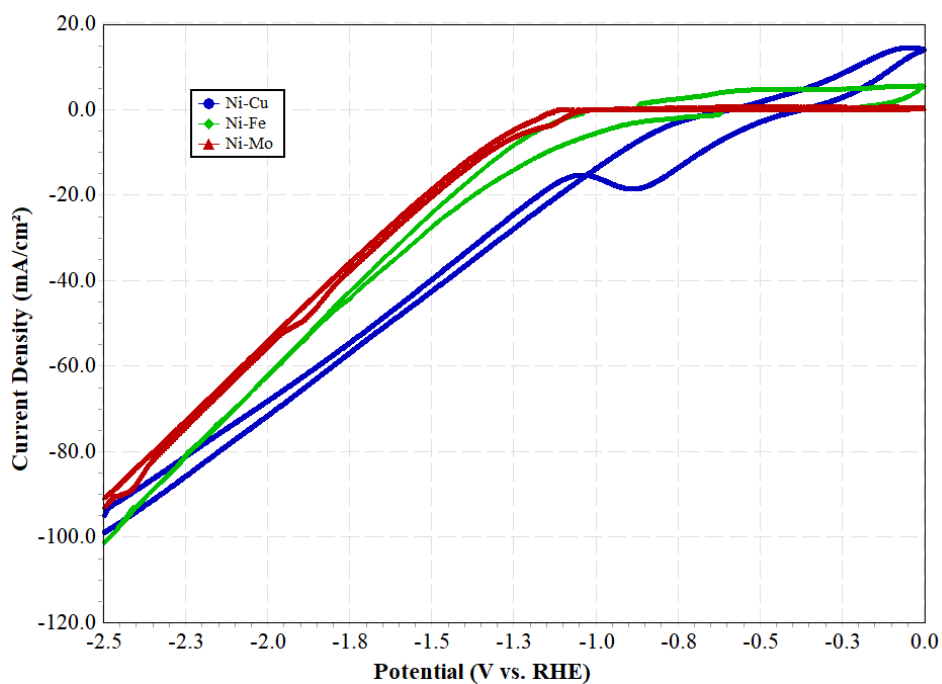


Figure 5.20 CV measurements of nickel alloy coated CPLA 3D-printed electrodes in 1 mol KOH solution

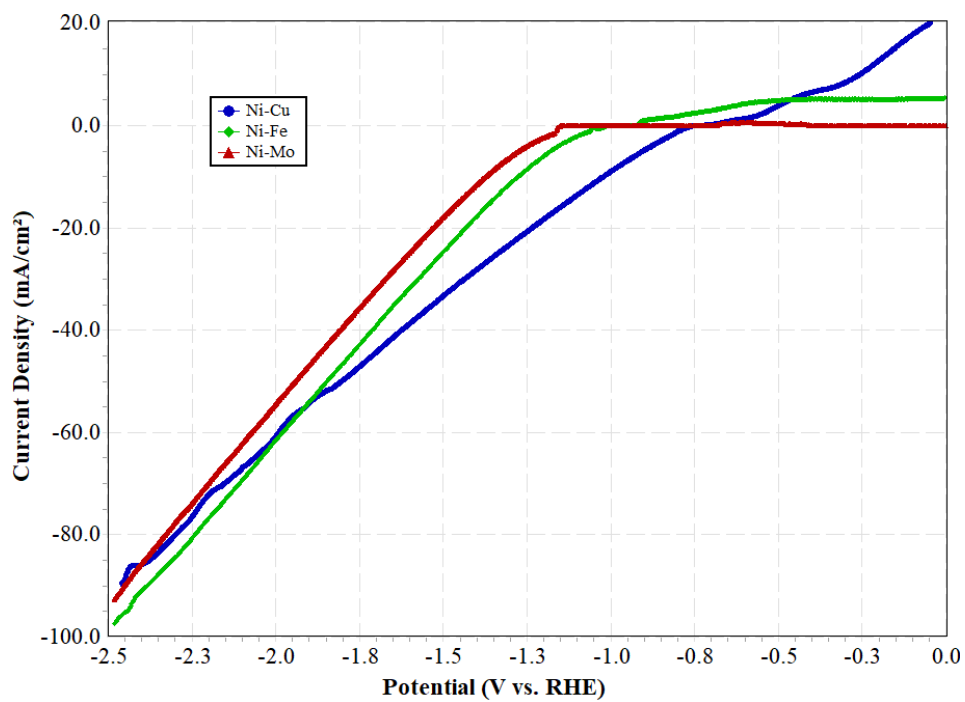


Figure 5.21 LSV measurements of nickel alloy coated CPLA 3D-printed electrodes in 1 mol KOH solution

5.3.2.1 Nickel Copper

Electrodeposition for various compositions of copper is investigated to better understand the properties of the catalyst. Figure 5.22 illustrates the CV measurements of three different copper depositions on nickel in 1 mol KOH electrolyte solution. All three electrodes have the same amount of deposition of nickel, only the amount of copper coating is increased with each electrode. Ni-Cu2x has two times the copper coating compared to Ni-Cu1x, and Ni-Cu3x as approximately three times the coating. The electrodes Ni-Cu1x, and Ni-Cu2x are coated at the same electrodeposition parameters, only the time for Ni-Cu2x is doubled. For Ni-Cu3x, the current at which the electrodeposition took place is reduced, and the coating time is increased. It can be observed that the current density of Ni-Cu3x (with three times more copper than Ni-Cu1x) is comparably higher. The relation of Ni-Cu1x, and Ni-Cu2x to each other, Ni-Cu2x has a slightly higher current for the same potential. The current densities are lower for lower voltages and similar for all three coating amounts. For the results, a longer copper deposition time to achieve more copper on the electrode surface can be seen to be beneficial.

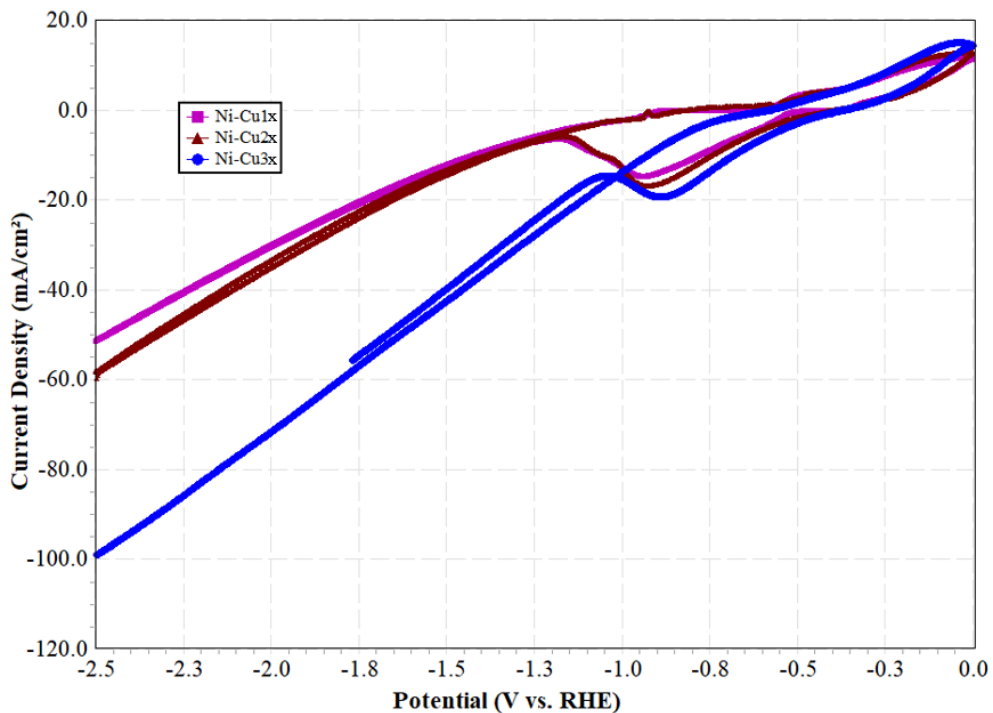


Figure 5.22 CV measurements of nickel-copper coated CPLA 3D-printed electrodes for different copper depositions in 1 mol KOH solution

The LSV measurements for the three different copper deposition amounts with nickel in 1 mol KOH solution are presented in Figure 5.23. Copper is plated on the CPLA 3D-printed electrodes for comparison with the nickel-copper alloy electrode. Both electrodes have the same amount of copper deposition. One notable difference between the Ni-Cu and Cu electrodes is the strength of the electrode. The nickel-copper electrode is much stronger, whereas the copper coating easily started to brake from the electrode surface.

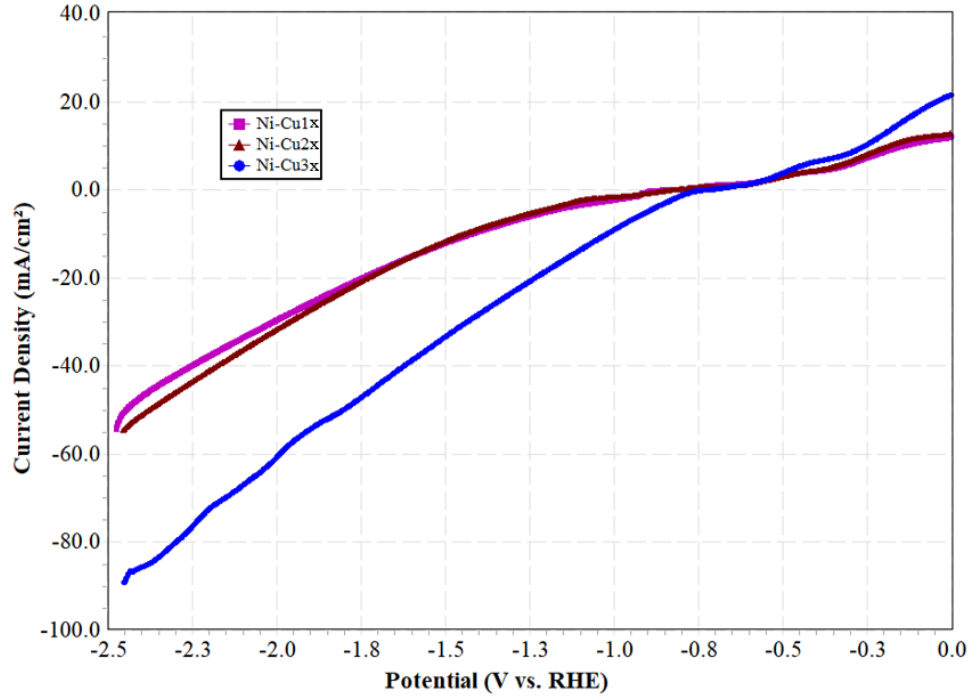


Figure 5.23 LSV measurements of nickel-copper coated CPLA 3D-printed electrodes for different copper depositions in 1 mol KOH solution

Figure 5.24 shows the LSV measurements for both the nickel-copper electrode and the copper electrode. The relation of the two electrodes is similar, at higher potentials the current densities are approximately the same. For potentials between 0.9 V and 2.1 V, the copper electrode has higher current densities at the same potential compared to the nickel-copper electrode. Higher copper depositions of the coating amount can significantly improve the current response of the electrodes. This is observed from the three different depositions amounts considered for the nickel-copper alloy.

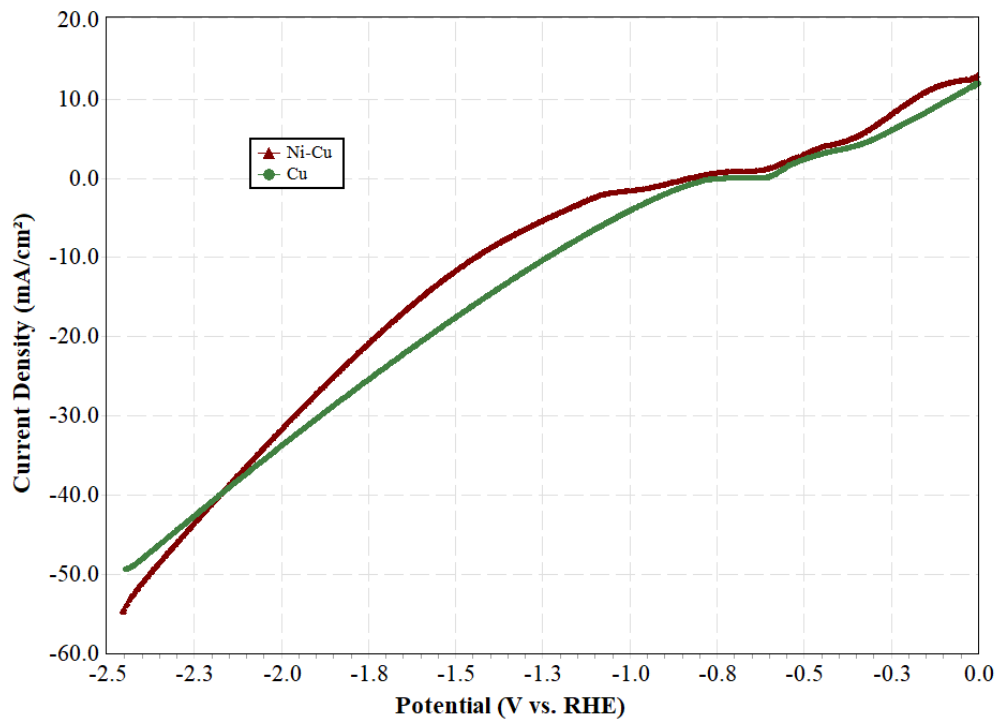


Figure 5.24 LSV measurements of nickel-copper coated vs copper-coated CPLA 3D-printed electrodes in 1 mol KOH solution

5.3.2.2 Nickel Molybdenum

Nickel with molybdenum is also coated on the CPLA 3D-printed electrodes. Two different compositions of molybdenum are considered. Ni-Mo1x has a molybdenum coating of 0.0728 g/cm^2 and Ni-Mo2x has a coating of 0.145 g/cm^2 which is two times of Ni-Mo1x. Figure 5.25 shows the CV measurements of the two nickel-molybdenum coated CPLA 3D-printed electrode samples. It can be seen from the figure that Ni-Mo2x has much higher current densities at the same potential compared to Ni-Mo1x. The forward and backward response of both electrodes is relatively similar. The current density for Ni-Mo1x and Ni-Mo2x is roughly zero at the same potential. At -2.5V the current density for Ni-Mo1x can be seen to be 60 mA/cm^2 . In comparison, Ni-Mo2x reaches a current density of 60 mA/cm^2 at around -1.9 V. The overpotential for Ni-Mo2x is much lower than it is for Ni-Mo1x. Interestingly, for a potential between -0.9 V and -1.3 V the current densities for Ni-Mo1x is measured to be higher than Ni-Mo2x. The overpotential at the current densities between this potential range would be slightly higher for Ni-Mo2x than Ni-Mo1x.

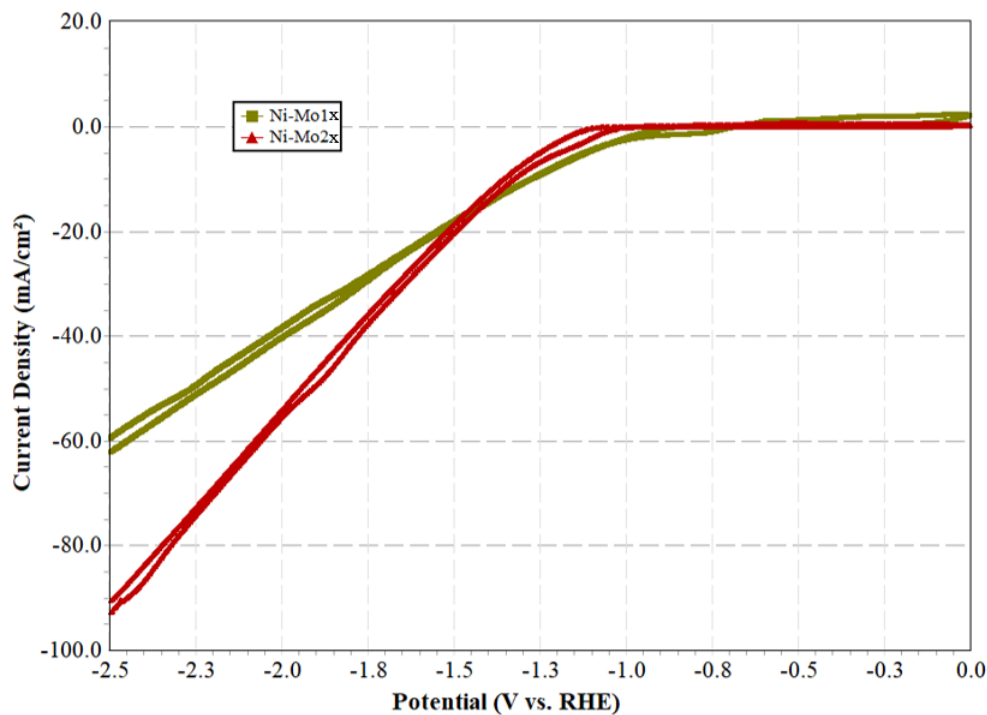


Figure 5.25 CV measurements of nickel-molybdenum coated CPLA 3D-printed electrodes for different molybdenum depositions in 1 mol KOH solution

Figure 5.26 presents the LSV measurements of the two nickel-molybdenum coated CPLA 3D-printed electrodes for two different deposition amounts of molybdenum. The measurements are relatively similar to the forward current response of the CV measurements. Similar current densities can be seen at the same potential for the Ni-Mo1x and Ni-Mo2x coated electrodes.

Figure 5.27 shows the LSV measurements of nickel-molybdenum sample with nickel coated first, and the nickel-molybdenum with both metals deposited together. The nickel-molybdenum (Ni-Mo) coated samples involve first coating the CPLA 3D-printed electrodes with nickel. Then the electrodes are coated with molybdenum for different compositions. In addition, Ni-Mo is also co-deposited on a CPLA 3D-printed electrode for comparison. An electrolyte bath consisting of both nickel sulfate (source of nickel ions) and ammonium molybdate (source of molybdenum ions) is used to coat both nickel and molybdenum at the same time.

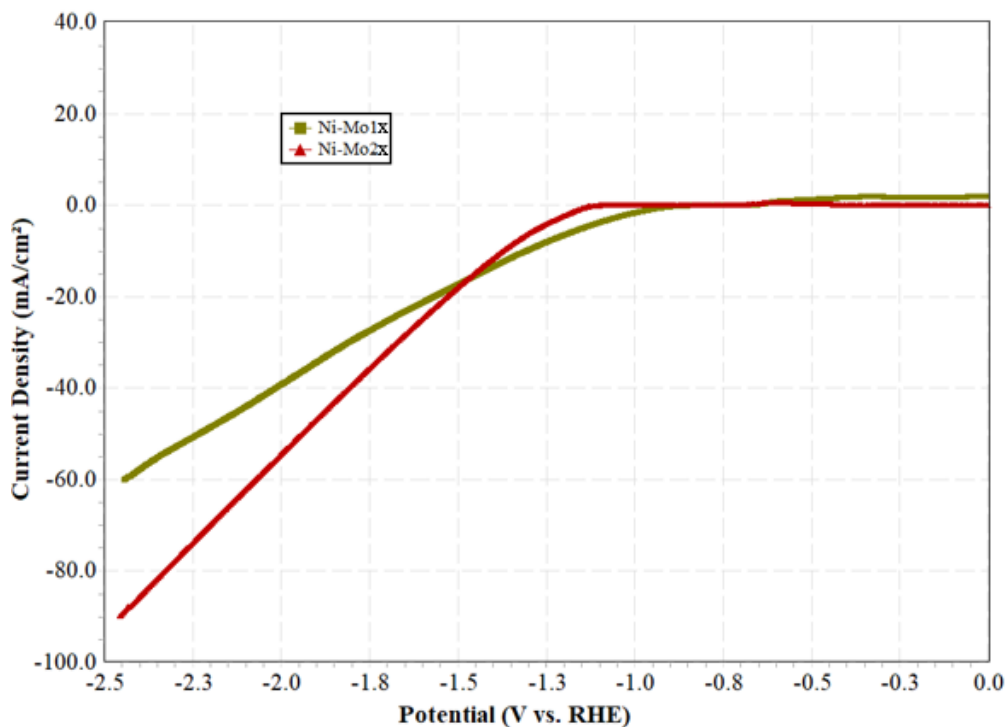


Figure 5.26 LSV measurements of nickel-molybdenum coated CPLA 3D-printed electrodes for different molybdenum depositions in 1 mol KOH solution

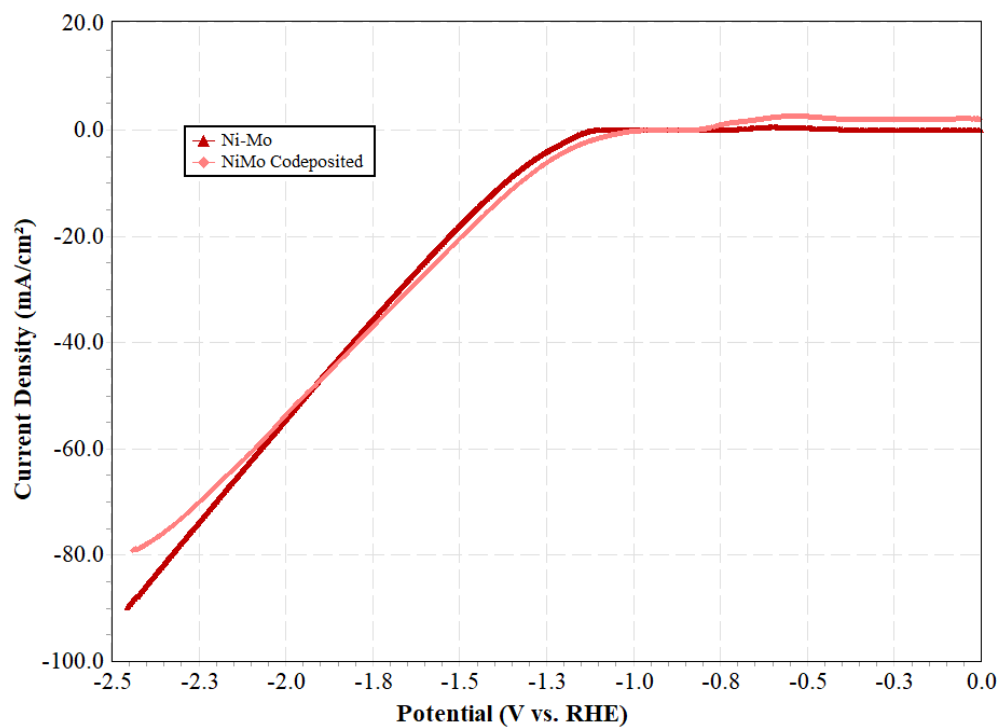


Figure 5.27 LSV measurements of nickel-molybdenum coated vs nickel-molybdenum co-deposited CPLA 3D-printed electrode in 1 mol KOH solution

For Ni-Mo samples represented in Figure 5.27, both have a coating of molybdenum of 0.145 g/cm^2 . It can be noticed from the figure that the current response of both the samples is relatively similar. At a potential of -2.5V , the nickel-molybdenum sample co-deposited has a slightly lower current density. In general, coating the electrode with nickel first, or co-depositing the two metals together did not show to make a huge difference in the current response. Although, coating the electrode with nickel first then the catalyst might be beneficial in some scenarios, such as reducing the input voltage required by the power supply. Due to the high resistance of the CPLA 3D-printed electrode, more power is required to coat the electrode. However, when the electrode is coated with nickel first, the second coat (molybdenum) does not require much more since the resistance of the electrode is significantly reduced by the nickel coating.

5.3.3 Impudence Measurements

The coated CPLA 3D-printed electrodes are tested using electrochemical impedance spectroscopy (EIS). The EIS measurements of the different samples are measured in 1 mol KOH in 400 ml distilled water solution. Figure 5.28 shows the bode plot representing impedance magnitude of the coated electrodes over frequency. The samples have a stable behaviour and tend to decrease from a frequency range of 0.1 Hz to 10 kHz . Major changes in the magnitude from 0.1 Hz to 10kHz are observed for the nickel coated CPLA 3D-printed electrode. The nickel coated electrode also has the highest impudence magnitude compared to the nickel alloy samples. The nickel-molybdenum coated electrode has the lowest impudence compared to all samples shown. In terms of the nickel alloy coated electrodes, nickel-iron sample has the highest impudence at low frequencies. At larger frequencies, all nickel alloy coated electrodes have approximately the same impudence.

Figure 5.29 shows the bode plot with the phase angle for the coated CPLA 3D-printed electrodes. A smooth transition is observed over a range of frequencies for the nickel coated and the nickel-iron coated CPLA printed electrodes. The nickel-molybdenum sample has the highest phase angle compared to the other samples, whereas the nickel coated electrode has the lowest phase angle. The negative phase angle are proportional to their

respective impedance magnitude. The samples that have a lower impedance magnitude, have a peak at a higher phase angle and vice versa.

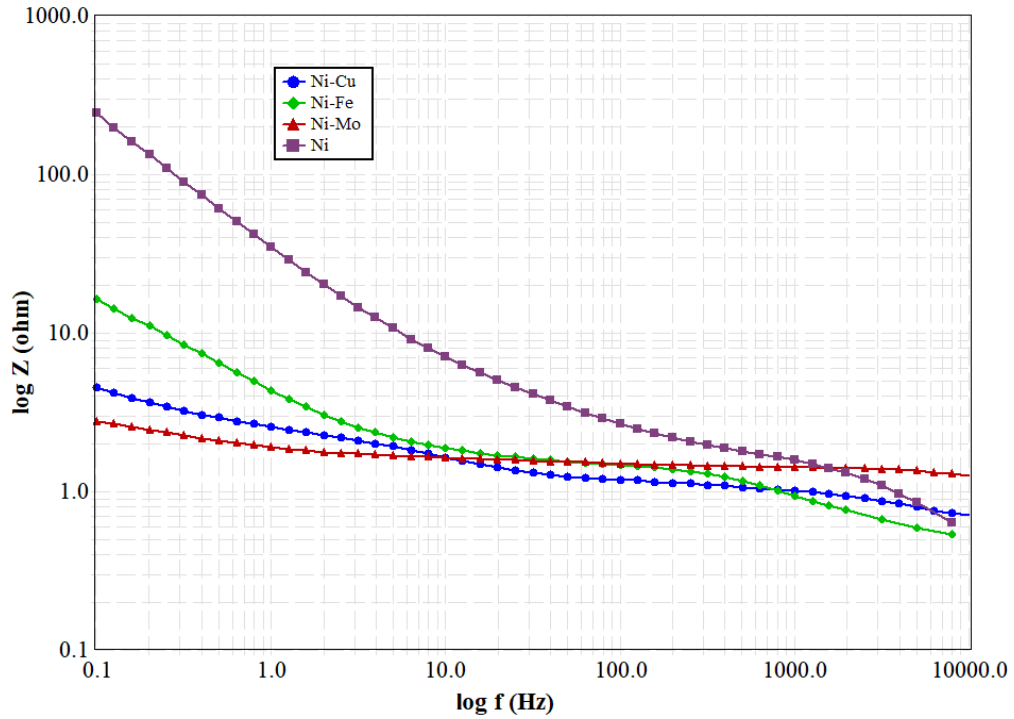


Figure 5.28 Bode plot for impedance magnitude for CPLA 3D-printed coated electrodes

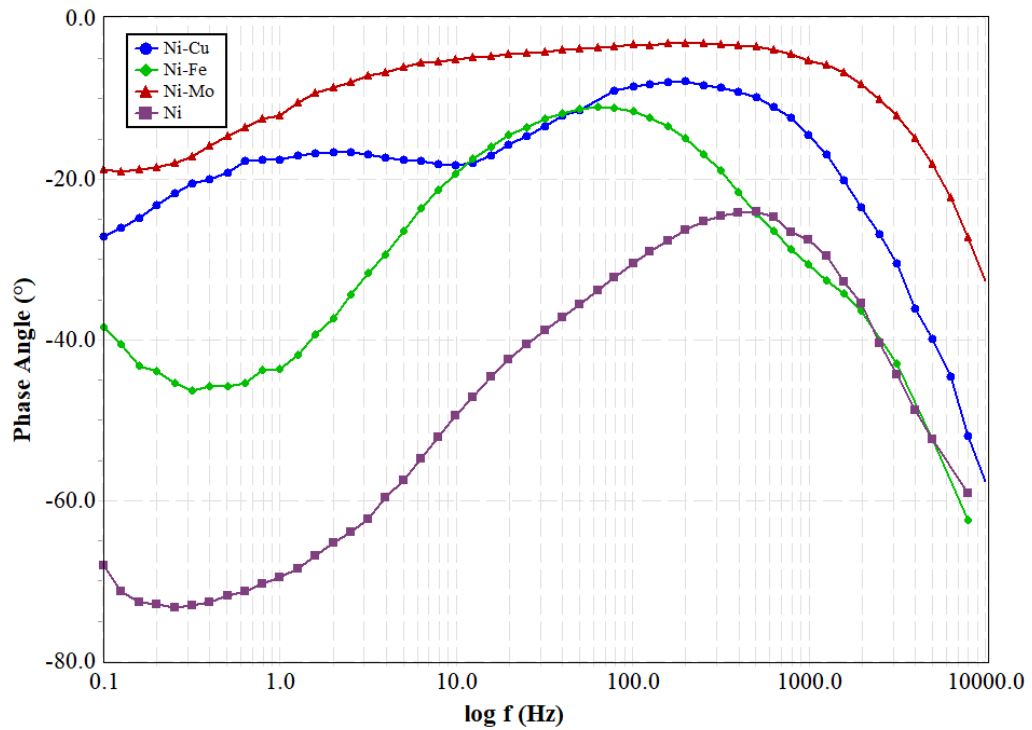


Figure 5.29 Bode plot for phase angle for CPLA 3D-printed coated electrodes

The Nyquist plot for the coated CPLA 3D-printed electrodes is shown in Figure 5.30. The plot shows the negative imaginary part of the impedance over the real part of the impedance. The nickel coated CPLA electrode has a significantly higher imaginary impedance compared to the nickel alloys. Nickel-molybdenum coated sample has the lowest impedance. In respect to the nickel alloy coated electrodes, the results show that the nickel-iron coated sample has the highest imaginary impedance over the real part. In general, the negative imaginary impedance tends to increase with an increase in the real.

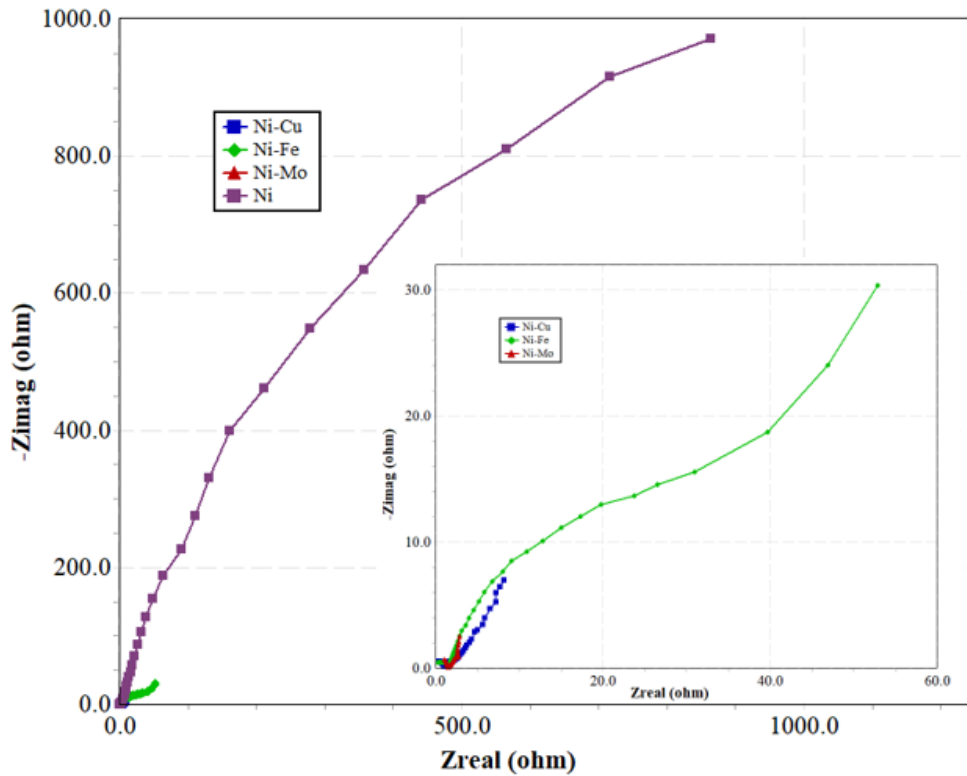


Figure 5.30 Nyquist plot for CPLA 3D-printed coated electrodes

5.3.4 Overpotential Results

The LSV measurements used to determine the overpotential of the coated CPLA 3D-printed electrodes are shown in Figure 5.31. The overpotentials calculated using the LSV measurements of the coated CPLA 3D-printed electrodes are illustrated in Figure 5.32. At a current density of 10 mA/cm² nickel-iron coated and nickel-copper have approximately the same overpotential, 270 mV, and 275 mV respectively. Nickel has the highest overpotential compared to all other samples considered. Nickel-molybdenum has a high overpotential at 10 mA/cm² compared to nickel-copper. However, at 20 mA/cm²

both nickel-copper, and nickel-molybdenum samples respectively have the same overpotential of 492 mV, and 499 mV respectively.

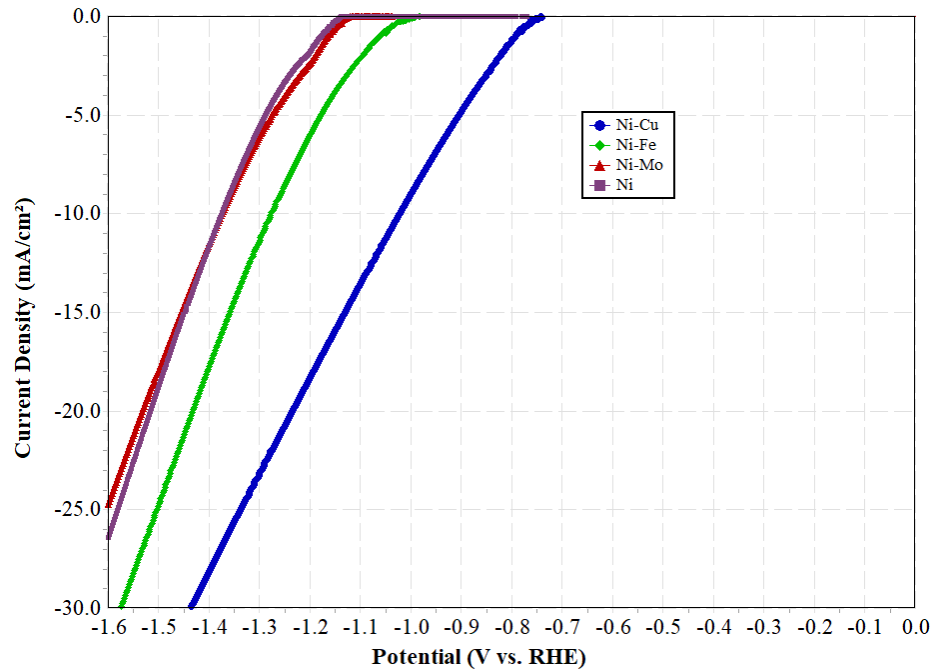


Figure 5.31 LSV measurements of coated CPLA 3D-printed electrodes for overpotential

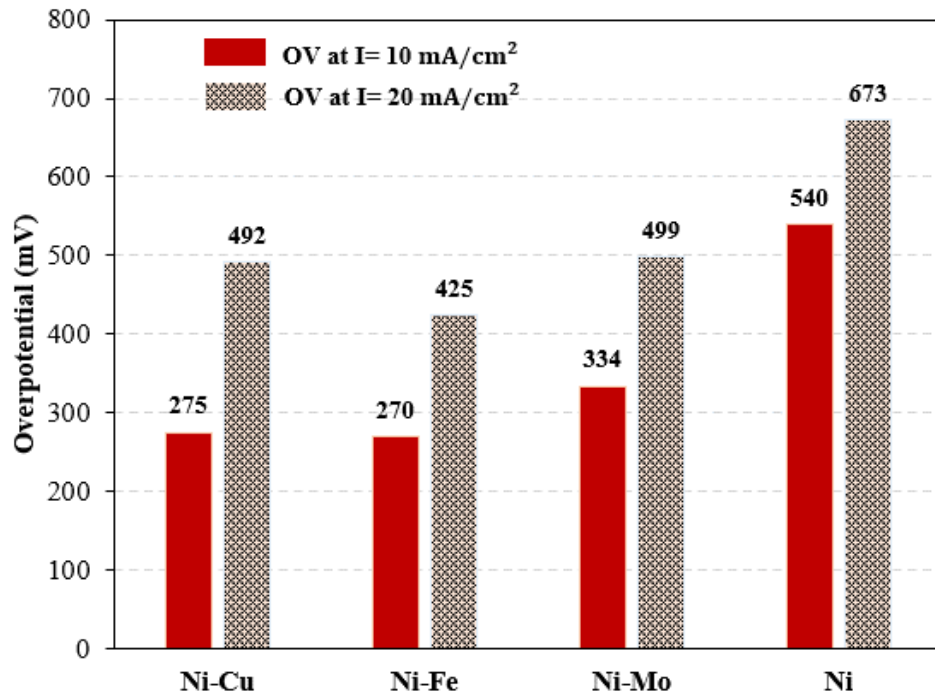


Figure 5.32 Overpotentials for CPLA 3D-printed coated electrodes

5.4 Flow Through Coated Electrodes

The flow through (D2) electrode design considered is 3D-printed with the conductive PLA and then coated following the same coating processes as the other electrodes using electrodeposition. The flow-through electrodes are coated with nickel, nickel-copper, and nickel-iron. Nickel is coated first on the electrodes, then the electrode is coated with either copper (for Ni-Cu) or nickel-iron co-deposition (for Ni-Fe). The D2 electrodes are tested using a similar electrochemistry system as the other electrodes. This section presents the electrochemical results gathered for the flow through electrodes. Results related to current density, impedance and overpotentials are discussed.

5.4.1 Current Density Measurements

The Cyclic Voltammetry (CV) measurements are taken for the coated CPLA 3D-printed flow through electrodes as well the uncoated electrode. Figure 5.33 shows CV measurements of the coated electrodes and the uncoated in 1 mol KOH solution. The uncoated electrode has a very current density, almost close to zero. This is due to the high resistance of the uncoated conductive PLA 3D-printed electrode. The nickel-copper coated flow through samples has the highest current density among the coated electrodes, and nickel has the lowest. The amount of coating on the nickel sample is 0.133 g/cm^2 , for nickel-copper is $0.0891 \text{ g/cm}^2 \text{ Ni}$, 0.0846 g/cm^2 and for the nickel-iron coating the coating is $0.178 \text{ g/cm}^2 \text{ Ni}$, $0.0851 \text{ g/cm}^2 \text{ Fe}$.

It is important to consider that some CV and LSV measurements of the electrodes show that the current density at potential is greater than zero. Due to certain impurities in the electrodes, there tends to be a current response at a potential of zero. The reference electrode can also be a factor. Under inadequate conditions with the reference electrodes, there can be an effect on the observed potential. Another potential cause is aging and possibly adhesion between layers is weak. This causes the coated metal layers on electrodes to come apart with time.

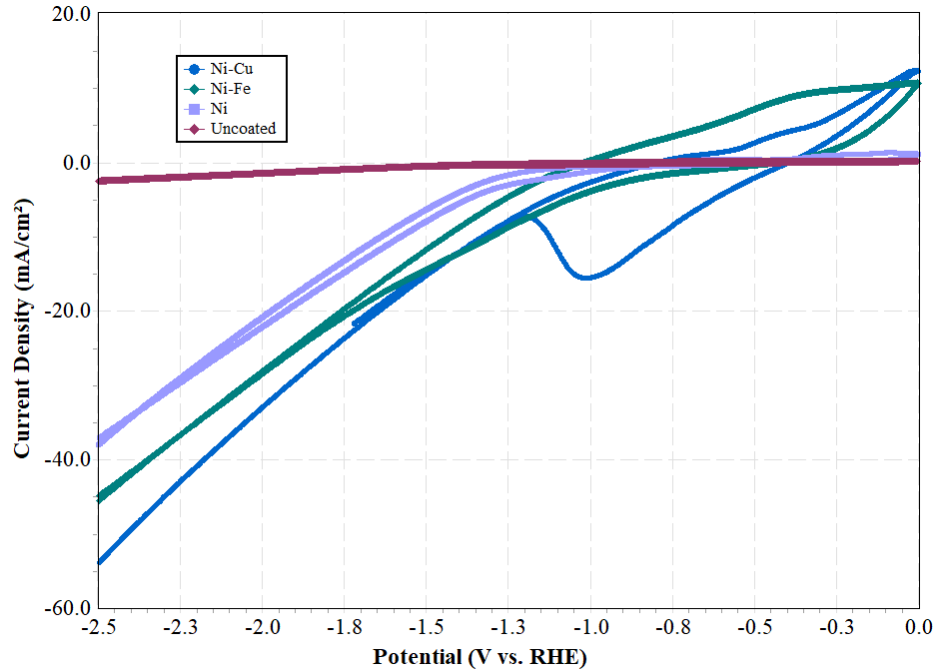


Figure 5.33 CV measurements of flow through coated electrodes and the uncoated electrode in 1 mol KOH solution

5.4.2 Impedance Measurements

Figure 5.34 shows the impedance magnetic for flow-through coated electrodes over a range of 0.1 Hz to 10 kHz frequency. The measurements for impedance are performed in 1 mol KOH solution using electrochemical impedance spectroscopy (EIS) measurements for nickel-copper coated and nickel-iron coated flow through samples. The nickel-iron coated electrode has a higher impedance at lower frequencies, but at higher frequencies the impedance is lower than the nickel-copper coated electrode. The impedance decreases with increase in frequency.

Figure 5.35 presents the bode plot with the phase angle for the coated flow through CPLA 3D-printed electrodes. The nickel-copper coated and nickel-iron coated flow through electrodes both have a smooth transition over the range of frequencies. Both electrodes have a phase angle peak at roughly the same phase angle. The amplitude of the nickel-iron electrode is bigger.

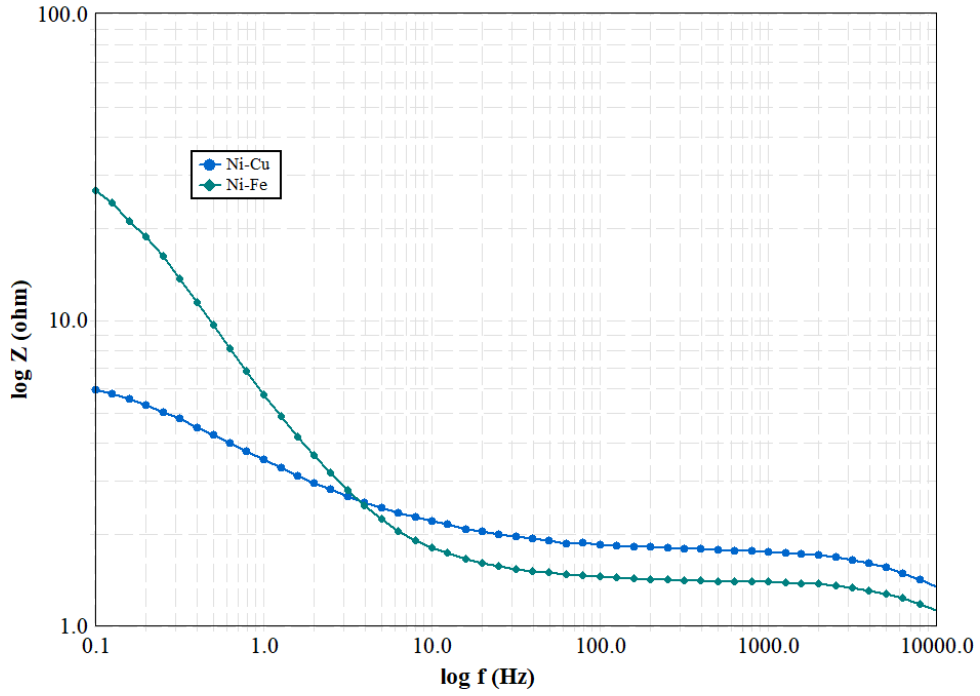


Figure 5.34 Bode plot for impedance magnitude for flow through (D2) coated electrodes

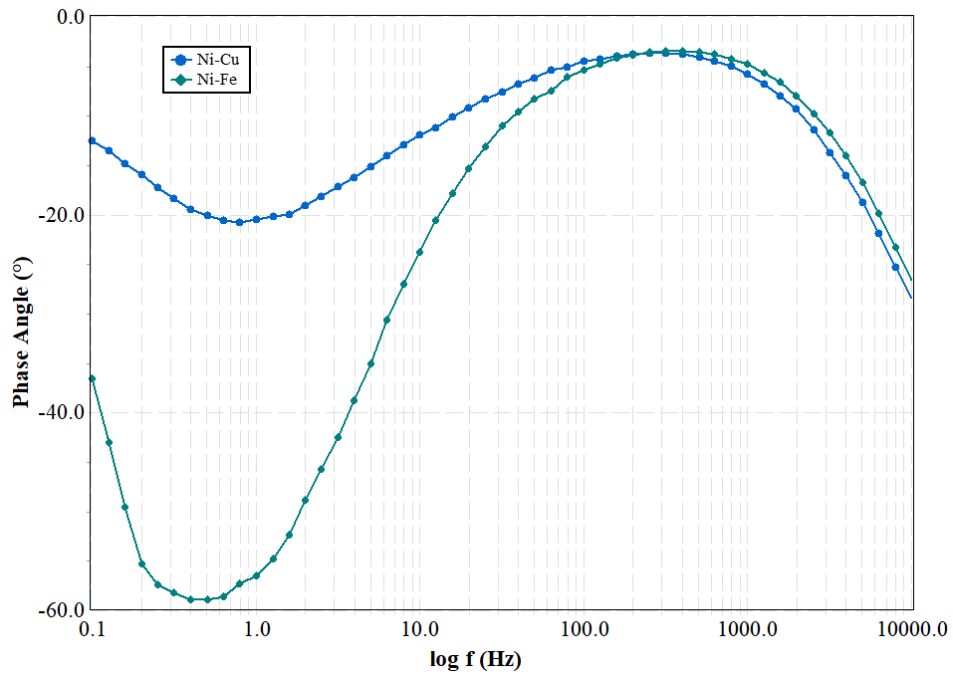


Figure 5.35 Bode plot for phase angle for flow through (D2) coated electrodes

Figure 5.6 shows the Nyquist plot of the nickel-copper coated and nickel-iron coated flow through electrodes. The nickel-iron coated electrode has a much higher impedance compared to nickel-copper. The impedance of both electrodes is similar to the one obtained for the coated CPLA 3D-printed and NCP 3D-printed electrodes of the same metals. The design of the electrode doesn't have an effect on the impedance, rather its related to the properties of the metal themselves.

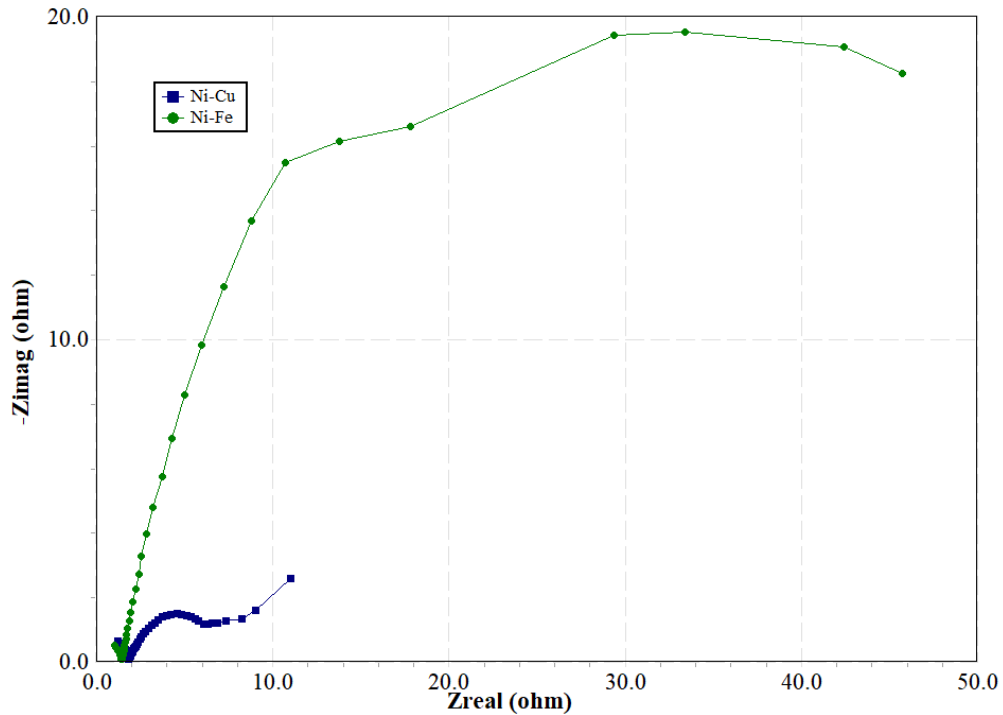


Figure 5.36 Nyquist plot for flow through (D2) coated electrodes

5.4.3 Overpotential Results

The LSV measurements of the coated CPLA 3D-printed flow through electrodes is shown in Figure 5.7. These measurements are used to calculate the overpotentials of the nickel-copper coated and the nickel-iron coated flow-through electrodes. The nickel coated electrode has a much lower current densities at the same potential compared to nickel-copper coated, and nickel-iron coated electrode. Similar to the coated CPLA 3D-printed electrodes, nickel would have the highest overpotential compared to Ni-Cu coated and Ni-Fe coated electrodes. that the nickel-iron coated electrode has a lower overpotential than nickel-copper coated flow through electrodes.

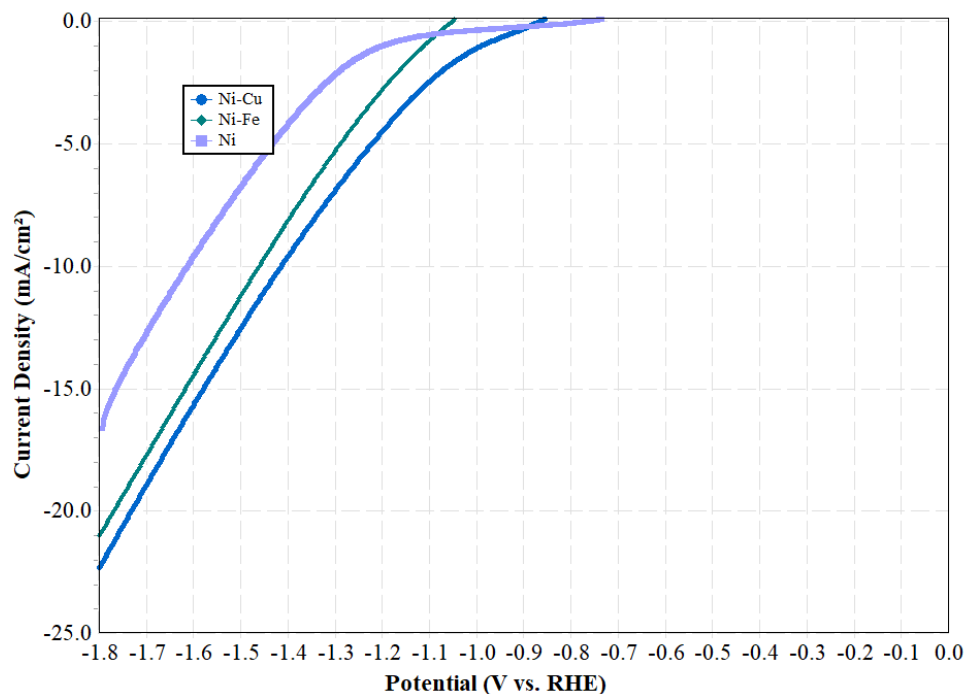


Figure 5.37 LSV measurements of flow through coated electrodes in 1 mol KOH solution

Figure 5.38 shows the overpotentials of the coated nickel-copper and nickel-iron flow through electrodes for three different current densities. It can be observed other coated electrodes in the thesis where Ni-Fe coated electrodes have the lowest overpotential. In comparison to the initial design coated CPLA 3D-printed electrodes, the overpotentials are much higher. Overpotentials are directly related to the properties of the metal. The metal deposited on the flow-through electrodes is less which is a contributing factor for higher overpotentials that are observed.

The overpotentials obtained are related to the impedance of the electrodes. Referring to the impedance measurements obtained, it can be observed that electrodes that have higher impedance tend to have higher overpotential. Due to the increased resistance, the electrode requires more energy to overcome the potential for reaching the same current. It should also be taken into consideration that these only account for the activation overpotential. In operation for hydrogen production, there may be an increase in overall overpotential due to an increase in ohmic overpotential. This would be a result of the resistance between the electrolyte and the electrode surface.

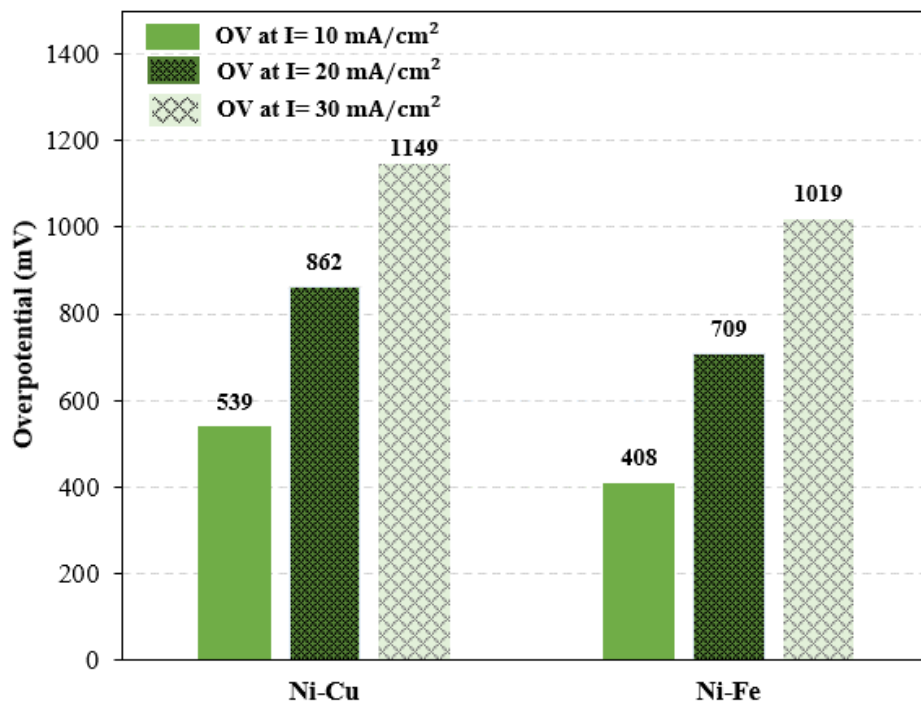


Figure 5.38 Overpotentials for flow through coated electrodes

5.5 Comparative with Related Literature Studies

The performance of the coated 3D-printed electrodes is compared with recent literature studies. Additive manufacturing has been investigated for electrochemistry for a wide range of applications, however only a few researchers have looked at 3D-printed electrodes for hydrogen evolution reaction using the methods in this thesis. Huner et al. [45] were among one of the few who 3D-printed electrodes using conductive PLA and then used electrodeposition as a coating technique. Figure 5.39 shows the current densities of the nickel-copper electrode coated in their study and the Ni-Cu1x from this thesis project. There were three nickel-copper electrodes considered in their study, and each have a different amount of the copper coating. These were composed of 0.0390 g/cm², 0.0404 g/cm², and 0.0420 g/cm². The Ni-Cu1x electrode studied in the thesis have a coating of 0.0423 g/cm² which is the least amount of copper composition deposited from the three sampled studied in the thesis (Ni-Cu1x, Ni-Cu2x, and Ni-Cu3x). The electrode with the copper coating of 0.0420 g/cm² from Huner et al. study is compared with the Ni-Cu1x, which has approximately the same amount of copper deposited. At -1.2V, both electrodes have roughly the same current density of -20 mA/cm².

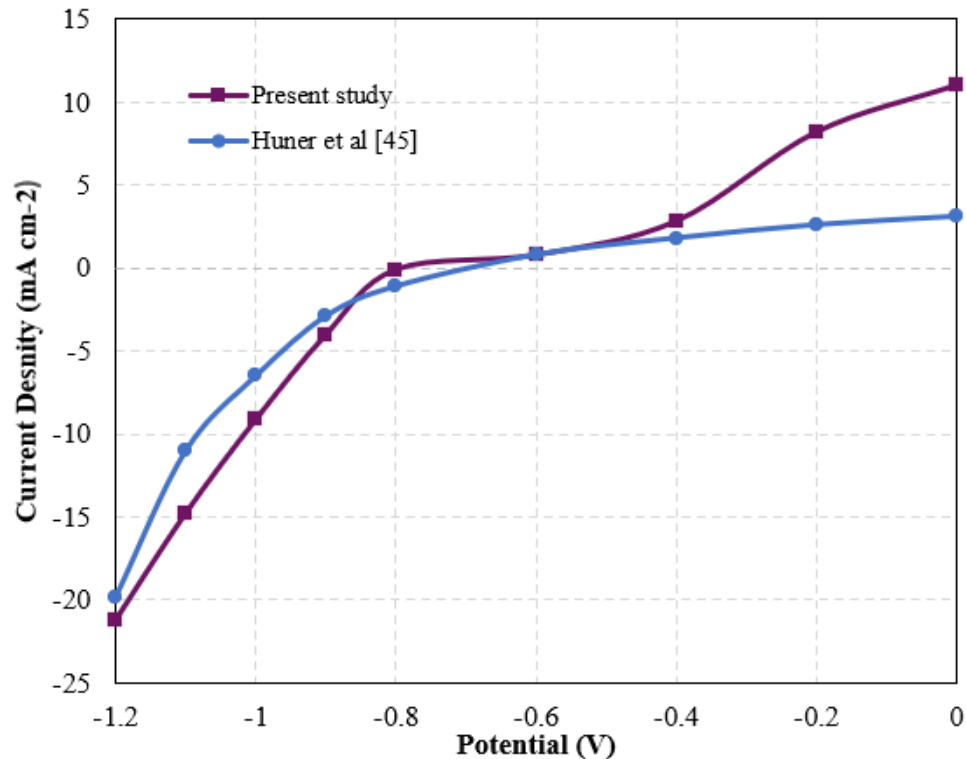


Figure 5.39 A comparison of current density obtained for the nickel-copper coated electrodes from this study with Huner et al. [45] study

The conditions at which electrodes from both studies are prepared were similar, they both are performed at room temperature using the same chemical compositions of the electrolyte bath. The exact current and time for the copper coating is not provided, but the full electrodeposition process is performed for 4h. For the Ni-Cu1x sample in the present study, the copper coating is only coated for 1h at a current of 0.7A. It is possible, the electrodes in Huner et al. study was likely coated for a longer duration than Ni-Cu1x at a lower current. It should also be noted that the geometry of the electrode in this study is different from Huner et al. study.

Further, the nickel-iron coated CPLA 3D-printed electrode from this study is compared with Han et al. [48] nickel-iron electrode produced using direct photo-curing. Figure 5.40 shows a comparison of overpotential obtained for the nickel-iron coated electrode in the present study with Han et al. [48] study. The direct comparison between the electrodes is the two different approaches used. It is evident that the overpotential of the electrode in their study is lower, and this is possibly due to the technique they used.

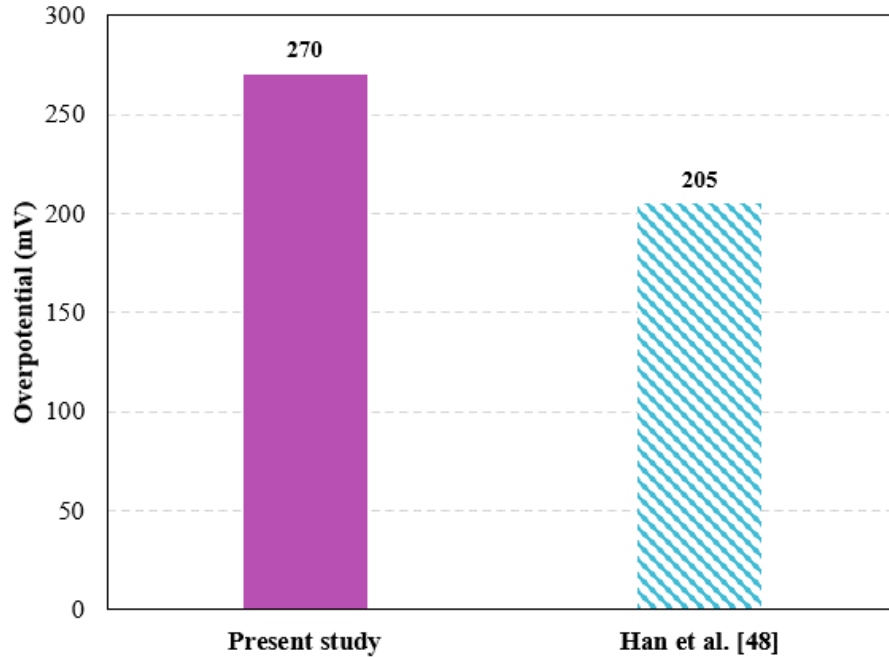


Figure 5.40 A comparison of overpotential obtained for the nickel-iron coated electrodes from this study with Han et al. [48]

Photo-curing is more accurate in terms of accuracy, but much more complex and requires more steps. For the nickel-iron electrode from this study, nickel-iron alloy coating using electrodeposition is found difficult because of the corrosive properties of iron. A larger deposition of the nickel coating is required in order to prevent iron from corroding after electrodeposition. This can be a possible factor for the higher overpotential obtained. Another factor which could contribute to lower potential for Han et al. study is more metal deposition. As seen from the results earlier, the current densities are higher for more metal depositions, and tend to have lower overpotentials.

5.6 Electrolysis Cathodic Testing Results for Hydrogen Potential

The different types of coated 3D-printed electrodes are tested as the cathode in an electrolysis testing cell for hydrogen production. The HQ-8 hydrogen sensor with Arduino is used to measure the amount of hydrogen produced. Due to the sensitivity of the sensor measurements are only recorded at the end of each run time. The power supply is turned off, and the final reading is only recoded at the end of each run when the readings stabilized. This is due to the delay between the time the hydrogen is produced until it reaches the sensor, therefore the hydrogen needs to be accumulated in the hydrogen storage cylinder

until a stable reading is obtained by the sensor. All readings are recorded in ppm and then converted to mg/m³ using the conversion formula given by equation 5.1 [77].

$$\frac{mg}{m^3} = ppm \times \frac{M}{22.4} \times \frac{273}{(273+T)} \times \frac{P}{1013} \quad (5.1)$$

where M is the molar weight of the substance (hydrogen), T is the temperature in Kelvins and P is the pressure in hPa.

The amount of hydrogen produced during the duration of the operation is calculated using the mg/m³ calculated and multiplying by the area of the hydrogen storage container (0.00532 m³) where the hydrogen reading is measured. The amount of hydrogen produced is then used to calculate the rate of hydrogen production assuming a constant rate of hydrogen during the period of time the coated 3D-printed cathode is supplied power for. To determine the changes in the hydrogen mass flow rate, some electrodes are tested for different run times to determine if the mass flow rate remained constant with time or changed. Due to the high error and sensitivity of the hydrogen sensor, each experiment is performed three times and the average value is taken and used for the results. All hydrogen testing experiments are conducted using a 316 stainless steel industrially prepared anode roughly the same size as the coated 3D-printed cathodes prepared in the study. The energy and exergy efficiencies of the electrolysis cell are also calculated based on the thermodynamic and hydrogen efficiency analysis discussed in section 4 of the thesis. This section presents and discusses the results for hydrogen mass flow and efficiencies of each tested cathode obtained from hydrogen production testing.

5.6.1 Hydrogen Production Rates

This section presents the results obtained for hydrogen production rates for the different coated 3D-printed cathodes tested for different testing times. The hydrogen mass flow rates obtained are based on the measured hydrogen produced at each testing time. All tests are performed for three times to minimize random error, and an average of the three runs is taken. First the electrodes are tested for only 15 minutes to determine the hydrogen mass flow rate at the start. The nickel-copper and nickel-iron coated electrodes are tested for 30 minutes. These electrodes are selected for additional testing based on their performance and strength, as well as their stability during coating using electrodeposition which made

them suitable candidate for cathodes for hydrogen production. The nickel-copper electrodes are found to be the most suitable for electroplating. In addition, the electrodes have good current response and reasonable overpotentials based on the electrochemical testing performed. Hence, the nickel-copper coated electrodes are also tested for 1 hour to further evaluate their performance.

Figure 5.41 shows the average (from the three runs) hydrogen mass flow rates for the coated NCP 3D-printed electrodes in the first 15 minutes of the cathode testing. For the coated NCP 3D-printed electrodes, it can be observed that the nickel-copper coated electrodes have the highest mass flow rates. The nickel coated electrodes have the lowest mass flow rate.

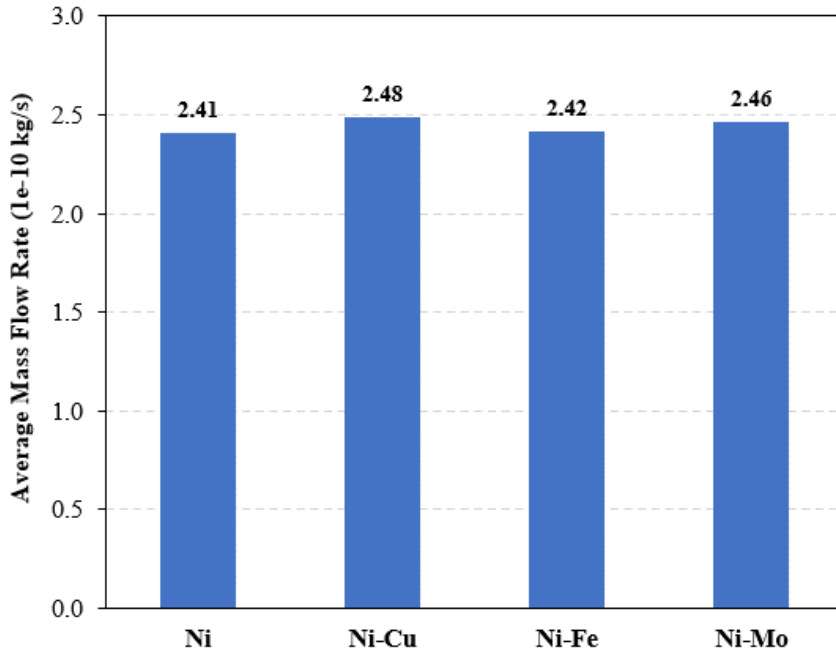


Figure 5.41 Average hydrogen mass flow rate for coated NCP 3D-printed electrodes for a run time of 15 minutes

Figure 5.42 shows the average mass flows from the three trials run for 15 minutes each for the coated CPLA 3D-printed electrodes. In comparison, for the coated CPLA coated electrodes, the nickel-molybdenum has the highest hydrogen production rate. The nickel coated CPLA electrodes have the lowest rate from all the tested cathodes. In terms of the durability, the coated CPLA 3D-printed electrodes are the best for hydrogen production

due to their strength. For the coated NCP 3D-printed electrodes, due to the painted surface the electrodes are too brittle. After a few hydrogen tests the electrodes would break apart.

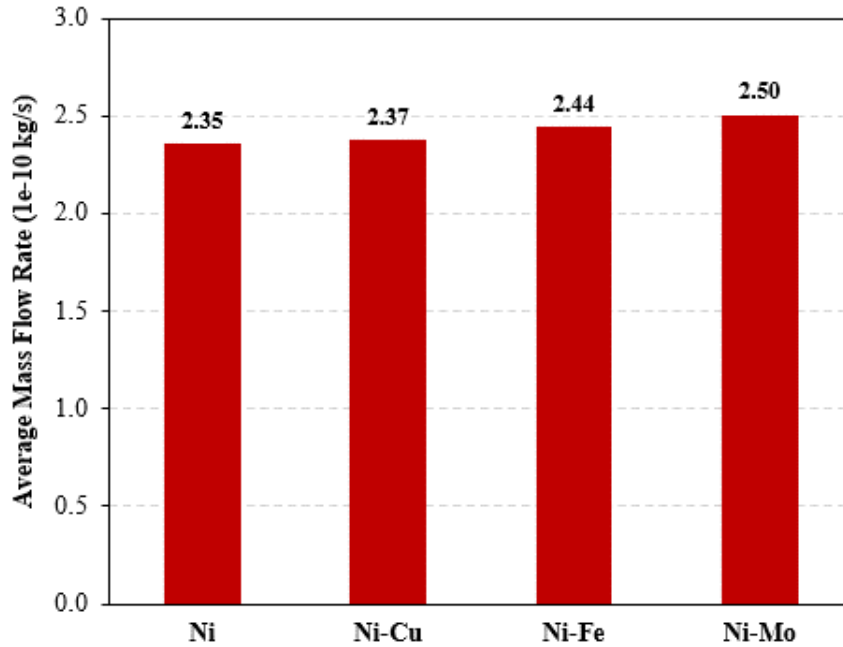


Figure 5.42 Average hydrogen mass flow rate for coated CPLA 3D-printed electrodes for a run time of 15 minutes

Figure 5.43 shows the average hydrogen mass flow measured for the three runs for the first 15 minutes of operation for the flow through electrodes. Only the nickel-copper coated and nickel-iron coated flow through electrodes are tested for hydrogen potential. The performance of the flow through electrodes is compared with the solid (initial design) coated CPLA 3D-printed electrodes.

It can be observed that the mass flow rate of the flow through electrodes is higher compared to the solid plate design electrode. The main reason for is that the flow through electrodes improve mass transport by prompting movement of the gasses produced (hydrogen) and the electrolyte. The faster evacuation of the gasses allows more electrolyte to interact with the electrode increasing the rate of hydrogen produced. It is important to note, the amount of the nickel-copper and nickel-iron coating on the flow through electrodes is less than of the initial electrode design.

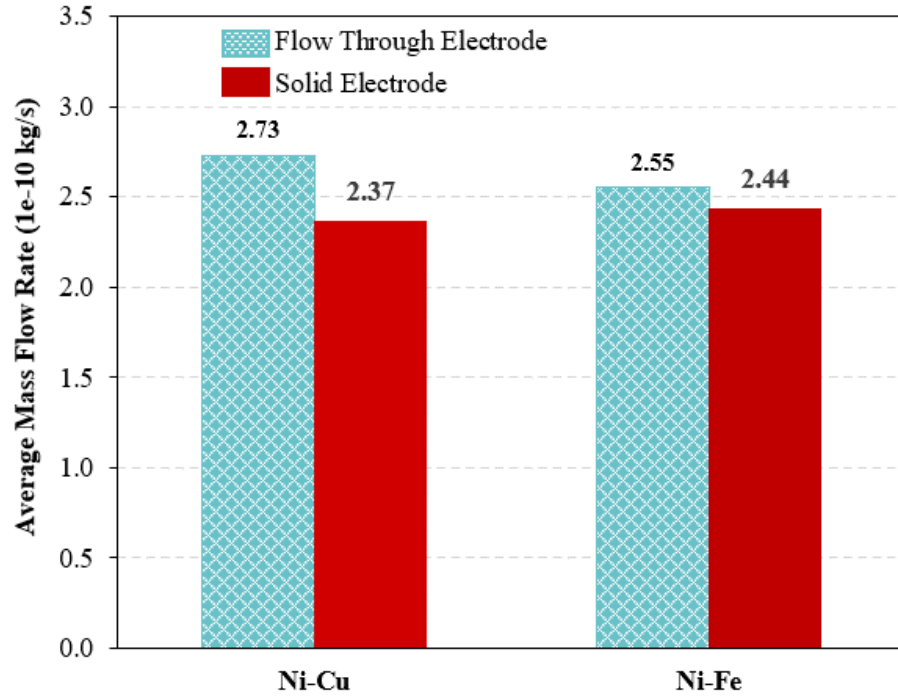


Figure 5.43 Average hydrogen mass flow rate for coated CPLA 3D-printed electrodes for flow through electrodes versus initial design for a run time of 15 minutes

The significance of the amount of metal coating related to hydrogen production will need to be investigated to determine if there is a difference. Regardless, the electrode performance is increased with the metal coating amount as seen with the studies from electrochemical testing of the thesis. Even though the initially designed electrodes have more amounts of the same metal, the flow through electrodes still perform better in comparison due to their porous design.

5.6.2 Hydrogen Rates for Extended Testing Run Time

The nickel-copper and the nickel-iron coated electrodes are tested again for extended hydrogen measurement times of 30 minutes three times. The results are averaged to determine the hydrogen mass flow rates. Figure 5.44 shows the flow rate of the nickel-copper and the nickel-iron coated NCP 3D-printed electrodes. The figure compares the mass flow rates measured for the 15-minute test versus the 30-minute test. For both coated electrodes the mass flow rate decreases within the first 30 minutes.

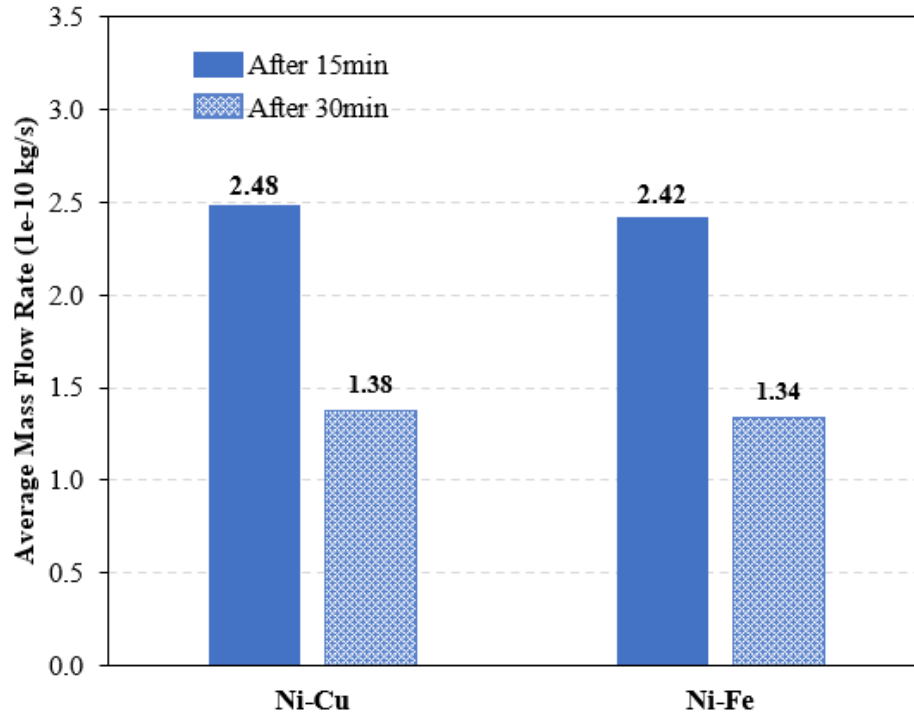


Figure 5.44 Average hydrogen mass flow rate for Ni-Cu and Ni-Fe coated NCP 3D-printed electrodes for a run time of 15 minutes versus 30 minutes

Figure 5.45 shows the average mass flow rates of the nickel-copper and the nickel-iron coated CPLA 3D-printed electrodes. Like the coated NCP 3D-printed electrodes, the hydrogen mass flow rates are also observed for a 15-minute hydrogen test and a 30-minute hydrogen test. Again, the hydrogen mass flow rate for the 30-minute significantly decreases. During the start of the electrodes the reaction is activated, and the electrodes are more efficient. With operation, the current in the circuit decreases due to many reasons such as the interaction between the electrolyte and the gasses produce which increase the ohmic potential due to increase in resistance. In this case, more voltage would be required to maintain the initial hydrogen mass flow. Since the supplied DC voltage is kept the same, ultimately the rate of hydrogen produced decreases. It is also observed that the current supplied is higher at the start of the experiments, by the end of each timed measurement, the current at the same voltage (2.5 V) significantly decreases.

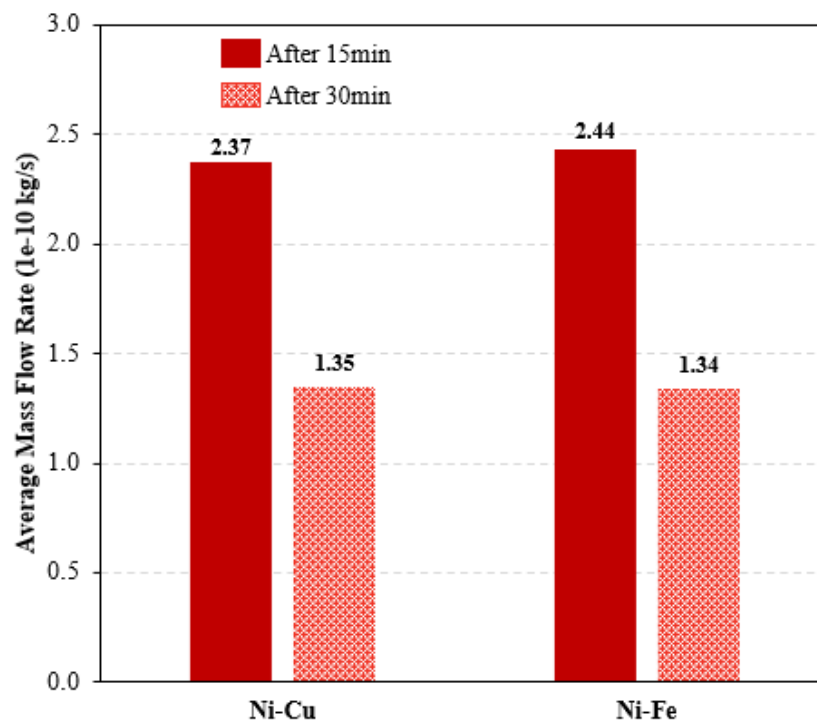


Figure 5.45 Average hydrogen mass flow rate for Ni-Cu and Ni-Fe coated CPLA 3D-printed electrodes for a run time of 15 minutes versus 30 minutes

To further evaluate the performance of the coated electrodes, the nickel-copper samples are tested for 1 hour three times to obtain average results. From the results of the experiments conducted at the three times (15 min, 30 min, and 1 h) a relation between the hydrogen mass flow rate and the operation time is developed. The tests are performed for the nickel-copper coated flow through and the initial design coated CPLA 3D-printed electrodes. Figure 5.46 compares the performance of the nickel-copper coated flow through and the solid coated CPLA 3D-printed electrodes for 1 hour. It can be seen that the mass flow rate is very high in the first 15 minutes, past which the flow rate decreases until it is stabilized. It can be observed that the flow-through electrode has a higher flow rate at the start compared to the initial design. With time the mass flow rate of the two electrodes is relatively similar.

The performance of the coated electrodes needs to be further investigated to understand the behaviour of the coated 3D-printed electrodes. Due to these variations, hydrogen testing is found to be crucial to understand the activity of coated 3D-printed electrodes. CV and LSV measurements are good for understanding the current response of the electrodes. However,

the measurements do not account for the variation in current operation time, the current response is only given at the different potentials.

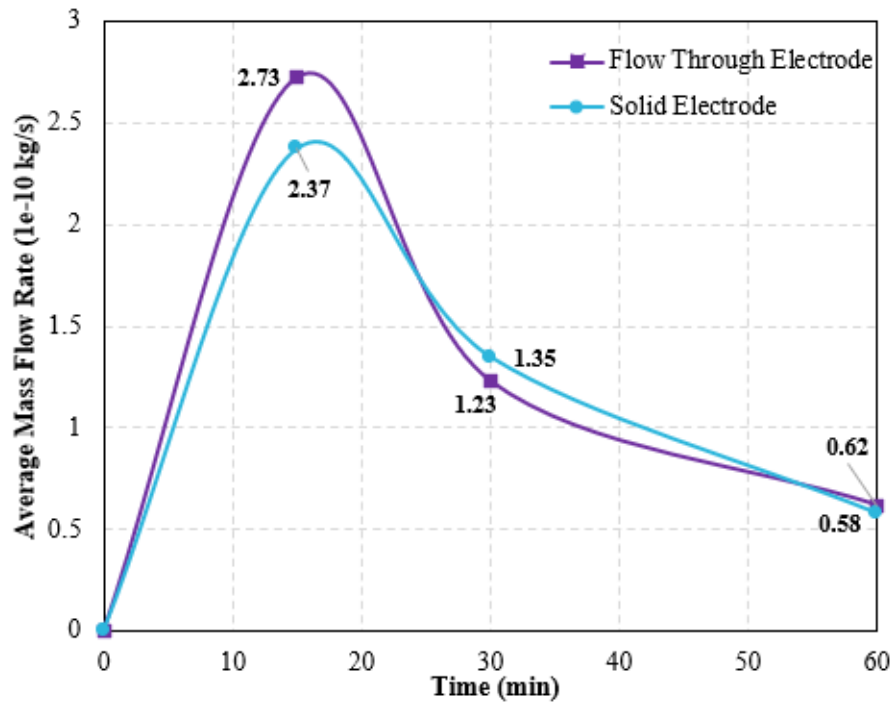


Figure 5.46 Average hydrogen mass flow rate for Ni-Cu coated CPLA 3D-printed flow through (D2) and solid (initial design) electrodes relation with operation time

5.6.3 Energy and Exergy Efficiency Results

The energy and exergy efficiencies of the cathodic electrodes are calculated based on the hydrogen mass flow rates obtained and the energy input into the electrolysis testing cell. The calculations are made based on the energy and exergy analysis presented in section 4 of the thesis. The voltage supplied for each experiment is 2.5 V. The total energy input into the electrolysis testing cell varied for each testing cathode depending on the resistance. The actual current which is supplied at this potential is measured when it stabilized. The current at start is generally higher, eventually the current stabilized, which is recorded and used to calculate the energy input into the electrolysis testing cell. The efficiencies are calculated based on the 15 minutes operation time, the rate of hydrogen produced is the highest for these experiments. Regardless of the declination in the mass flow rate after the first 15 mins, very slight or no changes are observed in the efficiency for extended testing times.

As the mass flow rate decreased the current supplied is reduced therefore reducing the energy input into the electrolysis.

Figure 5.47 shows the energy and exergy efficiencies of the coated NCP 3D-printed electrodes. The specific exergy of hydrogen is lower than its lower heating value, therefore the exergy efficiency obtained is lower than the energy efficiency. Referring to Figure 5.47 it can be observed that the energy and exergy efficiency of the nickel-molybdenum (Ni-Mo) electrodes is the highest compared to the other coated NCP 3D-printed electrodes. The Ni-Mo coated NCP 3D-printed electrode have the highest rate of hydrogen produced. In addition, the Ni-Mo coated electrode have the lowest amount of energy input.

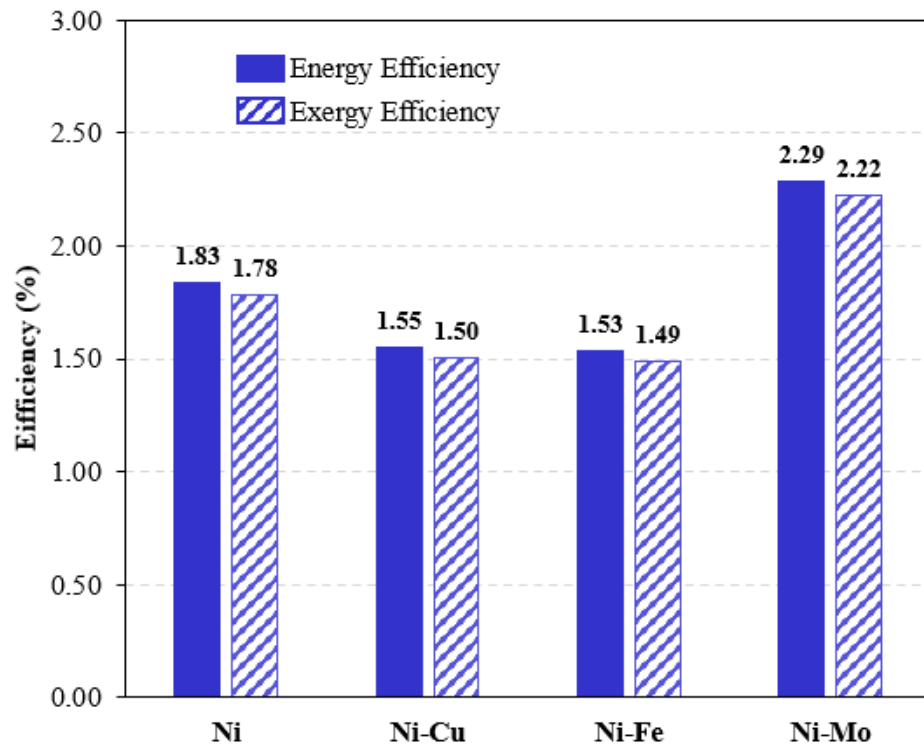


Figure 5.47 Energy and exergy efficiencies for coated NCP 3D-printed electrodes

Figure 5.48 shows the current densities of the coated NCP 3D-printed electrodes measured by the potentiostat and based on the actual current recorded during hydrogen testing. It can be seen from Figure 5.48 that the actual recorded current density at 2.5 V is the lowest compared to the other samples. Referring back to the overpotentials of the coated NCP 3D-printed electrodes, the Ni-Mo coated electrode has the lowest overpotential. This is one of the main reasons a high energy efficiency is obtained for the Ni-Mo coated

3D-printed electrode. The other coated electrodes have relatively similar efficiencies. Interestingly, the Ni coated NCP 3D-printed electrode has a slightly higher efficiency compared to the Ni-Cu and Ni-Fe coated electrodes. Sample J from the nickel coated NCP 3D-printed electrodes is tested for hydrogen production. This sample has the highest current density and lowest overpotential at high current densities compared to other nickel coated samples.

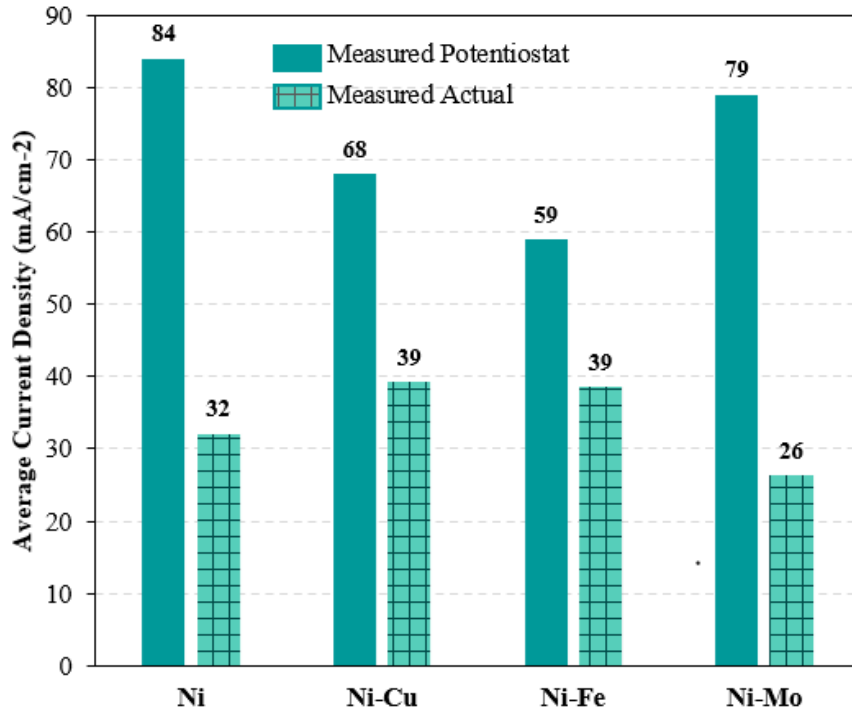


Figure 5.48 Current densities at 2.5V for coated NCP 3D-printed electrodes measured by potentiostat versus actual during hydrogen production

Figure 5.49 shows the energy and exergy efficiencies of the coated CPLA 3D-printed electrodes. For the coated CPLA 3D-printed electrodes, the efficiencies obtained can be seen to be higher compared to the coated NCP 3D-printed electrodes. Figure 5.50 shows the actual current density recorded during hydrogen production and the measured current density with the potentiostat. One main contribution to this is the lower current at the same potential as seen in Figure 5.50. From the coated CPLA 3D-printed electrodes, the nickel and nickel-molybdenum coated electrodes have the highest efficiencies.

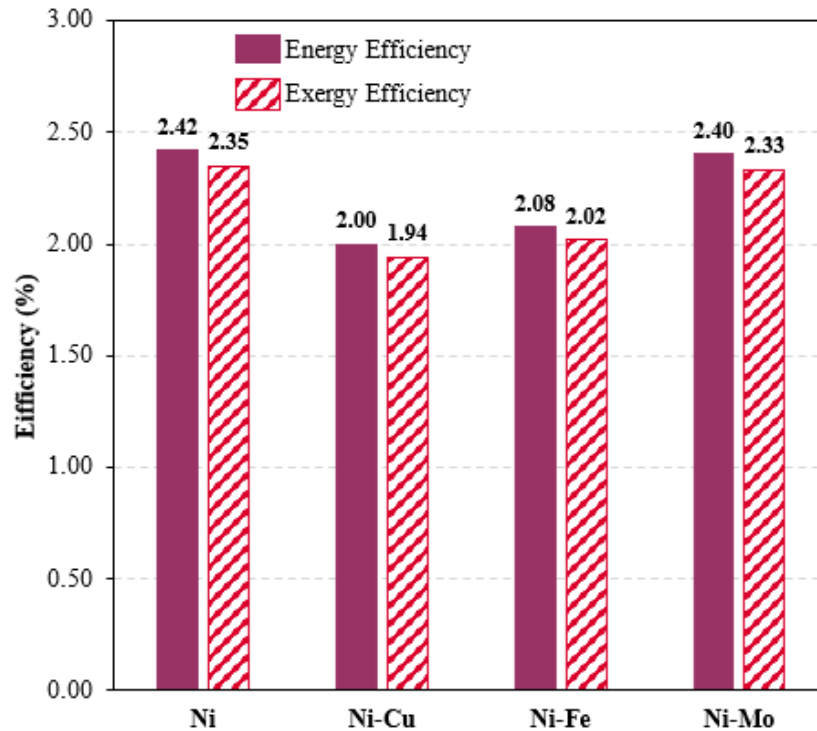


Figure 5.49 Energy and exergy efficiencies for coated CPLA 3D-printed electrodes

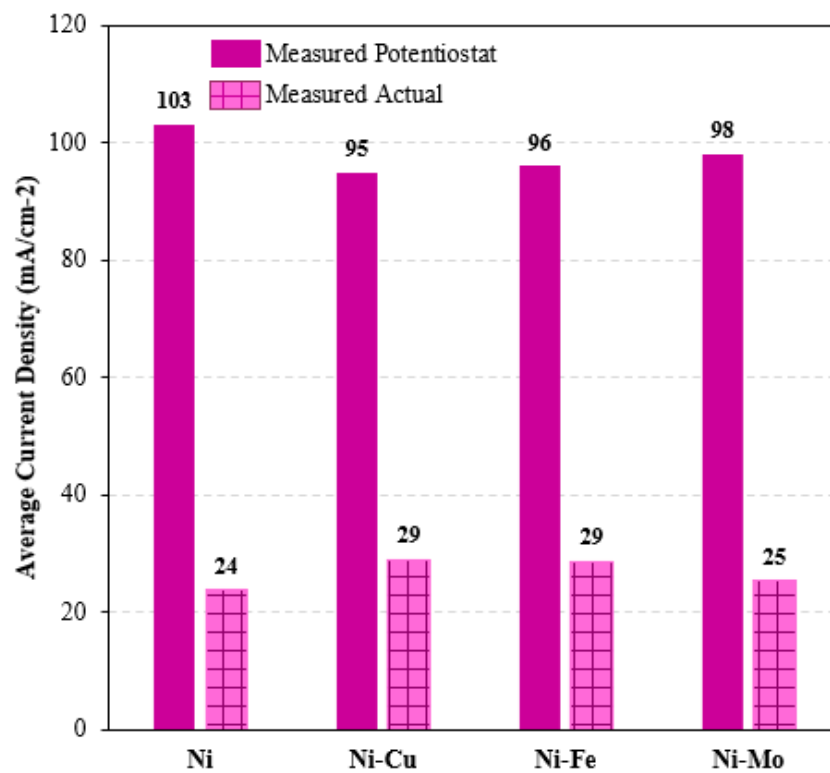


Figure 5.50 Current densities at 2.5V for coated CPLA 3D-printed electrodes measured by potentiostat versus actual during hydrogen production

Figure 5.51 shows the energy and exergy efficiencies of the coated flow through CPLA 3D-printed electrodes. The efficiency of the nickel-copper coated flow-through electrode is slightly higher compared to the nickel-iron coated electrode. One main reason for this is the increase in mass flow rate for the flow-through electrodes as seen earlier. In addition, the energy at the mass flow rate is reduced due to the decrease in current supplied at the same voltage. There is an increase in mass transport as a result of the porous design in the flow-through electrodes. This reduces the losses due to ohmic overpotential that occur between the electrolyte and the electrode. Therefore, increasing the efficiencies of the electrolysis.

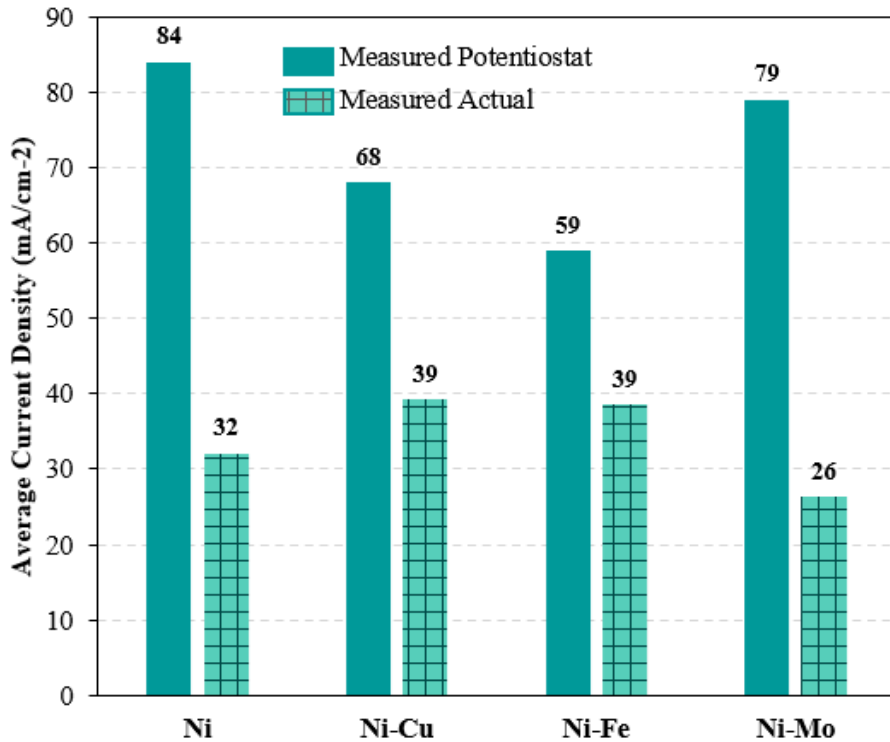


Figure 5.51 Energy and exergy efficiencies for coated flow through electrodes

The energy efficiencies of the flow-through and conventional (the originally designed) electrode are directly compared in Figure 5.52. It can be seen the efficiencies of the coated flow through electrodes is much higher than the initial design coated CPLA 3D-printed electrodes. The efficiencies of the flow-through electrodes for the same coating metal are approximately 74% higher. The higher efficiency is directly a result of faster mass transport and higher hydrogen production rate for the flow-through design. In addition, the flow through electrodes required less energy for the hydrogen produced compared to the initially

designed electrodes. The presented study shows that the flow through design have higher hydrogen production rates and much higher efficiencies compared to conventional electrode designs.

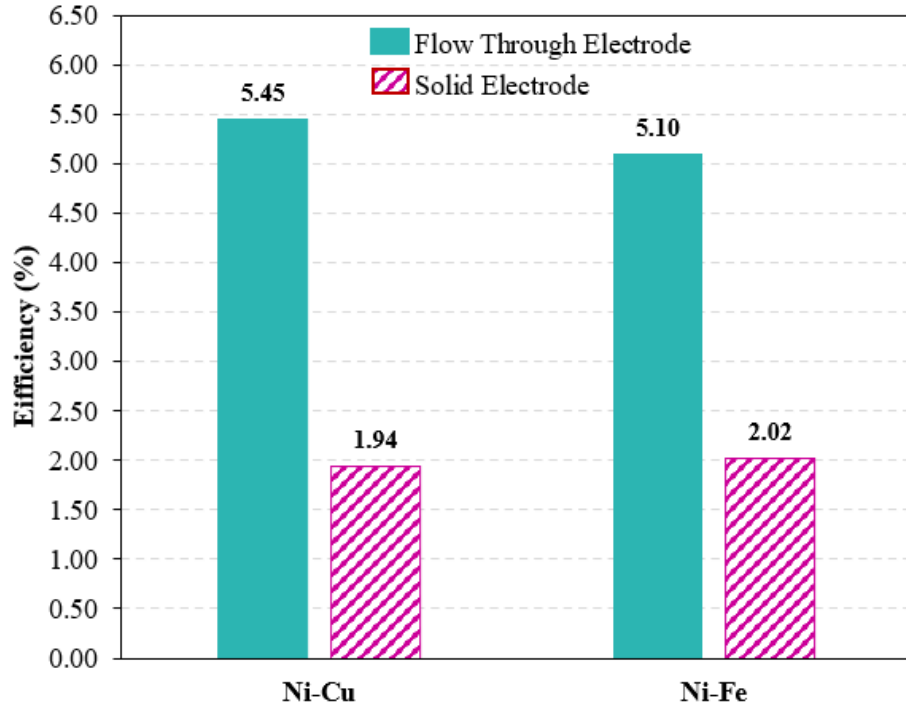


Figure 5.52 Energy efficiencies for Ni-Cu and Ni-Fe coated CPLA 3D-printed flow through (D2) versus solid (initial design) electrodes

One additional factor to also consider is the surface area of the electrodes. Electrodes with larger surface areas would be able to tolerate larger currents which would hence lead to larger hydrogen production. Even though in this study, the flow-through and the initially designed electrodes have different surface areas, these results are only based on the geometry on the electrodes. In this case, the flow-through electrodes have smaller surface areas due to the geometry. Further studies with the same surface areas need to be considered to evaluate the effect of surface area on the hydrogen production for the two designs.

CHAPTER 6: CONCLUSIONS AND RECOMMENDATIONS

In the thesis presented, 3D-printed electrodes were coated using electrodeposition for hydrogen production. Nickel was considered as the main coating metal for the electrodes. Additionally, various other catalysts were coated along with nickel to evaluate their performance for hydrogen evolution reaction. The coated electrodes were evaluated for current density, overpotential, impedance, hydrogen production rate, energy efficiency and exergy efficiency.

6.1 Conclusions

There is an urgent need for clean energy fuels for replacing fossil fuels. The rapid increase in usage of fossil fuels has led to a critical state of environmental conditions. The impact of carbon dioxide emissions released from the usage of fossil fuel is evident in the changes in climate encountered today. Changes in climate are noticeable all around the globe is continuously impacting the environment and life on earth. Hydrogen is an emerging clean fuel for replacement of fossil fuels. Zero emissions are released when hydrogen is used as a fuel. Some concerns with hydrogen production are that it's expensive to produce and hard to store. Electrolysis is a common device used for hydrogen production, more commonly for green hydrogen production. Better solutions are needed to reduce hydrogen production cost, increase the feasibility, and to make hydrogen production more easily accessible.

This thesis presents a novel approach for preparing the electrodes used in an electrolysis for hydrogen production. Electrolysis is one of the most efficient means of producing hydrogen. Electrodes, the anode, and the cathode play a crucial role in hydrogen production. Electricity is supplied from the anode to the cathode where a reaction occurs for splitting water. As a result, hydrogen and oxygen is produced due to the hydrogen evolution reaction (at the cathode) and the oxygen evolution reaction (at the anode) that occur in the electrolysis. In this thesis, a water membraneless alkaline electrolysis is considered, and the performance of the cathodes (coated 3D-printed electrodes) is evaluated in a 1 mol potassium hydroxide (KOH) added to the water supplied. There were two main methods considered for coating the 3D-printed electrodes using electrodeposition as the coating technique. For the first method, the electrodes were 3D-printed using normal

PLA (non-conductive). Two different types of nickel conductive paints were used to first coat the 3D-printed electrodes. This was because, electrodeposition requires the coating material to be conductive for electroplating to occur. The second method considered was to 3D print the electrodes using conductive PLA which allowed to directly coat the electrodes using electrodeposition. The performance of both approaches was evaluated. The second method with the conductive PLA approach was found to be more efficient due to various reasons. The approach reduced the number of steps and the time required to prepare the coated 3D-printed electrodes. In addition, using the conductive PLA allowed for more flexibility with the electrode design. More complex electrode designs can be coated with the conductive PLA. Printing complex shapes with the normal PLA and then coating them with the conductive paint would be more difficult. The paint is dense and would be very difficult to apply on complex shapes. A unique electrode design was considered for further study. The developed design is a flow-through electrode which promotes mass transport to increase the rate of hydrogen produced. The flow through electrode is printed with the conductive PLA and then coated using similar electrodeposition approaches. In general, the efficiencies of the coated 3D-printed was low for commercial applications. However, this technology can be beneficial as a design space which can help improve the efficiencies and performance of conventional electrode designs. The results of all coated 3D-printed electrodes prepared were obtained. The major findings from the thesis are presented as follows:

- Using the conductive paint approach was found to be more efficient. Whereas coatings on the conductive PLA 3D-printed electrodes was a more reliable approach for preparing the electrodes. The coatings on the conductive PLA were consistent throughout the surface compared to the ones on the conductive paint.
- The nickel coated electrodes had higher overpotentials compared to the nickel-copper, nickel-iron, and nickel-molybdenum coated electrodes. The overpotentials of Ni, Ni-Cu, Ni-Fe, and Ni-Mo coated on conductive PLA electrodes at a current density of 10 mA/cm² were found to be 540 mV, 275 mV, 270 mV, and 334 mV.
- Nickel-copper coatings were found to be the least challenging when electroplating and the most durable under testing and in electrolysis conditions.

- A nickel coated electrode four times the metal coating (0.178 g/cm^2) of another nickel coated electrode (0.044 g/cm^2) had a current density of -106 mA/cm^2 versus -44 mA/cm^2 at a potential of -2.5V .
- The nickel-copper electrode with three times more copper coating (0.144 g/cm^2) had a current density of -88 mA/cm^2 versus -45 mA/cm^2 .
- The nickel-molybdenum electrode with two times more of the Mo coating (0.145 g/cm^2) had a current density of -92 mA/cm^2 versus -60 mA/cm^2 .
- The flow through electrode design was found to be the better design as the hydrogen production rate was increased. In addition, the energy efficiency of the flow through electrode was $\sim 70\%$ higher compared to the traditional coated solid electrode design coated with the same metals.
- The energy efficiencies of the nickel-copper coated flow-through electrode and the originally designed electrodes were 5.45% and 1.94% respectively.
- The energy efficiencies of flow through and the initial designed nickel-iron coated electrodes was found to be 5.10% and 2.02% respectively.

6.2 Recommendations

Various areas in the study are identified for opportunities to expand on the research work. These group of recommendations are presented as follows:

- The current response and overpotentials for higher electrodeposition amounts showed promising results, electrodes with different deposition amounts of the same metal should be tested to better understand the behaviour of electrodes for hydrogen production.
- Different methods for controlling bath conditions should be considered to avoid the bath becoming acidic, which becomes critical in coating the conductive PLA. Possibly using different chemical compositions can be investigated.
- Other additive technologies should be considered for directly 3D printing the electrodes with metal deposits instead of coating the electrodes with metals.
- The sensor used to measure hydrogen concentration was very sensitive with high uncertainty. A method for measuring the instantaneous hydrogen production rate

should be implemented to be able to test for extended operation times. Using a flow meter for hydrogen production rate can be considered for future work.

- More studies should be investigated with the flow-through design. A modified version of the designs, with more holes and bigger openings should be considered and tested for hydrogen production. The flow through electrodes should also be coated with other metals and catalysts and tested for hydrogen production.
- Further studies should consider focusing on the design aspect and possibilities of the electrodes.
- A scaled-up version of the electrodes and a zero-gap multi electrode stalk cell can be considered for future work.

REFERENCES

- [1] “Introduction to Climate Action” United Nations Framework Convention on Climate Change. <https://unfccc.int/climate-action/introduction-climate-action> (accessed May 22, 2023).
- [2] “CO₂ Emissions in 2022 IEA Report.” International Energy Agency. [https://www.iea.org/reports/CO₂-emissions-in-2022](https://www.iea.org/reports/CO2-emissions-in-2022) (accessed May 22, 2023).
- [3] “World Energy Outlook 2022 Report IEA” International Energy Agency. <https://www.iea.org/reports/world-energy-outlook-2022/executive-summary> (accessed May 22, 2023).
- [4] “Net Zero by 2050 IEA Report.” International Energy Agency. <https://www.iea.org/reports/net-zero-by-2050> (accessed May 22, 2023).
- [5] “Energy IRENA Outlook Report” International Renewable Energy Agency. <https://www.irena.org/Energy-Transition/Outlook> (accessed May 22, 2023).
- [6] “Use of hydrogen U.S. EIA.” United States Energy Information Administration. <https://www.eia.gov/energyexplained/hydrogen/use-of-hydrogen.php> (accessed May 23, 2023).
- [7] “The Future of Hydrogen IEA Report.” International Energy Agency. <https://www.iea.org/reports/the-future-of-hydrogen> (accessed May 23, 2023).
- [8] “The hydrogen colour spectrum.” National Grid Group. <https://www.nationalgrid.com/stories/energy-explained/hydrogen-colour-spectrum> (accessed May 24, 2023).
- [9] “The colors of hydrogen.” WordPress Chem.4.us. <http://www.chem4us.be/blue-green-gray-the-colors-of-hydrogen/> (accessed May 24, 2023).
- [10] “Hydrogen Production: Electrolysis” United States Department of Energy. <https://www.energy.gov/eere/fuelcells/hydrogen-production-electrolysis> (accessed May 24, 2023).
- [11] “Global Top 20 Hydrogen Electrolyzer Manufacturers [2023].” Blackridge Research. <https://www.blackridgeresearch.com/blog/list-of-global-top-hydrogen-electrolyzer-manufacturers-companies-makers-suppliers-in-the-world/> (accessed May 24, 2023).
- [12] “Electrolyzers: a manufacturing industry that everyone wants to lead | CIC Energigune.” <https://cicenergigune.com/en/blog/electrolyzers-manufacturing-industry-everyone-lead> (accessed May 25, 2023).
- [13] G. Givirovskiy, V. Ruuskanen, L. S. Ojala, M. Lienemann, P. Kokkonen, and J. Ahola, “Electrode material studies and cell voltage characteristics of the in situ water electrolysis performed in a pH-neutral electrolyte in bioelectrochemical

- systems,” *Heliyon*, vol. 5, no. 5, p. e01690, May 2019, doi: 10.1016/J.HELIYON.2019.E01690.
- [14] T. D. Ngo, A. Kashani, G. Imbalzano, K. T. Q. Nguyen, and D. Hui, “Additive manufacturing (3D printing): A review of materials, methods, applications and challenges,” *Compos B Eng*, vol. 143, pp. 172–196, Jun. 2018, doi: 10.1016/J.COMPOSITESB.2018.02.012.
- [15] “Future now: 3D printing moves from prototyping to production” McKinsey. <https://www.mckinsey.com/capabilities/operations/our-insights/the-mainstreaming-of-additive-manufacturing> (accessed May 24, 2023).
- [16] “Electrolysers IEA.” International Energy Agency. <https://www.iea.org/reports/electrolysers> (accessed May 23, 2023).
- [17] C. Coutanceau, S. Baranton, and T. Audichon, “Hydrogen Production From Water Electrolysis,” *Hydrogen Electrochemical Production*, pp. 17–62, 2018, doi: 10.1016/B978-0-12-811250-2.00003-0.
- [18] A. Keçebaş, M. Kayfeci, and M. Bayat, *Solar Hydrogen Production*. Elsevier, 2019. doi: 10.1016/C2017-0-02289-9.
- [19] T. Tsoutsos, “Hybrid wind–hydrogen energy systems,” *Stand-Alone and Hybrid Wind Energy Systems*, pp. 254–281, 2010, doi: 10.1533/9781845699628.2.254.
- [20] X. Tang, L. Xiao, C. Yang, J. Lu, and L. Zhuang, “Noble fabrication of Ni–Mo cathode for alkaline water electrolysis and alkaline polymer electrolyte water electrolysis,” *Int J Hydrogen Energy*, vol. 39, no. 7, pp. 3055–3060, Feb. 2014, doi: 10.1016/J.IJHYDENE.2013.12.053.
- [21] F. Allebrod, C. Chatzichristodoulou, and M. B. Mogensen, “Cobalt and molybdenum activated electrodes in foam based alkaline electrolysis cells at 150–250 °C and 40 bar,” *J Power Sources*, vol. 255, pp. 394–403, Jun. 2014, doi: 10.1016/J.JPOWSOUR.2014.01.024.
- [22] V. M. Nikolic, G. S. Tasic, A. D. Maksic, D. P. Saponjic, S. M. Miulovic, and M. P. Marceta Kaninski, “Raising efficiency of hydrogen generation from alkaline water electrolysis – Energy saving,” *Int J Hydrogen Energy*, vol. 35, no. 22, pp. 12369–12373, Nov. 2010, doi: 10.1016/J.IJHYDENE.2010.08.069.
- [23] A. N. Colli, H. H. Girault, and A. Battistel, “Non-Precious Electrodes for Practical Alkaline Water Electrolysis,” *Materials*, vol. 12, no. 8, 2019, doi: 10.3390/MA12081336.
- [24] F. Rosalbino, S. Delsante, G. Borzone, and E. Angelini, “Electrocatalytic behaviour of Co–Ni–R (R = Rare earth metal) crystalline alloys as electrode materials for hydrogen evolution reaction in alkaline medium,” *Int J Hydrogen*

- Energy*, vol. 33, no. 22, pp. 6696–6703, Nov. 2008, doi: 10.1016/J.IJHYDENE.2008.07.125.
- [25] P. Esmaili, I. Dincer, and G. F. Naterer, “Energy and exergy analyses of electrolytic hydrogen production with molybdenum-oxo catalysts,” *Int J Hydrogen Energy*, vol. 37, no. 9, pp. 7365–7372, May 2012, doi: 10.1016/J.IJHYDENE.2012.01.076.
- [26] B. Hüner *et al.*, “An Overview of Various Additive Manufacturing Technologies and Materials for Electrochemical Energy Conversion Applications,” *ACS Omega*, vol. 7, no. 45, pp. 40638–40658, Nov. 2022, doi: 10.1021/ACSOMEGA.2C05096/ASSET/IMAGES/MEDIUM/AO2C05096_0015.GIF.
- [27] M. P. Browne, V. Urbanova, J. Plutnar, F. Novotný, and M. Pumera, “Inherent impurities in 3D-printed electrodes are responsible for catalysis towards water splitting,” *J Mater Chem A Mater*, vol. 8, no. 3, pp. 1120–1126, Jan. 2020, doi: 10.1039/C9TA11949C.
- [28] “3D-printing for electrolytic processes and electrochemical flow systems.” *Journal of Materials Chemistry*. <https://pubs.rsc.org/en/content/articlelanding/2020/ta/d0ta07939a/unauth> (accessed May 27, 2023).
- [29] H. Quan, T. Zhang, H. Xu, S. Luo, J. Nie, and X. Zhu, “Photo-curing 3D printing technique and its challenges,” *Bioact Mater*, vol. 5, no. 1, p. 110, Mar. 2020, doi: 10.1016/J.BIOACTMAT.2019.12.003.
- [30] S. Yu *et al.*, “Novel nanomaterials for environmental remediation of toxic metal ions and radionuclides,” *Emerging Nanomaterials for Recovery of Toxic and Radioactive Metal Ions from Environmental Media*, pp. 1–47, Jan. 2021, doi: 10.1016/B978-0-323-85484-9.00002-9.
- [31] D. Sobha Jayakrishnan, “Electrodeposition: the versatile technique for nanomaterials,” *Corrosion Protection and Control Using Nanomaterials*, pp. 86–125, 2012, doi: 10.1533/9780857095800.1.86.
- [32] J. Rathouský, K. Wessels, M. Wark, and T. Oekermann, “Texture properties of nanoporous TiO₂ films prepared by anodic electrodeposition using a structure-directing agent,” *Stud Surf Sci Catal*, vol. 170, no. B, pp. 1494–1501, Jan. 2007, doi: 10.1016/S0167-2991(07)81021-4.
- [33] E. Cattaneo and B. Riegel, “Chemistry, Electrochemistry, And Electrochemical Applications | Nickel,” *Encyclopedia of Electrochemical Power Sources*, pp. 796–809, Jan. 2009, doi: 10.1016/B978-044452745-5.00062-9.

- [34] Q. Li, J. O. Jensen, and N. J. Bjerrum, “Chemistry, Electrochemistry, And Electrochemical Applications | Aluminum,” *Encyclopedia of Electrochemical Power Sources*, pp. 695–708, Jan. 2009, doi:10.1016/B978-044452745-5.00951-5.
- [35] Z. Zhang *et al.*, “A Concentrated AlCl₃-Diglyme Electrolyte for Hard and Corrosion-Resistant Aluminum Electrodeposits,” *ACS Appl Mater Interfaces*, vol. 12, no. 38, pp. 43289–43298, Sep. 2020, doi: 10.1021/ACSAMI.0C12602/ASSET/IMAGES/LARGE/AM0C12602_0011.JPEG.
- [36] A. Vicenzo and P. L. Cavallotti, “Copper electrodeposition from a pH 3 sulfate electrolyte,” *J Appl Electrochem*, vol. 32, no. 7, pp. 743–753, Jul. 2002, doi: 10.1023/A:1020191111298/METRICS.
- [37] A. K. Shukla and B. Hariprakash, “Chemistry, Electrochemistry, And Electrochemical Applications | Iron,” *Encyclopedia of Electrochemical Power Sources*, pp. 744–750, Jan. 2009, doi: 10.1016/B978-044452745-5.00063-0.
- [38] R. M. Schaffert and B. W. Gosser, “A Sulfate-Chloride Solution for Iron Electroplating and Electroforming,” *Transactions of The Electrochemical Society*, vol. 84, no. 1, p. 319, Oct. 1943, doi: 10.1149/1.3071576.
- [39] P. N. Bartlett, M. A. Ghanem, I. S. El Hallag, P. De Groot, and A. Zhukov, “Electrochemical deposition of macroporous magnetic networks using colloidal templates,” *J Mater Chem*, vol. 13, no. 10, pp. 2596–2602, Sep. 2003, doi: 10.1039/B304496C.
- [40] H. zhen CAO, C. jian TONG, H. bin ZHANG, and G. qu ZHENG, “Mechanism of MoO₂ electrodeposition from ammonium molybdate solution,” *Transactions of Nonferrous Metals Society of China*, vol. 29, no. 8, pp. 1744–1752, Aug. 2019, doi: 10.1016/S1003-6326(19)65082-X.
- [41] X. Li, “Electrodeposition of multi-component alloys: Thermodynamics, kinetics and mechanism,” *Curr Opin Electrochem*, vol. 39, p. 101289, Jun. 2023, doi: 10.1016/J.COEELEC.2023.101289.
- [42] D. Yan, “Computational Simulation of Copper (Cu) and Nickel-Copper (Ni-Cu) Alloy Electrodeposition,” 2019.
- [43] J. O. Dukovic, “Computation of current distribution in electrodeposition, a review,” *IBM J Res Dev*, vol. 34, no. 5, pp. 693–705, 1990, doi: 10.1147/RD.345.0693.
- [44] B. Hüner, N. Demir, and M. F. Kaya, “Ni-Pt coating on graphene based 3D printed electrodes for hydrogen evolution reactions in alkaline media,” *Fuel*, vol. 331, p. 125971, Jan. 2023, doi: 10.1016/J.FUEL.2022.125971.
- [45] B. Hüner, N. Demir, and M. F. Kaya, “Electrodeposition of NiCu bimetal on 3D printed electrodes for hydrogen evolution reactions in alkaline media,” *Int J*

Hydrogen Energy, vol. 47, no. 24, pp. 12136–12146, Mar. 2022, doi: 10.1016/J.IJHYDENE.2021.10.009.

- [46] B. Hüner, N. Demir, and M. F. Kaya, “Hydrogen Evolution Reaction Performance of Ni-Co-Coated Graphene-Based 3D Printed Electrodes,” *ACS Omega*, vol. 8, no. 6, pp. 5958–5974, Feb. 2023, doi: 10.1021/ACSOMEGA.2C07856/ASSET/IMAGES/LARGE/AO2C07856_0014.JPG.
- [47] J. C. Bui, J. T. Davis, E. S. Cousens, and D. V Esposito, “3D Printed Electrodes for Membraneless Electrolyzers,” *ECS Meeting Abstracts*, vol. MA2018-01, no. 44, p. 2520, Apr. 2018, doi: 10.1149/MA2018-01/44/2520.
- [48] Z. Han, G. Wang, J. Zhang, and Z. Tang, “Direct photo-curing 3D printing of nickel-based electrocatalysts for highly-efficient hydrogen evolution,” *Nano Energy*, vol. 102, p. 107615, Nov. 2022, doi: 10.1016/J.NANOEN.2022.107615.
- [49] I. Sullivan *et al.*, “3D printed nickel-molybdenum-based electrocatalysts for hydrogen evolution at low overpotentials in a flow-through configuration,” *ACS Appl Mater Interfaces*, vol. 13, no. 17, pp. 20260–20268, May 2021, doi: 10.1021/ACSAMI.1C05648/ASSET/IMAGES/LARGE/AM1C05648_0005.JPEG.
- [50] P. Zhou *et al.*, “Anodized Steel: The Most Promising Bifunctional Electrocatalyst for Alkaline Water Electrolysis in Industry,” *Adv Funct Mater*, vol. 32, no. 26, p. 2202068, Jun. 2022, doi: 10.1002/ADFM.202202068.
- [51] G. Chisholm, P. J. Kitson, N. D. Kirkaldy, L. G. Bloor, and L. Cronin, “3D printed flow plates for the electrolysis of water: an economic and adaptable approach to device manufacture,” *Energy Environ Sci*, vol. 7, no. 9, pp. 3026–3032, Aug. 2014, doi: 10.1039/C4EE01426J.
- [52] J. Gage Wright, B. P. Charnay, J. A. Rabinowitz, R. G. Mariano, and M. W. Kanan, “Rapid Prototyping of Lab-scale Electrolysis Cells Using Stereolithography and Electroless Plating,” Apr. 2023, doi: 10.26434/CHEMRXIV-2023-P200M.
- [53] G. Yang *et al.*, “Fully printed and integrated electrolyzer cells with additive manufacturing for high-efficiency water splitting,” *Appl Energy*, vol. 215, pp. 202–210, Apr. 2018, doi: 10.1016/J.APENERGY.2018.02.001.
- [54] M. Próchniak and M. Grdeń, “Electrochemical deposition of nickel from aqueous electrolytic baths prepared by dissolution of metallic powder,” *Journal of Solid State Electrochemistry* 2021 26:2, vol. 26, no. 2, pp. 431–447, Nov. 2021, doi: 10.1007/S10008-021-05084-9.
- [55] R. Y. Ying, “Electrodeposition of Copper-Nickel Alloys from Citrate Solutions on a Rotating Disk Electrode: I. Experimental Results,” *J Electrochem Soc*, vol. 135, no. 12, pp. 2957–2964, Dec. 1988, doi: 10.1149/1.2095469/XML.

- [56] Y. Wang, N. Williamson, R. Dawson, and N. Bimbo, “Electrodeposition of nickel–iron on stainless steel as an efficient electrocatalyst coating for the oxygen evolution reaction in alkaline conditions,” *J Appl Electrochem*, vol. 53, no. 5, pp. 877–892, May 2022, doi: 10.1007/S10800-022-01817-4/FIGURES/8.
- [57] M. I. Jaramillo-Gutiérrez, S. M. Sierra-González, C. A. Ramírez-González, J. E. Pedraza-Rosas, and J. A. Pedraza-Avella, “Effect of electrodeposition parameters and surface pretreatment on the electrochemical hydrogen production using nickel-plated stainless steel electrodes,” *Int J Hydrogen Energy*, vol. 46, no. 11, pp. 7667–7675, Feb. 2021, doi: 10.1016/J.IJHYDENE.2019.09.205.
- [58] J. Brauns and T. Turek, “Alkaline Water Electrolysis Powered by Renewable Energy: A Review,” *Processes 2020, Vol. 8, Page 248*, vol. 8, no. 2, p. 248, Feb. 2020, doi: 10.3390/PR8020248.
- [59] Y. S. K. De Silva, P. H. Middleton, and M. L. Kolhe, “Performance comparison of mono-polar and bi-polar configurations of alkaline electrolysis stack through 3-D modelling and experimental fabrication,” *Renew Energy*, vol. 149, pp. 760–772, Apr. 2020, doi: 10.1016/J.RENENE.2019.12.087.
- [60] H. Rajaei and J. W. Haverkort, “Compact monopolar electrochemical stack designs using electrode arrays or corrugated electrodes,” *Electrochim Acta*, vol. 332, p. 135470, Feb. 2020, doi: 10.1016/J.ELECTACTA.2019.135470.
- [61] G. Yang *et al.*, “A novel PEMEC with 3D printed non-conductive bipolar plate for low-cost hydrogen production from water electrolysis,” *Energy Convers Manag*, vol. 182, pp. 108–116, Feb. 2019, doi: 10.1016/J.ENCONMAN.2018.12.046.
- [62] K. C. Sandeep *et al.*, “Experimental studies and modeling of advanced alkaline water electrolyser with porous nickel electrodes for hydrogen production,” *Int J Hydrogen Energy*, vol. 42, no. 17, pp. 12094–12103, Apr. 2017, doi: 10.1016/J.IJHYDENE.2017.03.154.
- [63] “Wanptek Dps Series DC Power Supply User Manual.” Available: <https://manuals.plus/wanptek/dps-series-dc-power-supply-manual#axzz86NpX7FIJ> (accessed Jul. 02, 2023).
- [64] “Isotemp Hotplates, Stirrers and Stirring Hotplates Operation Manual”. Available: <http://www.marshallscientific.com/v/vspfiles/files/manuals/FisherScientificHotplatesStirrers.pdf>
- [65] “Operating Instructions Mettler Toledo B-S/Fact Line of Balances ”. Available: www.mt.com/classic (Accessed: Jul. 02, 2023)
- [66] “Operator’s Manual Tabletop Ultrasonic Cleaners”. Available: <https://neurophysics.ucsd.edu/Manuals/Fisher/Fisher%20Scientific%20Operator's%20Manual%20Tabletop%20Ultrasonic%20Cleaners.pdf> (Accessed: Jul. 02, 2023)

- [67] “Mastercraft Battery Powered Digital Temperature Reader Instructional Manual.” Available: <https://media-www.canadiantire.ca/manual/product/0574554/057-4554-manual-en-029182da-ae44-401b-b0d7-14a099742b9e.pdf> (Accessed: Jul. 02, 2023)
- [68] “Conductivity Probe User Manual – Vernier.” Available: <https://www.vernier.com/manuals/con-bta/> (Accessed: Jul. 02, 2023)
- [69] “Pocket Digital Multimeter Instruction Manual model no. 052-0060-2”. Available: <https://media-www.canadiantire.ca/manual/product/0520060/0520060p-en-fr-ea15b320-e2db-4d4f-bec4-b3bc85396f6f.pdf> (Accessed: Jul. 02, 2023)
- [70] “Corning pH 450 Instruction Manual”. Available: https://archive-resources.coleparmer.com/Manual_pdfs/Corning%20Meter%20Manuals/Corning440pHBenchMeterManual.pdf (Accessed: Jul. 02, 2023)
- [71] “Furno 300 Dual Temperature Heat Gun Owner’s Manual”. Available: https://www.wagnerspraytech.com/wp-content/uploads/2017/05/0503748F_Furno300.pdf (Accessed: Jul. 02, 2023)
- [72] “Conductive PLA Proto-pasta.” ProtoPasta. [Online]. <https://www.protopasta.com/pages/conductive-pla>. (Accessed: Jul. 02, 2023)
- [73] “841AR Liquid Super Shield TM Nickel Conductive Paint” MG Chemicals. [Online]. Available: www.mgchemicals.com (Accessed: Jul. 02, 2023)
- [74] “841WB Liquid Super Shield TM Nickel Conductive Paint.” MG Chemicals Available: <https://mgchemicals.com/downloads/tds/tds-841wb-l.pdf> (Accessed: Jul. 02, 2023)
- [75] “Flammable Gas Sensor,” Winsensor. [Online]. Available: www.winsensor.com(Accessed: Jul. 02, 2023)
- [76] G. Instruments, “Reference 3000 Potentiostat/Galvanostat/ZRA Operator’s Manual,” 2012, [Online]. Available: www.gamry.com/service-support/ (Accessed: Jul. 02, 2023)
- [77] “Hydrogen Concentration Conversion.” Gastec Corporation. [Online]. <https://www.gastec.co.jp/en/technology/knowledge/concentration/> (Accessed: Jul. 02, 2023)